UNIVERSITY OF CAPE TOWN
IYUNIVESITHI YASEKAPA • UNIVERSITEIT VAN KAAPSTAD

Sasol Advanced Fuels Laboratory

An Investigation into the Effects of Diesel Fuel Properties on the Injection Characteristics of a Common Rail Injection System

---

Author:

Brenainn A. Cross

Supervised by:

Mr. Paul Schaberg

A dissertation submitted to the Department of Mechanical Engineering at the University of Cape Town, in partial fulfillment of the requirements for the degree of Master of Science in Mechanical Engineering.

Cape Town, South Africa

January 2012

Declaration

1. I know the meaning of plagiarism and declare that all the work in the document, save for that which is properly acknowledged, is my own.

2. I have used the Harvard convention for citation and referencing. Each significant contribution to, and quotation in this project from the works of other people has been attributed, and has been cited and referenced.

3. I have not allowed, and will not allow anyone to copy my work with the intention of passing it off as his/her own work.

Signature: _____

Abstract

Modern diesel engines must meet a number of performance criteria related to fuel consumption, emissions levels, engine noise and vibrations. The diesel fuel injection system is the primary mode of combustion control, and hence is important in helping to meet these engine requirements.

This study set out to investigate the effects of diesel fuel properties on the behaviour of a common rail fuel injection system, with particular emphasis on the injection rate shape characteristics. The investigation included the design and commissioning of experimental equipment for the measurement of fuel properties at typical common rail pressures, as well as the measurement of instantaneous fuel flow rate by a modified Bosch Indicator method. Data was then collected for two different diesel fuels, operating in two different fuel injector designs. The two fuels were EN590 (a European reference fuel) and GTL (a fuel derived from natural gas). The two injectors were a Bosch solenoid type injector, and a Bosch piezo type injector.

Some difficulties were experienced with the pressure of the fuel delivered by the fuel pump, and as such it was necessary to make use of regression models to generate 'clean' data, allowing for better comparisons between fuels and injectors at common operating points.

Injection data was collected at pulse widths of 0.2 ms to 1.5 ms, and regression models were developed for the data where pulse widths were longer than 0.5 milliseconds.

Across the injection pressure range of 600 bar to 1200 bar, the fuel density was found to have a significant effect on the injected mass, with a 10.4 % increase in fuel density resulting in increases of up to 6.6 % in the injected mass for the solenoid injector and up to 5.6 % for the piezo injector. Fuel viscosity, although not included in the models, was

predicted to have had effects on the injected mass, where an increase of 100 % in viscosity would result in a decrease in the injected mass of the order of 3 %.

The EN590, having a higher density, and lower viscosity than the GTL, displayed injected mass values of up to 7.9 % higher than the GTL. The initial rate of rise in the flow rate was also roughly 30 % higher in the piezo injector than in the solenoid injector.

Some improvements to the testing procedures used in this study were recommended, including a closer look at the method for measuring the injected mass at pulse widths less than 0.5 ms. It was also noted that the length of fuel pipe between the fuel pump and the fuel injector should be kept as close as possible to the length of the fuel pipe in the actual engine. This would ensure that any upstream effects on the fuel supply pressure would be accurately mimicked during testing. Lastly, it was recommended that a needle lift sensor be used for injection flow rate measurement, allowing for more accurate measurement of the injection durations.

Acknowledgements

Thanks are extended to the following people/entities for contributions made towards this project:

- The Sasol Advanced Fuels Laboratory – Initiator and sponsor of the project.
- Mr. Paul Schaberg – Project supervisor.
- Dr. Gareth Floweday – For assistance with data processing.
- Mr. Adrian Velaers – For technical advice pertaining to fuel injectors.
- Mr. Mark Wattrus – For significant assistance with the LabVIEW control system used.
- Mr. Jean-Paul Pelteret – For assistance with the collection and review of literature.
- Mr. Gavin Tomlinson – For assistance with laboratory equipment.
- Mr. Glen Newins – For manufacturing of the designed parts.

Table of Contents

List of Figures

List of Tables

Glossary of Terms

Acoustic velocity/Sonic velocity – *This is effectively the speed at which a sound wave travels through a substance under given conditions.*

Biodiesel – *Diesel which is manufactured using bio-mass (as opposed to diesel manufactured from fossil fuels).*

Bulk modulus – *The bulk modulus of a substance is a measure of the compressibility of that substance, and is expressed as a change in the hydrostatic pressure surrounding the substance as a function of the change in volume occupied by the substance.*

Common rail – *The common rail is a short section of pipe in modern diesel injection systems. The common rail is maintained at a constant pressure, and is the 'common' reservoir of fuel which supplies fuel to each fuel injector.*

Continuity equation – *An equation for flow of a compressible fluid based on the conservation of mass. It states that the mass of fluid entering a particular junction per unit of time equals the mass exiting that junction per unit of time.*

Density – *The mass of a particular substance, measured as a function of the volume it occupies in space, is referred to as the density of that substance.*

Dynamic viscosity – *When external forces act on a fluid, shear forces are experienced within the layers of the fluid. The measure of these shear forces as a function of the rate at which the external forces are applied is referred to as the viscosity of the fluid.*

ECU – *This is the Engine Control Unit, and is basically an on-board computer which controls the engine on a vehicle. Most modern engines have an ECU installed.*

Fuel injector – *An injector unit is installed in the head of each cylinder in a direct injection engine. The fuel injector acts as a valve which allows the fuel to enter the combustion chamber when necessary. The timing of the opening and closing of the fuel injectors is controlled by the engine's ECU.*

Injection duration - *The actual time for which flow occurs for a particular injection event.*

Injection event – *Described as one complete cycle of opening and closing of a fuel injector, resulting in a measured quantity of fuel being delivered to the engine's combustion chamber.*

Injection pressure – *The control pressure at which fuel is maintained in the common rail.*

Injection system – *Delivers fuel from the fuel tank to the engine. It consists of a fuel pump, fuel pipes, and fuel injectors.*

Kinematic viscosity – *The ratio of a fluids' dynamic viscosity to its mass density is referred to as the fluids' kinematic viscosity.*

Needle – *The main needle inside a fuel injector forms a seal on its seat just before the injectors' nozzle. The movement of this needle forms the opening and closing action of the fuel injector.*

Nozzle – *A mechanical fitting with single or multiple holes through which a fluid flows. A nozzle is usually designed to give a desired pattern of flow upon exit.*

Piezo-electric crystal – *A crystal which when subjected to mechanical deformation, emits an electric charge. Similarly, when subjected to an electric charge, a piezo-electric crystal will deform.*

Pressure transducer – *An instrument which measures the pressure at the point at which it is situated.*

Pulse-width – *The length of time the ECU instructs the fuel injector to open for a particular injection event.*

Pycnometer – *A flask/tube used for the measurement and comparison of fluid densities.*

Regression analysis – *A statistical tool whereby a data set is analysed for the purpose of generating additional data sets. The key idea being that the behaviour of these additional data sets remains consistent with the behaviour of the original data set.*

Riser – *A small pin inside a solenoid fuel injector which assists in controlling the opening and closing action of the main needle.*

Solenoid – *A solenoid consists of a magnet and an electric coil. When the solenoid is energised, a magnetic field is set up by the electric coil, and this magnetic field reacts to the magnetic field of the magnet to produce a linear motion.*

Thermocouple – *A probe which measures the temperature at the point at which it is situated.*

Nomenclature

Greek Symbol	Quantity	Units
β	Bulk Modulus	Pa
ρ	Density	kg/m^3
ρ_M	Density in the measuring tube	kg/m^3
ρ_R	Density in the common rail	kg/m^3
μ	Dynamic viscosity	Pa.s
μ_P	Poisson's ratio	none
υ	Kinematic viscosity	m^2/s

Symbol	Quantity	Units
A	Flow area	m^2
c	Acoustic Velocity	m/s
d	Diameter	m
L	Length	m
m	Mass	kg
P	Pressure	Pa
P_M	Measuring tube pressure	Pa
P_R	Common rail pressure	Pa
q	Volumetric flow	m^3
Q	Total Volumetric flow	m^3
Re	Reynold's number	none
t	Time	s
T	Temperature	K
u	Velocity	m/s
v	Velocity	m/s
V	Volume	m^3

1. Introduction

Modern diesel engines on both heavy and light duty vehicles are designed to meet a number of various performance requirements. These include, amongst others, adhering to emissions legislation, falling within engine noise requirements, lowering engine vibrations, and optimising the fuel consumption. Many different factors in the design of diesel engines contribute towards satisfying these requirements.

The primary mode of combustion control in a diesel engine is through the diesel injection system. This is one area where innovative design plays a significant role in engine optimisation and, in particular, the use of a common rail injection system allows for fine tuning and optimisation of the engine's performance (Schommers et al, 2000). The common rail system is a high pressure injection system with an electrically controlled, hydraulically actuated injector which allows for the variation of parameters such as injection duration, injection pressure, the number of injection events, and injection timing (Stumpp et al, 1996). Modern systems use injection pressures ranging from about 300 bar to in excess of 2000 bar (Ganser, 2000).

The injector system design is not the only factor affecting fuel injection characteristics. The physical properties of the fuel itself can have a significant effect on injection behaviour. Modern diesel fuels are derived from a variety of hydrocarbon sources and each different source produces a fuel with different physical properties (Morgan et al, 1998).

Changes in these properties, such as density and bulk modulus, affect the injection timing and the mass flow rate through the nozzle (Tat et al, 2003). Fuel spray pattern and atomization are also important aspects of fuel injection but these were not investigated in this study.

In an attempt to quantify the effects of fuel properties on fuel injection characteristics, the author tested two different diesel fuels (with differing physical properties), in a flow measurement apparatus. Further, in order to quantify the effects of injection system design, two differently designed injectors were tested with this apparatus. The two fuels used in the study were EN590, a European fuel used in this research as a reference, and a test fuel derived from natural gas (from here on referred to as GTL). The two injection systems differed only in the injector unit, where the first was a solenoid-driven common rail injector and the second a piezo-electrically driven common rail injector.

1.1 Problem Definition

The purpose of this study was to investigate the effects of GTL and EN590 diesel fuel properties on the injection characteristics in a common rail injection system. With 'diesel fuel properties' and 'injection characteristics' being fairly broad terms, it was necessary to set certain boundaries within which the study would focus. In terms of fuel properties, this translated into focussing on the diesel density, acoustic velocity, and bulk modulus. For the injection characteristics, the areas of particular interest were the injected mass values, and the shape of the injection rate curves. With these parameters identified, a secondary set of objectives was generated, namely, the construction, commissioning and verification of experimental apparatus which would allow for the measurement of the aforementioned quantities.

1.2 Objectives

The investigation of the aforementioned effects and characteristics proceeded from the following list of objectives:

Experimental Objectives

- Determine the bulk modulus, acoustic velocity, and density of the fuels to be tested at typical operating pressures and temperatures for a common rail injection system.
- Verify the accuracy of the above-mentioned fuel property measurements.
- Design and commission equipment capable of accurately measuring the instantaneous fuel mass flow rate through a common rail injector.
- Verify the accuracy of the fuel flow rate measurement.

Theoretical Objectives

- Use the measured results to draw sound conclusions relating to the effects of the fuel properties on the fuel injection behaviour.
- Evaluate these conclusions on the basis of other similar literature.

1.3 Report Layout

In order to aid the reader in navigating this document, here follows the basic structure for its layout. For a more in-depth guide to the information contained in this document please refer to the table of contents.

Literature Review (Chapter 2)

In order to put this study into context, this chapter describes previously conducted research on topics of similar interest. A literature review precedes any research project and assists in laying the foundations for the emphasis of the study.

Theoretical Background (Chapter 3)

This chapter describes the basics of the theories upon which the work in this study is based. It aims to give the reader an in-depth understanding of the physics behind high pressure fuel injection and details the mathematics behind the methods used in the experimental portion of the study.

Design of Equipment and Methodology (Chapter 4)

This chapter contains a description of the design of the equipment used in this study and the reasoning behind the different methods used in obtaining the necessary physical fuel injection and fuel property data. For design drawings please refer to Appendix C.

Results (Chapter 5)

A summary of the collected data is presented and the relevant behavioural trends are shown in the form of numerical tables and graphical plots. Data from other literature sources is also presented here as a comparison.

Analysis and Discussion (Chapter 6)

The results from this study are analysed and discussed here and the author presents comments on the trends and effects of fuel properties on diesel injection. Regression analyses are also presented for some of the flow data.

Conclusions (Chapter 7)

This study set out to investigate the effects of fuel properties on diesel injection behaviour and, based on the discussion chapter, relevant conclusions are drawn here about the findings of this study.

Recommendations (Chapter 8)

This chapter outlines some of the challenges faced throughout the course of this study and the author offers some possible improvements to the experimental processes as well as ideas for the scope of future work which continues from this study.

References (Chapter 9)

References for all of the associated literature are presented in this chapter. The Harvard convention was employed for all referencing and citation purposes.

Appendices

The appendices of this report contain the fuel properties, injected mass data, and design drawings for some of the experimental equipment.

2. Literature Review

2.1 Measurement of Fuel Properties

The more challenging of the experimental portions of this study was the measurement of the fuel properties at typical common-rail operating pressures. The effects of fuel properties on injection characteristics could only be fully investigated if the fuel properties at the given operating conditions were accurately determined; therefore it was necessary to make use of a simple yet reliable method for measuring the fuel properties in question. Given the effects of temperature on fuel properties, it was equally important that these measurements were made at constant and known temperatures.

The fuel properties to be measured were bulk modulus, density, and speed of sound (or acoustic velocity. These are defined as follows:

The bulk modulus of a fluid is the measure of that fluid's compressibility. That is to say, that for a given change in pressure, the fluid will experience a corresponding change in volume. The relationship is as follows (Douglas, Gasiorek, Swaffield, 2001):

$$\beta = -\frac{dP}{dV}V \quad \text{(Pa)} \qquad \text{(Eq 2-1)}$$

Where β is the bulk modulus of the fluid, dP is the change in applied pressure, and dV is the corresponding change in volume.

Density is the mass per volume measurement for any given substance and, for gases and liquids, density varies significantly with temperature.

Density:

$$\rho = \frac{m}{V} \qquad (\mathrm{kg/m^3}) \qquad \text{(Eq 2-2)}$$

Lastly, the speed of sound (or acoustic velocity) in a substance is the speed at which a pressure wave travels through the substance. At very high pressures where the compressibility of liquids is taken into consideration, the speed of sound in any particular liquid varies significantly with pressure.

Tat and Van Gerpen (2003) measured the speed of sound, density, and bulk modulus of biodiesel using the apparatus in figure 2-1, in order to quantify the effects of these properties on injection timing and the resulting engine performance.

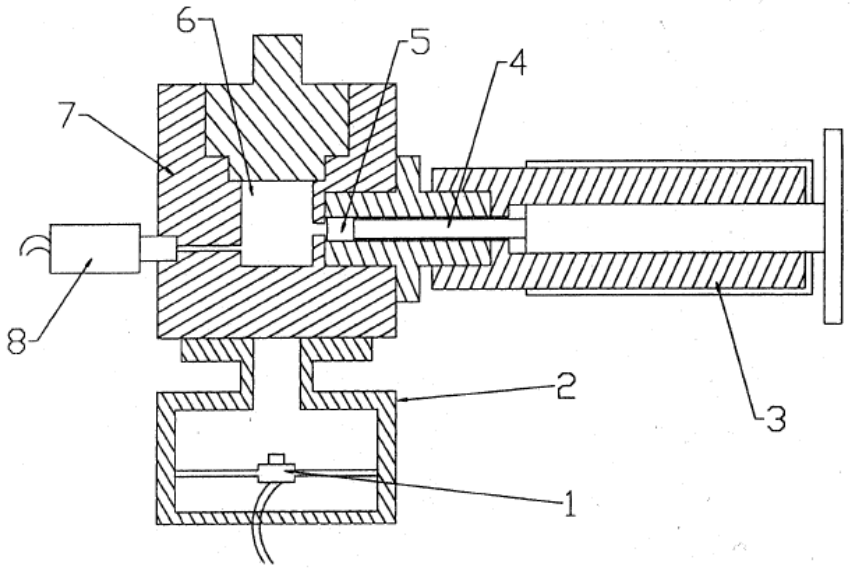

1. 10 MHz ultrasonic transducer.
2. cooled chamber for transducer.
3. pressure screw
4. plunger
5. piston
6. sample chamber
7. pressure vessel
8. pressure transducer

Figure 2- 1. Cross-section of apparatus as used by Tat and Van Gerpen (2003) for the measurement of density and speed of sound in biodiesel.

Referring to figure 2-1, the transducer at '1' emitted an ultrasonic pulse, and the reflections of the pulse were captured on an oscilloscope. The speed of the pulse travelling through the fuel in the sample chamber was then calculated as per figure 2-2. The density of the fuel sample was measured before each test, and by measuring the travel of the piston, the change in the volume of the sample chamber was known, hence the fuel density under the operating pressure was also known.

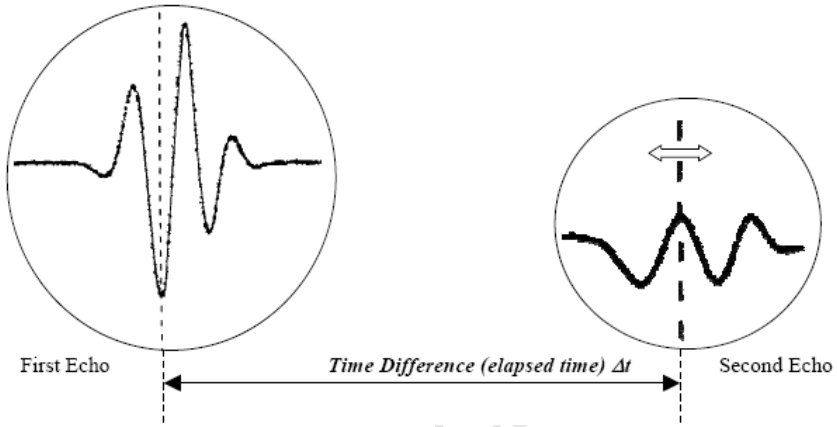

Figure 2- 2. Ultrasonic signal reflections for the speed of sound measurement in biodiesel (Tat and Van Gerpen, 2003)

A correction factor was included in the density measurement to allow for the expansion of the vessel at high pressure. The measured values for speed of sound and density were then used to calculate the bulk modulus of the fuel as follows (Gouw and Vlugter, 1967 and Rolling and Vogt, 1960, Tat and Van Gerpen, 2003):

$$\beta = c^2 \rho \qquad \text{(Eq 2-3)}$$

Where c is the speed of sound and ρ is the density at the operating pressure. Two difficulties with this method, as reported by Tat and Van Gerpen (2003), were the successful removal of all air bubbles from the sample chamber, and the elimination of any leaks in the system. It was also noted that the maximum operating pressure used in these tests was 345 bar, which is significantly lower than typical common rail injection pressures, which can reach in excess of 2000 bar (Ganser, 2000).

Szybist et al (2005) conducted a study to reduce biodiesel NOx emissions through the evaluation of formulation strategies. Part of this study involved the measurement of the bulk modulus of biodiesel. The fuel sample was placed inside a pycnometer which was further placed inside a pressurised vessel called a Jerguson Gauge as shown in figure 2-3. The vessel was pressurised to a known pressure with helium and the change in volume of the fuel sample was observed through a clear quartz viewing window, effectively a direct measurement of the bulk modulus of the fuel. The Jerguson Gauge was capable of handling pressures up to 4000 psi (275 bar).

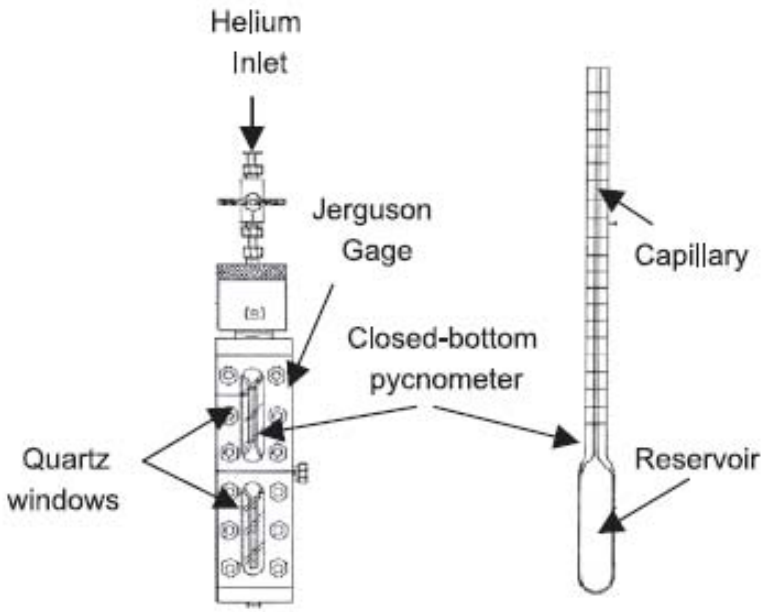

Figure 2- 3. Modified Stainless Jerguson Gauge used by Szybist et al (2005)

Huhtala and Vilenius (2001) presented a study of a common rail system which included measurement of the fuel properties. The pressure range over which these properties were measured was between 200 bar and 1450 bar. The method involved the measurement of the acoustic velocity in the fuel between two pressure transducers, as shown in figure 2-4.

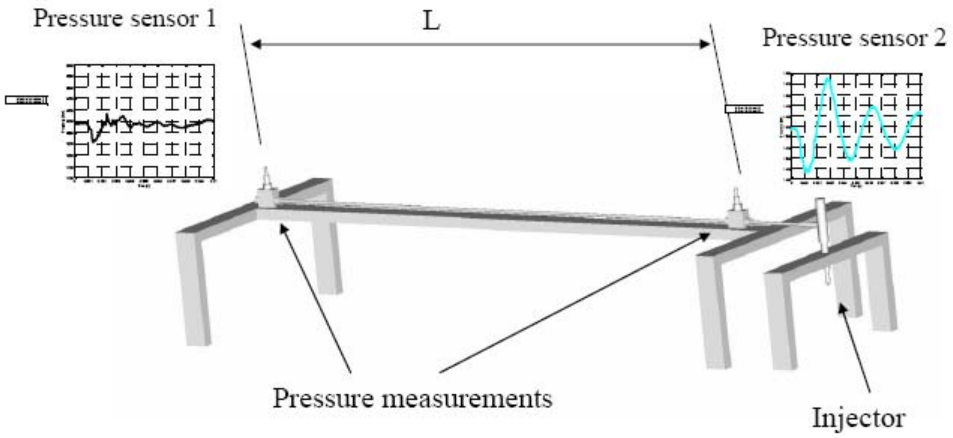

Figure 2- 4. Apparatus as used by Huhtala and Vilenius (2001) for the measurement of acoustic velocity in diesel fuel.

The acoustic velocity measurement was then used to infer the diesel density and bulk modulus at the operating pressure using the cross-correlation method as proposed by Jinghong et al (1994). See Chapter 3 of this report for a detailed description of the cross-correlation method.

Ball and Trusler (2001) conducted acoustic velocity measurements in n-hexane and n-hexadecane at temperatures between 298 K and 373 K, and at pressures up to 100 MPa. The apparatus was an ultrasonic cell type, as shown in figure 2-5 below.

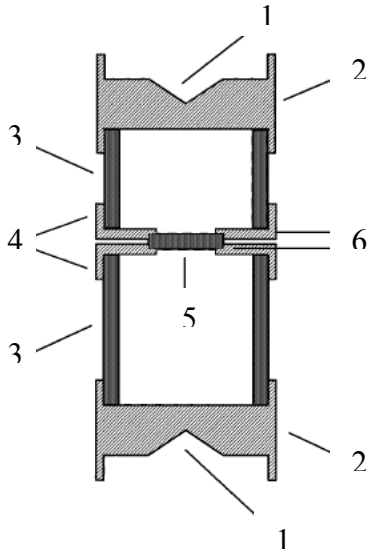

Figure 2- 5. Apparatus as used by Ball and Trusler (2001).

Similar in principle to the measurement technique used by Tat and van Gerpen (2003), the difference here was that the transducer was submersed in the test fluid. The transducer (5) was placed with two reflector plates (1) at different distances. After energising the transducer, two return signals were captured, slightly out of phase with each other. This method thus yielded two measurements of the acoustic velocity per test. The results were reported to agree with data from literature to within 0.3%, however it was the experience of the author that no further n-hexadecane data at similar test conditions could be found in the literature.

2.2 Measurement of Mass Flow through an Injector

The advantages gained from accurately controlling the quantity of fuel injected with each engine cycle are vast (see Chapter 1) and hence the subject of fuel flow measurement is widely documented and is a high priority for diesel engine researchers.
In 1966 Wilhelm Bosch presented a new method of measuring the quantity of fuel delivered by a fuel injector. The apparatus was termed the 'Bosch Indicator' and, in summary, this method involved connecting the delivery end (nozzle) of the injector to a tube which was pre-filled with fuel, and pressurised in order to simulate in-cylinder back-pressure conditions. Upon injection, a pressure wave was developed in this downstream (measuring) tube and was captured, via a strain gauge, on an oscilloscope. The analysis of this pressure trace allowed Bosch to accurately determine the quantity of fuel injected. In Chapter 3, Wilhelm Bosch's presentation of the Bosch Indicator system (Bosch, 1966) will be discussed in further detail. The flow measurement equipment designed for the purposes of this study was based on Bosch's design; however other methods for fuel flow measurement were investigated and are discussed here.

Thomas Ryan (1996) presented an innovative technique for the measurement of the instantaneous momentum of a fuel jet. The measured fuel jet was impacted on a plate equipped with pressure sensitive Piezo-film as shown in figure 2-6, and the measured momentum changes were then converted into fuel flow measurements. This system lends

itself to the measurement of asymmetries in the injected fuel jets but requires very accurate setup and installation of the Piezo-film in order to obtain accurate flow measurement results.

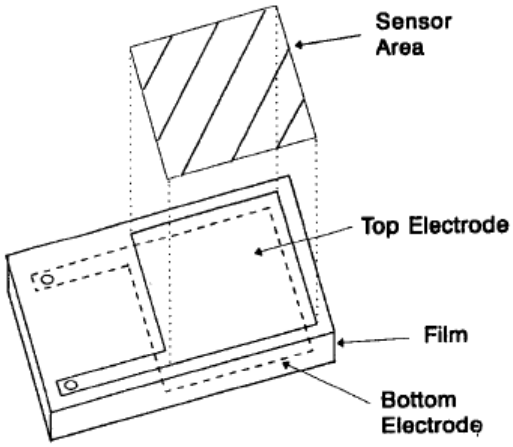

Figure 2- 6. Film sensor arrangement (Ryan, 1996).

Schmid et al (2001) presented a nozzle-integrated fuel flow measurement device based on theory similar to that of a hot-wire anemometer. As a normal hot-wire anemometer would not withstand the high pressures and velocities associated with fuel injection, Schmid's micro-device was fabricated from a ceramic substrate and thin film sensors. The "hot-film anemometer" was used to measure the heat transfer coefficient and hence fuel flow rate. This method required access to machinery necessary for producing micro-machined components and the application of this device was aimed at use for an in-service injector on an operating engine. Although the costs for these sensors were low in terms of mass production, the capital costs for a once-off application could be high in comparison with other flow measurement devices.

W. Zeuch's method is similar in principle to Bosch's design, but differs in that the fuel is injected into a pressurised fuel chamber, as shown in figure 2-7, as opposed to Bosch's pressurised fuel pipe. A highly accurate flow meter is also utilised in this setup for

calibration purposes. The calculation of the injected volume is calculated directly from the following relationship (Ishikawa et al, 2000):

$$\Delta P = \beta \frac{\Delta V}{V} \qquad \text{(Eq 2-4)}$$

Where V is the constant volume of the chamber and β is the bulk modulus of the fuel. Results comparing Bosch's method with Zeuch's method were presented by Takamura et al (1992) and show excellent correlation between the two methods. Zeuch's method requires a slightly more complicated design though, as the volume of the chamber into which the fuel is injected must be adjusted to match the corresponding injection quantity. The reason for this is that, for very small volume injections, the respective pressure rise is very small. Decreasing the chamber volume accordingly increases the pressure rise, which is then easier to measure accurately. The use of a very accurate fuel flow meter also introduces extra costs to the design.

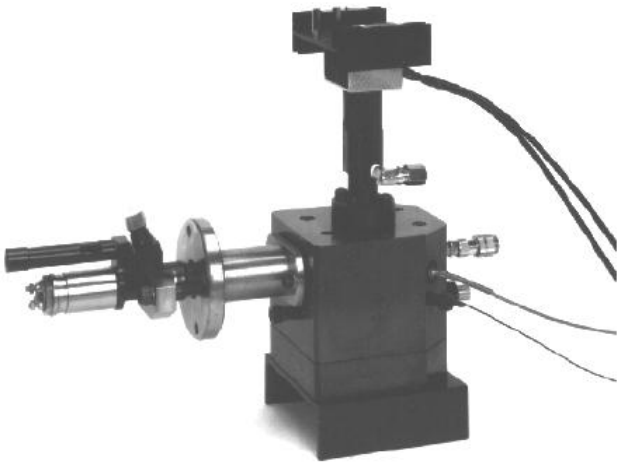

Figure 2- 7. Apparatus as used by Ishikawa et al (2000), Zeuch's method.

Some other approaches to fuel flow measurement have been via the mathematical modelling route. Zhu and Reitz (2000), and Smith and Timoney (1992) present just two of the many cases where an attempt has been made to describe complex fluid behaviour

in fuel injection systems with mathematical modelling. Although these studies produce useful tools for injection and combustion analysis, they are based on assumptions which are not necessarily applicable. Values for physical properties such as bulk modulus, friction factors and heat transfer quantities, which are difficult to measure, are assumed where the researcher lacks any better input. These assumptions naturally introduce inaccuracy of the respective results, as illustrated by figure 2-8. For the purposes of this study, it was decided that real experimental results were required in order to accurately quantify the effects of fuel properties on fuel injection characteristics.

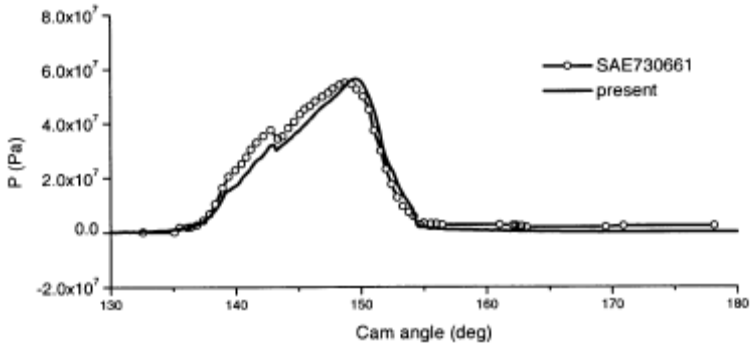

Figure 2- 8. Comparison of modelled results versus actual data (Zhu, 2000)

The advantages of Bosch's design over the above-mentioned alternatives are as follows:

- The Bosch design is simple to implement and is low cost.
- The results from the Bosch method are very accurate; errors within 3-4% were quoted by Bosch.
- Bosch's design has been implemented by a number of other researchers and is a recognized method for measuring fuel flow rate. (Stan, 1999; Benajes et al, 2004; Mulemane et al, 2004)

As already mentioned, the design for the flow measurement equipment used in this study was thus based on Bosch's design.

2.3 The Effects of Fuel Properties on Fuel Injection Characteristics

Based on the guidance of the project supervisor, and on some available literature, the author was able to determine which of the physical properties of a diesel fuel are major factors influencing fuel injection characteristics.

Boudy and Seers (2009) made use of a simulation model (AMESim) to study the effects of biodiesel fuel properties on fuel injection characteristics. They highlighted fuel density, bulk modulus and viscosity as the major factors, and concluded that, in part, the mass flow through an injector is affected by the Reynold's number (See Eq 2-5) of the fuel flow in the injector feed pipe.

Reynold's number (Douglas, Gasiorek, Swaffield, 2001) is defined as:

$$\mathrm{Re} = \frac{\rho v d}{\mu} \qquad \text{(Eq 2-5)}$$

They reported that the friction losses and pressure fluctuations in the injector feed pipe affected fuel flow and that, even though the changes were slight, the density inversely affected the injected mass during single injection events, as seen in figure 2-9.

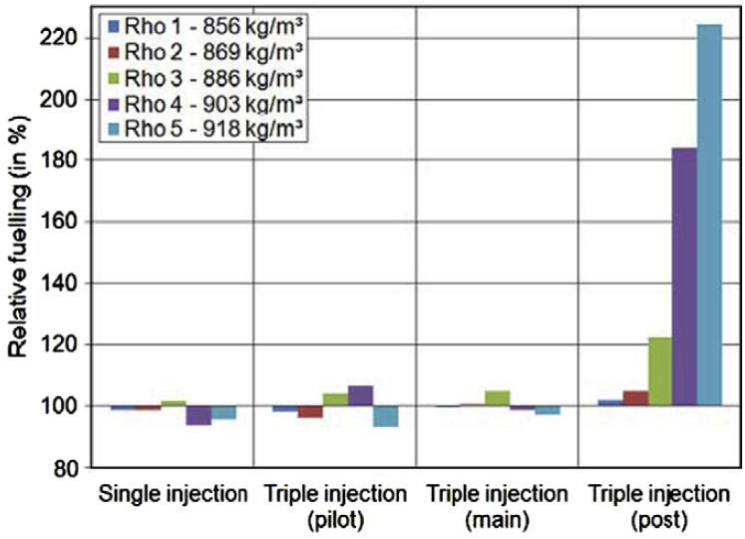

Figure 2- 9. Relative fuelling of diesel fuels with varying densities (Boudy and Seers, 2009)

Boudy and Seers used "relative fuelling" as a means to compare test fuels with a reference fuel. The relative fuelling was a comparison of the actual injected mass quantities when operating with different fuels at the same conditions. The fuel densities indicated in figure 2-9 varied by up to 8.8 % when compared with the reference fuel for the simulations. The largest decrease in relative fuelling for the single injection events appears to be of the order of 5%, but was not explicitly mentioned in the report. Density was reported to be the main factor in affecting the injected mass and, overall, fuel properties were said to make a larger difference when dealing with multiple injection strategies as opposed to single injection strategies.

Increases in fuel dynamic viscosity were also reported to result in an increase in the relative fuelling. Figure 2-10 illustrates that increases in dynamic viscosity of up to 80 % yielded increases in the relative fuelling of up to 2.8 % for single injection events.

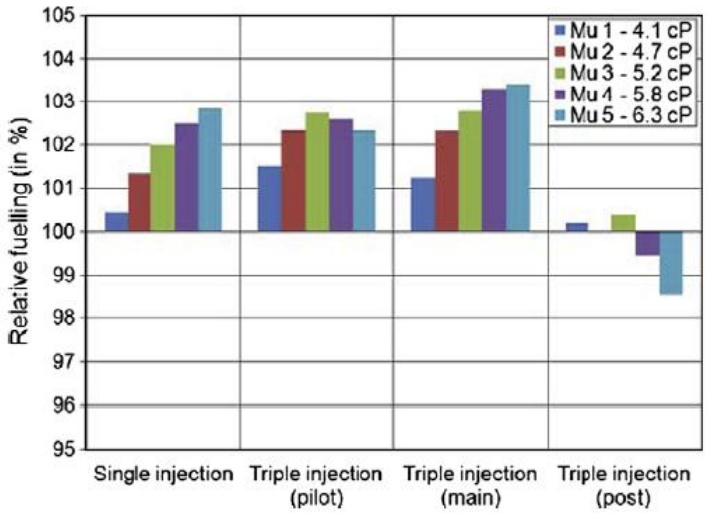

Figure 2- 10. Relative fuelling of diesel fuels with varying viscosities (Boudy and Seers, 2009)

Huhtala and Vilenius (2001) also alluded to the fact that upstream conditions affected fuel flow rates through the injector. They reported that the acoustic velocity of the fuel affected the resonance of the pressure head available at the injector, causing fluctuations

in the injected mass, however they did not provide any compelling data to back up this statement. Factors affecting the injector behaviour also included the length of the fuel supply line and the positioning of the pump supply relative to the injector feed pipe.

Seykens et al (2004) modelled a common rail injection system for heavy duty diesel engines using the AMESim code, and validated the model with experimental results obtained using a Zeuch-type apparatus as shown in figure 2-7. They investigated the influence of fluid properties on the injection process by comparing measurements using diesel to those using Rapeseed oil Methyl Ester (RME). At 20°C, the density of the RME was reported to be 7% higher than that of the diesel, and the kinematic viscosity of the RME 43% higher than that of the diesel. RME was reported to have a mean volumetric injection rate of 6.9% lower than that of the standard diesel as shown by figure 2-11. This translates to the RME having a mean mass injection rate of 0.2% lower than the diesel.

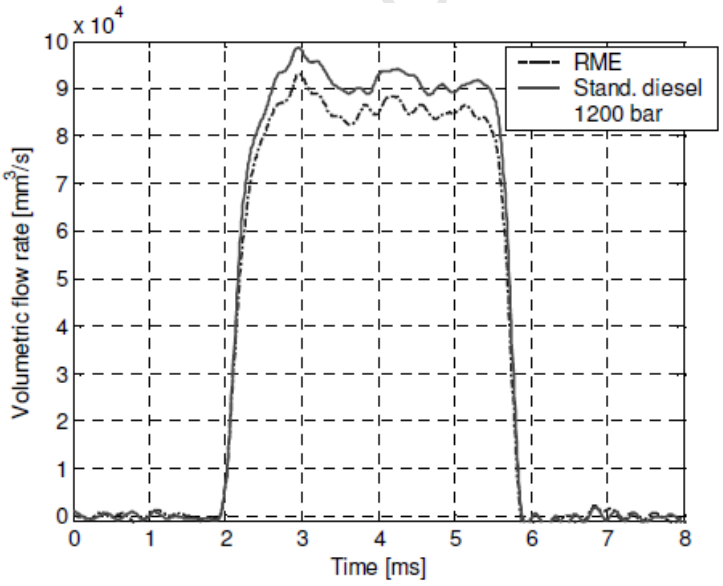

Figure 2- 11. Comparison of volumetric injection rates for RME versus Standard diesel (Seykens et al, 2004)

It was reported that no evidence was found to suggest that diesel properties influenced the timing of the injection events

3. Theoretical Background

3.1 Fuel Property Measurement Theory

As set out in the objectives for this study, it was necessary to accurately measure bulk modulus, density, and acoustic velocity at operating pressures similar to those typical of common rail injection systems. From the review of techniques used in the literature, it was evident that the direct measurement of density and bulk modulus at pressures in this range would not be possible using apparatus similar to that used by Tat and Van Gerpen (2003), or by Szybist et al (2005). These methods were only designed to measure at pressures of up to 345 bar, and 275 bar respectively. A more suitable solution to this problem was to measure the acoustic velocity at the high pressure conditions, and to then mathematically infer the density and bulk modulus properties. To this effect, Jinghong et al (1994) presented the cross-correlation method which infers the fuel density and the combined bulk modulus of the fuel and the pipe material from the acoustic velocity measurement. The mathematical relationships were as follows:

Equation 3-1 describes the effective combined bulk modulus of the fuel and the pipe material at a given pressure (Jinghong et al, 1994),

$$\beta_{ei} = \frac{L^2 \rho_i}{t_i^{\,2}} \qquad \text{(Eq 3-1)}$$

Where 'β_{ei}' is the effective combined bulk modulus of the fuel and the pipe which carries the fuel, 'L' is the length of pipe between the two pressure transducers, 'ρ_i' is the fuel density at the operating pressure and 't_i' is the time taken for the pressure wave to travel between the two transducers at the operating pressure.

Also (Huhtala and Vilenius, 2001),

$$\rho_i = \rho_0 e^{\frac{P_i - P_0}{\beta_{ei}}} \quad \text{(Eq 3-2)}$$

Where 'ρ_0' is the density of the fuel at atmospheric pressure and test temperature, 'P_i' is the operating pressure, and 'P_0' is atmospheric pressure. As seen from equations 3-1 and 3-2, β_{ei} and ρ_i are inter-dependent; therefore it was necessary to iterate in order to obtain the correct values for these variables. This iteration procedure was done using Microsoft Excel® 2003's 'solver' function (making use of a 'quasiNewton' method – [Microsoft Excel® 2003 Help Documentation]). Density values were substituted into equation 3-1, yielding corresponding effective bulk modulus values, which were in turn substituted into equation 3-2. This iterative process continued until the difference between the density value entered into equation 3-1 and the density value yielded by equation 3-2 was negligible. The relationship between density, effective bulk modulus, and acoustic velocity is as follows (Jinghong et al, 1994):

$$c = \sqrt{\frac{\beta_{ei}}{\rho_i}} \quad \text{(Eq 3-3)}$$

In order to quantitatively compare different fuels, the bulk modulus of each fuel itself must be known. Therefore it was necessary to separate out the bulk modulus of the fuel from the bulk modulus of the pipe material as follows: (Watton, 1989)

$$\beta_{Pipe} = \frac{1}{\frac{2}{E_{Pipe}}\left(\frac{d_{in}^2 + d_{out}^2}{d_{out}^2 - d_{in}^2} + \mu_P\right)} \quad \text{(Eq 3-4)}$$

Where 'E_{Pipe}' is the elastic modulus of the pipe material, 'd_{in}' is the inner diameter of the pipe, 'd_{out}' is the outer diameter of the pipe, and 'μ_P' is Poisson's ratio for the pipe material.

Also,

$$\beta_{Fluid} = \frac{1}{\frac{1}{\beta_{ei}} - \left(\frac{V_{Pipe}}{V_{Tot}\beta_{Pipe}} \right)} \qquad \text{(Eq 3-5)}$$

Where 'V_{Pipe}' is the volume of the pipe material, and 'V_{Tot}' is the total volume.

After solving for the relevant fuel properties by direct measurement and the use of the above formulae, the next step in the investigation was to quantify their effects on the injection characteristics. Understanding and quantifying these effects would require a good knowledge of the way in which a common rail injector functions, as well as accurate measurement of the flow through the injector.

3.2 Operating Principles of a Bosch Common Rail Injection System

The first injection system used in this study was a 2002 Bosch common rail diesel injection system. In order to aid the reader in understanding and appreciating the work covered in this report, here follows a detailed description of the principles of operation for this injection system. Figure 3-1 shows the detail of the common rail injector.

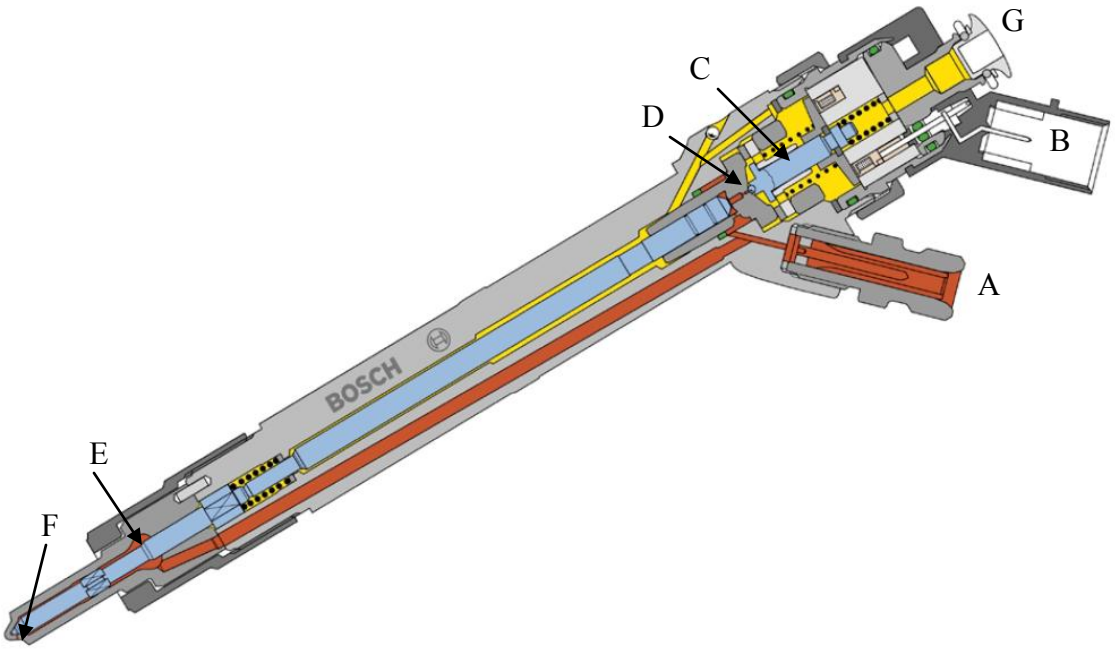

Figure 3- 1. Section showing Bosch common rail diesel injector detail (Schommers et al, 2000)

The high pressure diesel pump supplies fuel at the operating pressure to point 'A' on the injector, and the path taken by the fuel internally is shown by the red areas in the figure. In the injector's closed state, the resultant force acting on the blue needle 'E' is holding the needle down against the sealing face at 'F'. This resultant force comprises forces due to hydraulic pressure on the needle ends, and the spring force acting on the needle body. When the injector is required to open, the engine's ECU sends a signal to point 'B', actuating the solenoid. The riser at 'C' then lifts from its seat, allowing the fuel in the small chamber above the needle to flow through a channel ('D'). The release of this fuel above the needle results in a pressure drop at this point, and hence the resultant force on the blue needle changes, causing it to lift from its sealing face at 'F'. At this point, fuel flows through the injector nozzle and into the combustion chamber. When the injector is required to close again, the ECU de-actuates the solenoid, closing the riser 'C' against its seat again. Fuel in the small chamber above the needle builds pressure again and the balance of forces on the needle reverts again to the closed state. During this process, the small quantity of fuel released at 'D' for each injection leaves the injector body at 'G' and is returned to the vehicle's fuel tank.

The second injection system used in this study was a 2007 Bosch piezo-type common rail injection system. The difference between this injection system and the previous system lies in the fuel injector unit. Although the principle of hydraulic actuation remains, where the previous system used an injector which was controlled via a solenoid, the piezo-type system used a piezo-actuator module to control the injector. The piezo-type injector was also re-designed so that the main moving parts had a much lower mass. This lower inertia design, coupled with the piezo-actuator (which responds much faster than the solenoid) enables the piezo-type injector to be capable of up to five injection events per engine cycle. A disadvantage of employing the use of the piezo type injectors is that they are significantly more expensive than the solenoid type.

3.3 Fuel Flow Rate Measurement Theory

Wilhelm Bosch published a paper in 1966 detailing the design and theory behind the Bosch Fuel Rate Indicator system for the characterisation of individual fuel injections. The basic concept was to inject fuel into a pipe (from here on referred to as the 'measuring tube') already containing fuel at a pre-determined back pressure. This back pressure served the purpose of simulating pre-injection in-cylinder conditions in a diesel engine. The values quoted by Bosch for this back pressure ranged from 0 bar to 50 bar. The injection of fuel into the measuring tube set up a pressure wave described by equation 3-6 (Bosch, 1966):

$$dP = c\rho du \qquad \text{(Eq 3-6)}$$

Where 'dP' is the incremental pressure rise in the measuring tube, 'c' is the acoustic velocity of the fuel, 'ρ' is the density of the fuel, and 'du' is the corresponding velocity increase of the flow in the measuring tube.

With the use of the continuity equation, Bosch went on to show that the volume injected per unit time can be calculated as shown in equation 3-7:

$$\frac{dq}{dt} = \frac{A}{c\rho} P \qquad \text{(Eq 3-7)}$$

Where A is the internal flow area of the measuring tube.

When equation 3-7 is integrated over the entire injection duration, the total volume injected per stroke can be calculated:

$$Q = \frac{A}{c\rho} \int_{t_0}^{t} P dt \qquad \text{(Eq 3-8)}$$

Another consideration in the design of the Bosch Indicator was to enable continuous operation such that the pressure wave set up by injection event number N did not reflect back in the measuring tube and cause interference with the pressure wave set up by injection event number N+1. The original Bosch design solved this problem with the use of an orifice plate downstream of the point of injection. This orifice plate assisted in the decay of the pressure waves set up by each injection event. The length of the measuring tube was also matched to the frequency of the injections and their respective reflections for different simulated engine speeds. In the current study however, the measuring tube was simply lengthened and the losses due to pipe wall friction ensured that the pressure waves decayed completely before returning to the point of injection.

4. Design of Equipment and Methodology

For this study it was necessary to design and manufacture equipment for the measurement of the physical properties and flow properties of diesel at typical common rail operating pressures. The equipment and experimental procedures are detailed in this chapter.

4.1 Acoustic Velocity Measurement Equipment

For the most part, the experimental setup for the measurement of acoustic velocity was the same as the setup used for the injector flow tests. In order to increase the accuracy of the results from these tests however, the pressure was generated by a calibrated dead-weight tester shown in figure 4-1, conventionally used for calibrating pressure transducers. The dead weight tester provided a constant and accurately known pressure upstream of the fuel injector, as opposed to the fluctuating pressure provided by the high pressure pump. The use of the dead weight tester also significantly lowered the volume of fuel required for the tests. This was particularly important when testing a very costly substance such as n-hexadecane.

Figure 4- 1. Dead weight tester.

The pressure in the dead weight tester line was transmitted to the fuel line by means of a sliding piston device shown below in figure 4.2.

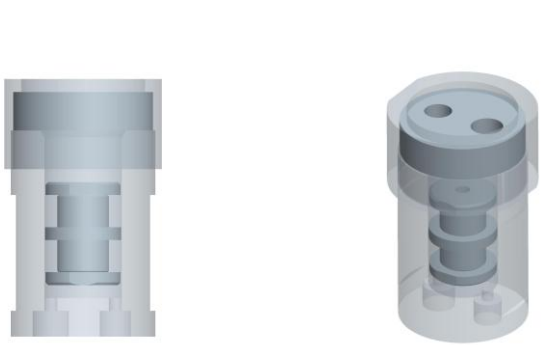

Figure 4- 2. 3-D CAD models of the sliding piston pressure transmitter.

The purpose of this device was to successfully transmit the pressure from the dead weight tester to the fuel line on the test rig without allowing the dead-weight tester's hydraulic oil to contaminate the test fuel in the fuel-line. The lack of a differential pressure between the two ends of the piston ensured that there was no leakage across the piston. Figure 4-3 illustrates the layout of the apparatus for measuring acoustic velocity:

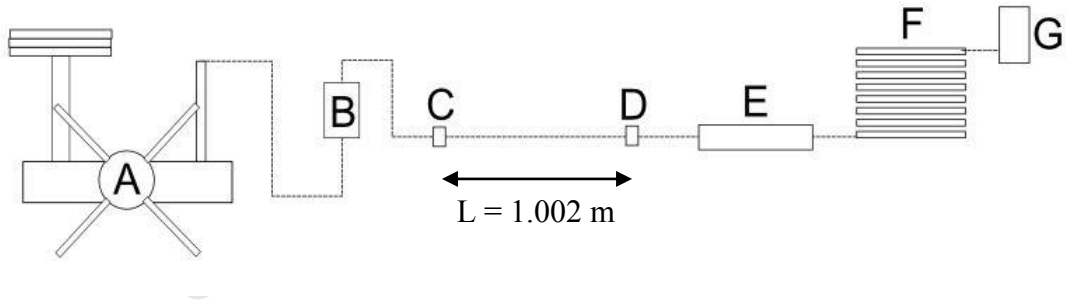

Figure 4- 3. Schematic of the apparatus layout.

Referring to figure 4-3, the dead weight tester (A) delivered oil at a known pressure to the pressure transmitter (B). This pressure was then transferred directly to the fuel in the pipe between 'B' and the injector holder (E). Two in-line pressure transducers were installed at 'C' and 'D', the distance between these transducers was 1.002 m. The downstream side of the injector holder was connected to the measuring tube (F), and finally, to the pressure regulating valve at 'G'.

4.2 Acoustic Velocity Measurement Procedure

The principle behind this experiment was to trigger a single injection event in the fuel injector, the effect of which was to cause a pressure disturbance upstream of the injector. The time taken for this disturbance to travel between the two in-line pressure transducers ('C' and 'D' in Figure 4-3) was then measured, giving the acoustic velocity of the fuel at the test pressure.

The solenoid injector was not suitable for the acoustic velocity tests as it displayed leakage of fuel back to the fuel tank when not operating. This was not suitable as it would result in loss of the pressure built up by the dead-weight tester. The Piezo injector on the other hand, did not display any leakage of fuel back to the fuel tank when not operating, and was thus suitable for this setup.

As previously mentioned, due to the pronounced effect of temperature on fuel density, it was necessary to exercise accurate temperature control on the fuels throughout all experimentation in this study. The temperature was thus controlled by heating the length of the fuel line between 'B' and 'E' in figure 4-3 with an electric heating element wrapped around the exterior of the pipe. The fuel line heating element was set to 80°C, resulting in the fuel heating up to approximately 56°C.

These tests were run at 5 different pressures and results were repeated 5 times for each test pressure, although at pressures near 1000 bar, the sliding piston device displayed some fuel leakage and as such limited data points were obtained near this pressure. The liquid used for verification of the acoustic velocity tests was n-hexadecane. The results from this investigation were compared to available acoustic velocity, density and bulk modulus data for n-hexadecane at similar pressures. Thereafter, EN590 and the GTL were tested.

The captured traces for each of the two pressure sensors were plotted on the same time axis and, in the same manner as displayed by Huhtala and Vilenius (2001), the time

differential between major curve features was calculated. The measurement of this time delay was conducted visually using cursors on the plot of the captured traces. Knowing the distance between the two transducers, it was then simple to calculate the acoustic velocity for each fuel at the different test pressures. This value of acoustic velocity was then used to derive bulk modulus and fuel density using the cross-correlation method as described in Chapter 3.

4.3 Mass Flow Measurement Equipment

As mentioned in chapter 2, the author opted to use the Bosch method for flow measurement through the fuel injector. A CAD model of the apparatus used in this study is shown below in Figure 4-4; the design of this apparatus was mostly based on Bosch's original design.

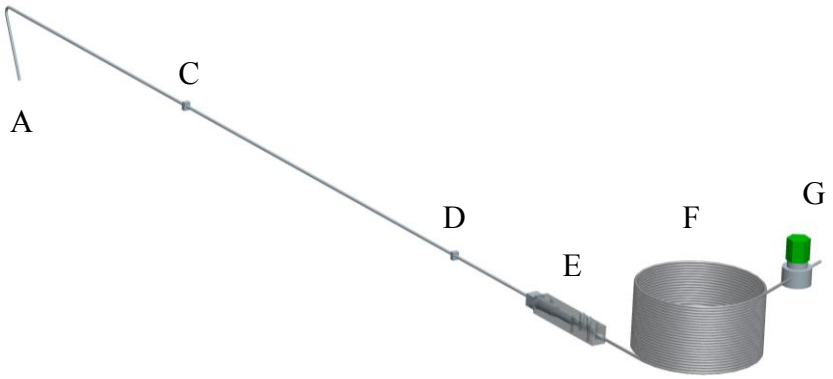

Figure 4- 4. CAD model of the apparatus layout.

The high pressure diesel pump in figure 4-5a supplied the common rail in figure 4-5b with fuel at the test pressure. The common rail is normally intended to supply fuel to 4 injectors in a vehicle, and thus has 4 tapping points along its length. For the purposes of the tests in this study, 3 of these tapping points were plugged and the 4th point was connected to the fuel line at 'A' in figure 4-4. The two pressure transducers installed along the length of the fuel line at 'C' and 'D' were used to monitor the upstream fuel pressure during testing. The fuel line supplied fuel to the injector which was housed

inside the machined casing 'E'. Downstream of the injector, the fuel entered the measuring tube 'F'. The pressure in this tube coil was accurately controlled by the regulating valve 'G'. The set point for the back pressure was 80 bar. After passing through the regulating valve, the fuel from each test was collected in a glass beaker. The fuel collected was then weighed, as shown in figure 4-6, and the mass of the collected fuel was used to calibrate each test.

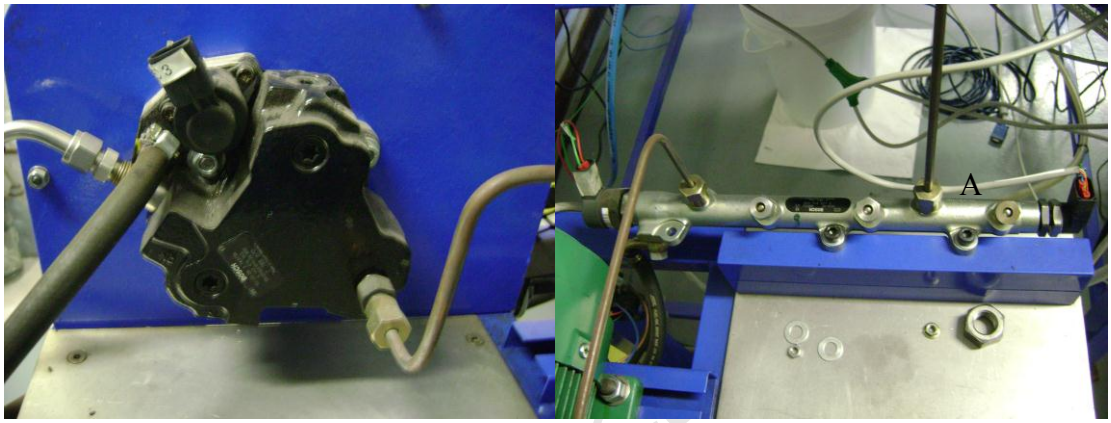

(a) High pressure diesel pump **(b) Common rail**

Figure 4- 5. High pressure supply system for the fuel injector.

Figure 4- 6. Weighing of the fuel to calibrate each flow test.

The machined casing for the fuel injector shown in figure 4-7 had two ports, 'G' and 'H', tapped into the downstream section for the installation of pressure transducers. Initially it was thought that two different pressure sensors with different operating ranges and different sensitivities might be required in order to successfully capture both main and pilot injection events. It was however later discovered that just one pressure sensor was necessary and thus the second port was plugged. The pressure sensor used was an AVL 0-200 bar Piezo-electric pressure sensor. (GM12D)

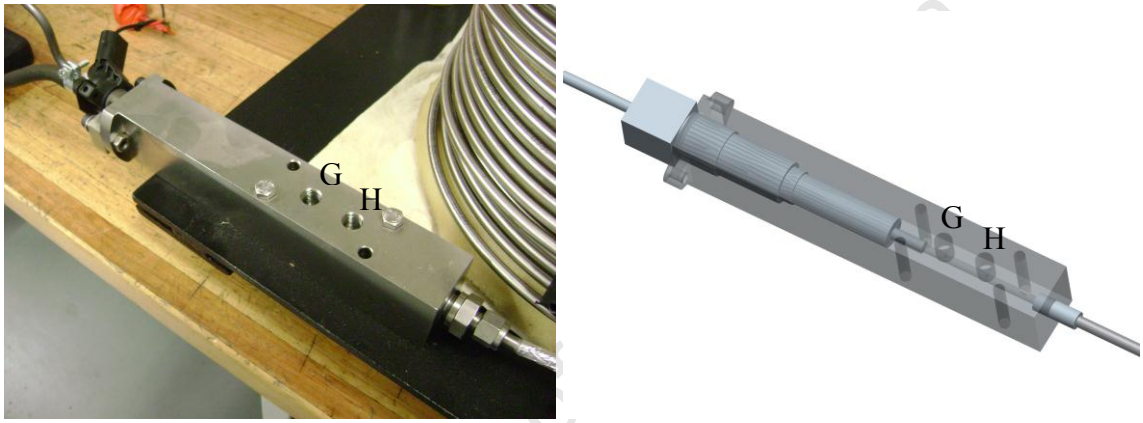

(a) Casing with pressure sensor ports. **(b) Transparent 3-D CAD model of casing.**

Figure 4- 7. Machined injector casing.

In W.Bosch's original design of the indicator system, he included two sets of tubes downstream of the fuel injector. The first tube was the measuring tube in which the pressure rise due to each injection event was measured. The second tube was connected to the first via an orifice plate and the purpose of this was to dissipate the pressure signals caused by each injection event. In the current study, the author altered this design slightly by doing away with the orifice plate and the second tube. The first tube was simply made much longer than in Bosch's design, as seen in figure 4-8, and the pressure signal from each injection event dissipated sufficiently before reflecting back to the point where it originated.

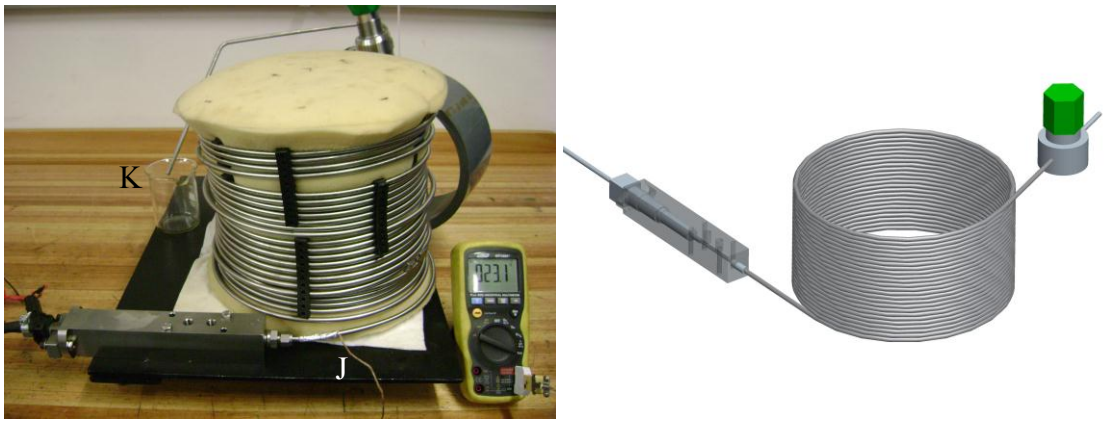

(a) Measuring tube with thermocouple probe. **(b) 3-D CAD model of the measuring tube.**

Figure 4- 8. Long measuring tube downstream of the injector

As shown in Figure 4-8a above, a thermocouple was placed downstream of the injector at 'J' to monitor the fuel temperature in the measuring tube. The beaker for collecting the fuel from each test was placed at 'K'.

Lastly, for the tests with the Piezo-type fuel injector, a back pressure of 10 bar was needed in the injector's fuel return line in order for the injector to function properly. This was implemented as shown in Figure 4-9.

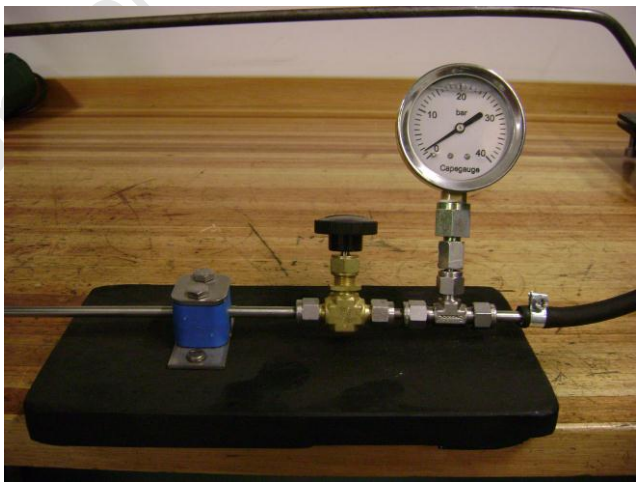

Figure 4- 9. Needle valve and pressure gauge on piezo injector's return line.

4.4 Mass Flow Measurement Procedure

Before each set of flow tests, the fuel system was cleaned and primed with a fresh drum of the required fuel, shown in figure 4-10. This cleaning process included draining all the pumps, valves and pipes, and then running some of the new fuel through the system to wash out any residue left by the previous fuel. Once the system was ready, the high pressure pump and the injector were left to run continuously for about 30 minutes at full load in order to allow the fuel in the drum to reach a stable temperature (approximately 60°C). The fuel exiting the measuring tube was re-circulated back into the fuel drum. This helped to eliminate errors in the test results caused by temperature fluctuations in the fuel. The heating element on the fuel line was also set to 80°C which, depending on the injection pressure set point, resulted in the fuel temperature stabilising at between 56°C and 65°C just upstream of the injector. This temperature measurement was taken using the temperature function on the piezo-resistive sensor installed on the fuel line upstream of the fuel injector (At 'D' in Figure 4-4). This sensor was a Kistler 4067A model.

Figure 4- 10. Drums supplying fuel to the high pressure pump.

The injectors used in this study were controlled via a PC, and a National Instruments® Compact-RIO FPGA controller. The software and injector driver modules used to control

the injectors were developed by Drivven USA. The PC interface is shown below in Figure 4-11.

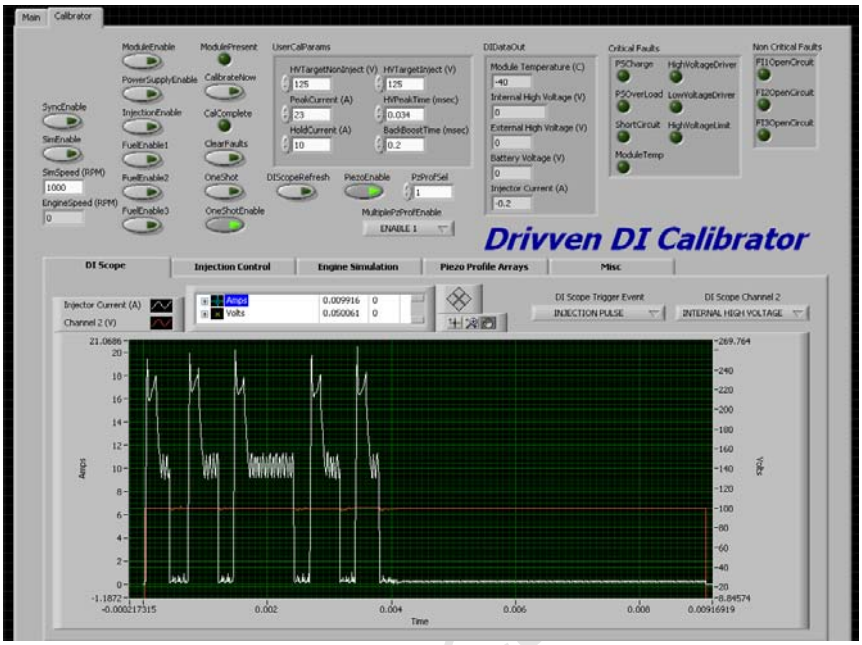

Figure 4- 11. Screenshot of the Drivven GUI for controlling the injectors.

This commercial product is intended for injector calibration purposes, however it provided sufficient functionality for the purposes of the study, including full injector parameter control, and compatibility with both solenoid and piezo-type injectors. The Drivven software for the injector control (shown in figure 4-11) and the software used to control the common rail system was all developed on a LabVIEW platform. The common rail pressure was also controlled via the LabVIEW interface, with a simple duty-cycle function being linked to the rail pressure relief valve. The LabVIEW code for controlling the common rail system and the rail pressure relief valve was developed by Geoff Miller, a previous M.Sc. student with the Sasol Advanced Fuels Laboratory (SAFL). Significant modifications to this LabVIEW code were made by Mark Wattrus, also a student with the SAFL.

The flow tests for each fuel were performed at 4 different injection pressures, and 9 different injection pulse-widths. At each combination of pressure and pulse-width, a set of 1000 injection events was recorded, with the pressure trace from each injection event

being captured and time-averaged on a digital oscilloscope. This averaging function was a feature of the digital oscilloscope which calculated and output the mean pressure trace over the test period. This function did not, however, allow for the capture of each individual pressure trace, and therefore it was this averaged signal which was the input for the calculation of the mass flow rate and total injected mass. As previously mentioned, for each set of 1000 injections, the fuel exiting the measuring tube was collected in a glass beaker and weighed as in figure 4-6. This mass measurement was then used to calibrate the calculations.

The fuel mass flow rate tests were conducted at a simulated engine speed of 1000 rpm. The system was set up as a four-stroke engine, and so this translated to 500 injections per minute. This was done in order to eliminate some of the fluctuations in upstream pressure delivery from the high pressure pump and the common rail. As mentioned earlier, the back pressure used to simulate in-cylinder conditions was set to 80 bar. Although Wilhelm Bosch (1966) used a back pressure of the order of 40 bar in his presentation of the Bosch indicator, it was decided that an in cylinder pressure of 80 bar would be a better representation of modern diesel engine conditions. Other studies from literature have used back pressures of up to 100 bar (Bianchi et al, 2003) and even up to 180 bar. (Desantes et al, 2005).

During each test, the average fuel temperature downstream of the injector was measured. Changes in this temperature reflected the corresponding density changes of the fuel downstream, and thus the appropriate factors were also included in the calculation stages.

5. Results

The results generated in the testing stages of this study are laid out in this chapter. The key trends and characteristics illustrated here with graphs and tables, and statistical analyses will be discussed further in chapter 6.

As previously mentioned, the two diesel fuels used for investigation in this study were as follows:

1. European reference diesel fuel EN590.
2. Test diesel fuel derived from natural gas (GTL).

Properties for these fuels are tabulated in Appendix A.

5.1. Fuel Property Results

The experimental determination of acoustic velocity played an integral part in characterizing the different diesel fuels. The experimental method thus required validation. N-hexadecane was used as a reference fuel, and the experimental data was then compared with existing n-hexadecane data taken from literature.

The acoustic velocity data for each of the fuels in this study was measured by dividing the distance between the two pressure sensors by the time taken for the pressure wave to travel between them. This time difference was measured as shown in figure 5-1 below.

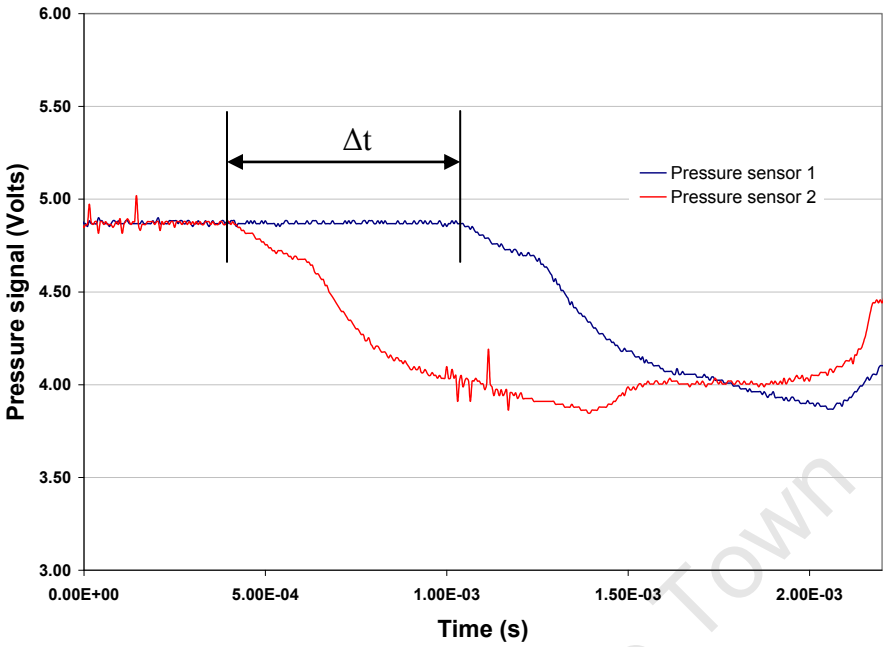

Figure 5- 1. Pressure signals for acoustic velocity measurement.

Acoustic velocity data was collected at five different pressures, with five repeat tests being conducted at each pressure. The data presented here is the averaged data for each operating point. The variability of the acoustic velocity data is illustrated in figure 5-2 by the uncertainty band symbols. (I). Two standard deviations (±2σ) have been indicated at each test point, representing the area within which 95% of test results would fall. From here on, the same standard of ±2σ will be used to indicate variability in graphs where it is applicable. A full set of the captured and inferred fuel data is presented in Appendix A.

Ball and Trusler (2001) presented data for the acoustic velocity of n-hexadecane at various pressures and temperatures. Figure 5-2 includes plots of this data against the acoustic velocity data from this study.

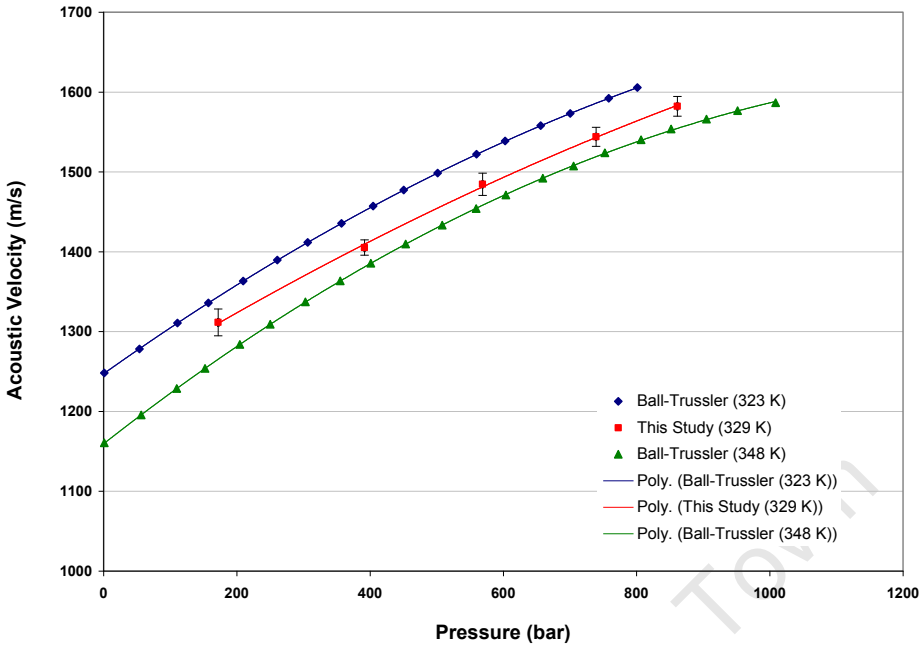

Figure 5- 2. Acoustic velocity data for n-hexadecane at various pressures and temperatures.

After measuring the acoustic velocity, density and bulk modulus values were inferred using the cross-correlation method as described in chapter 3. The density data for n-hexadecane taken from literature did not cover the exact operating points as covered in this study. The German Association for Petroleum Sciences and Coal Chemistry (DGMK-project 4510, 1976) tested n-hexadecane at various pressures and a fixed temperature of 25°C, while Cerdeirina et al (2001) tested n-hexadecane at various temperatures and at fixed atmospheric pressure. It was thus necessary to use the findings presented by these authors to generate data in the range required for this study, and against which the author's data was compared. This hexadecane data was generated using a statistical regression.

The regression used the following empirical relationship for n-hexadecane:

$$\rho_R = 748.9 + 0.3483(P_R - 1)^{0.5} + 0.0413(P_R - 1) - 0.6777(T_R - 329) \qquad \text{(Eq 5-1)}$$

Where

ρ is the density in (kg/m^3),

P is the test pressure in the supply rail (bar), and

T is the test temperature in (Kelvin).

Although the regression equation form had no physical basis, it was a very good fit to the data from literature, and had a coefficient of determination (R^2) of 0.999. It should be noted that extrapolation of data using this relationship is not advisable for temperature ranges far beyond those upon which the relationship was based.

Table 5-1 shows a comparison of the regression data with the data taken from literature.

Table 5- 1. Literature data for n-hexadecane density at various temperatures and pressures.

Test Pressure	Test Temperature	Data from Literature [a]	Regression Data	Error
(bar)	(K)	(kg/m^3)	(kg/m^3)	%
1	298.15	769.94	769.80	-0.02
1	313.15	759.50	759.62	0.02
1	333.15	746.10	746.05	-0.01
196	298.15	782.20	782.58	0.05
294	298.15	787.80	787.80	0.00
392	298.15	793.10	792.85	-0.03
588	298.15	803.00	802.64	-0.04
784	298.15	811.90	812.18	0.03
882	298.15	816.20	816.21	0.00

[a] Data taken from DGMK Project-4510 (1976) and Cerdeirina et al (2001)

The density data for n-hexadecane obtained from the cross-correlation method (discussed in section 3.1) is compared to the regression data in figure 5-3:

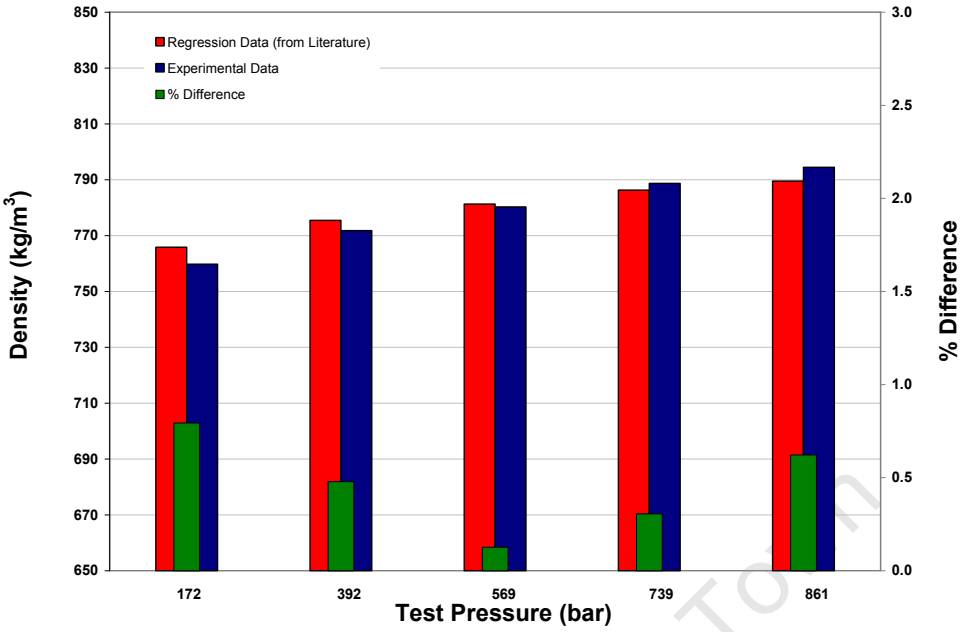

Figure 5- 3. Experimental and Regression data for n-hexadecane density.

The inferred bulk modulus values for n-hexadecane are shown against the DGMK's data in figure 5-4.

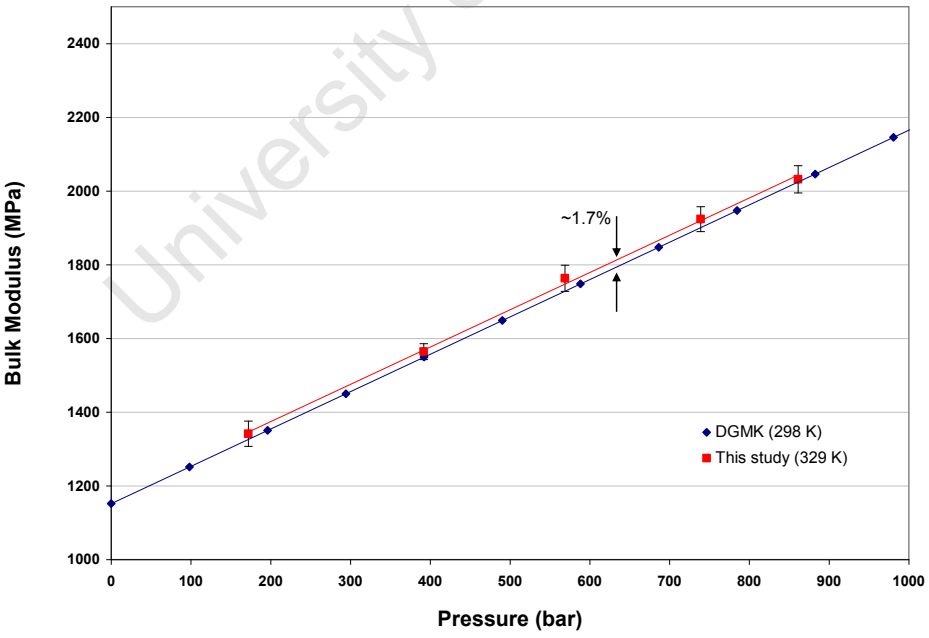

Figure 5- 4. Bulk modulus vs pressure values for n-Hexadecane.

Having tested the properties of n-hexadecane, and proven that the methodology produces results which compare well with the literature, the next procedure was to measure the physical properties for the GTL, and for EN590. The acoustic velocities for these fuels were measured under the same conditions as for n-hexadecane above, and the results are shown in figure 5-5:

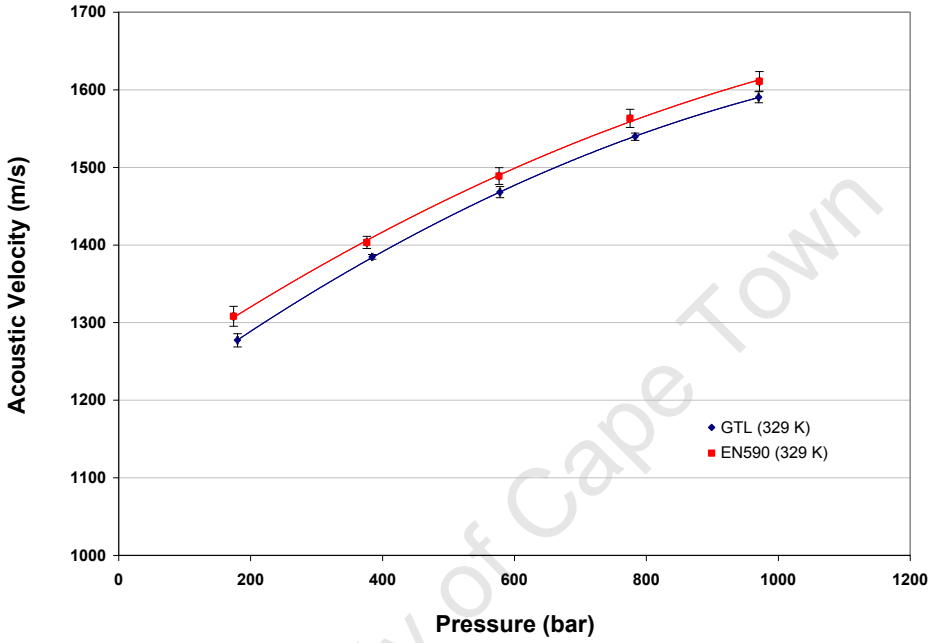

Figure 5- 5. Acoustic velocity data for diesel fuels at various pressures.

The density data for the GTL and for EN590 were as follows:

Table 5- 2. Experimental data for GTL densities at various pressures.

Test Pressure	Test Temperature	GTL
(bar)	(K)	(kg/m^3)
180	329	749
384	329	758
578	329	765
783	329	771
970	329	776

Table 5- 3. Experimental data for EN590 densities at various pressures.

Test Pressure	Test Temperature	EN590
(bar)	(K)	(kg/m^3)
174	329	813
376	329	822
577	329	829
775	329	834
971	329	840

Empirical relationships for the density, pressure and temperatures of GTL and EN590 were now required, however in the absence of any significant temperature variation over the experimental data set, it was necessary to make use of the temperature coefficient from equation 5-1. This was considered to be a close-enough value based on the fact that n-hexadecane is a major component of the diesel fuels. The resulting relationships were as follows,

For GTL:

$$\rho_R = 732.4 + 1.139(P_R - 1)^{0.5} + 0.0081(P_R - 1) - 0.6777(T_R - 329) \qquad \text{(Eq 5-2)}$$

For EN590:

$$\rho_R = 796.9 + 1.122(P_R - 1)^{0.5} + 0.0083(P_R - 1) - 0.6777(T_R - 329) \qquad \text{(Eq 5-3)}$$

Where

ρ_R is the density in (kg/m^3),

P_R is the test pressure in (bar), and

T_R is the test temperature in (Kelvin).

The coefficients of determination (R^2) for equations 5-2 and 5-3 were both 0.999.

The inferred density and bulk modulus data (using equations 3-1 through 3-5) is presented graphically in figures 5-6 and 5-7. No variability is indicated in these figures,

as the magnitude of the standard deviation is negligible in comparison to the presented values. This illustrates that the density and bulk modulus values inferred via the cross-correlation method display a lack of sensitivity to slight variations in the acoustic velocity data.

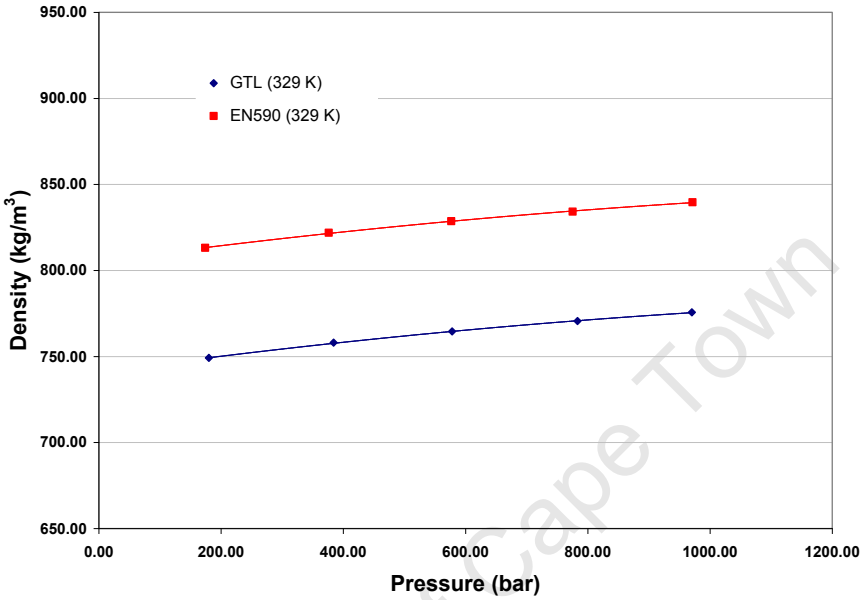

Figure 5- 6. Density data for diesel fuels at various pressures and constant temperature of 329 K.

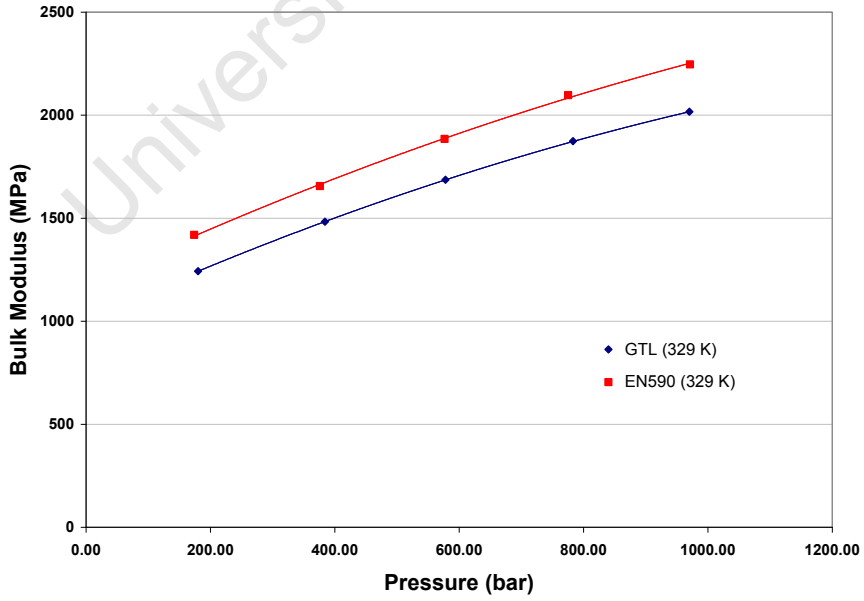

Figure 5- 7. Bulk modulus data for diesel fuels at various pressures and constant temperature of 329 K.

5.2. Injector Mass Flow Results

Flow Measurement Calibration

As described in chapter 4, the injector flow rate measurements were calibrated against the mass of the fuel collected in the beaker after each test. This calibration was carried out by scaling the Y-axis of the pressure-time plots. A typical calibration is illustrated by figure 5-8 below:

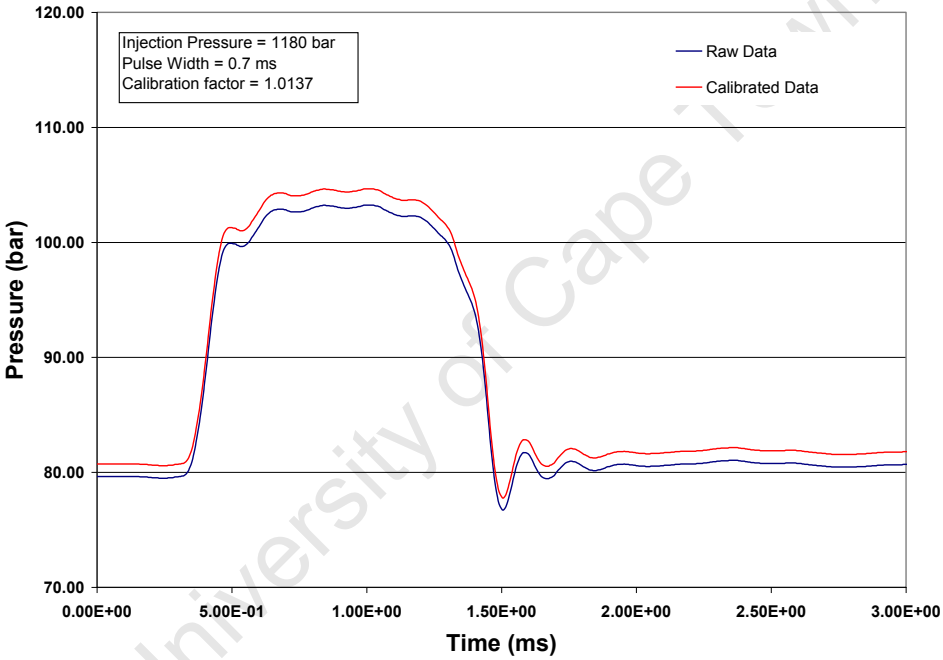

Figure 5- 8. Calibration of the pressure trace for GTL in the Solenoid injector.

The maximum, minimum, and average calibration factors (CF) for the tests performed in this study are summarized below in table 5-4, where the average factor is calculated as the average deviation from a factor of 1:

$$CF_{AVG} = \frac{\sum_{0}^{n} |1 - CF_n|}{n} \qquad \text{(Eq 5-4)}$$

Table 5- 4. Calibration factors for the injector flow measurements performed in this study.

	GTL in the Solenoid injector	EN590 in the solenoid injector	GTL in the piezo injector	EN590 in the piezo injector
Maximum Calibration Factor	1.0248	1.0492	1.0336	1.0602
Minimum Calibration Factor	0.9935	0.9234	0.9852	0.9562
Average Calibration factor	0.0063	0.0272	0.0095	0.0370

Solenoid Injector Results

The first tests for both fuels were performed using the solenoid injector. The mass flow through the injector unit was measured at injection pressure set points of 600, 800, 1000, and 1200 bar. The pulse widths used for the tests were 0.2, 0.3, 0.4, 0.5, 0.7, 0.9, 1.1, 1.3, and 1.5 ms. These test conditions were chosen to represent the typical operating range of the injector under normal engine operation. The plots that follow are the flow curves which were captured at each set of conditions. The set points for injection pressure and pulse width are indicated by the legends, however the plots themselves indicate the actual flow duration.

Figures 5-9 through 5-12 below illustrate the injection rate shape curves for the GTL diesel in the solenoid injector at each test pressure.

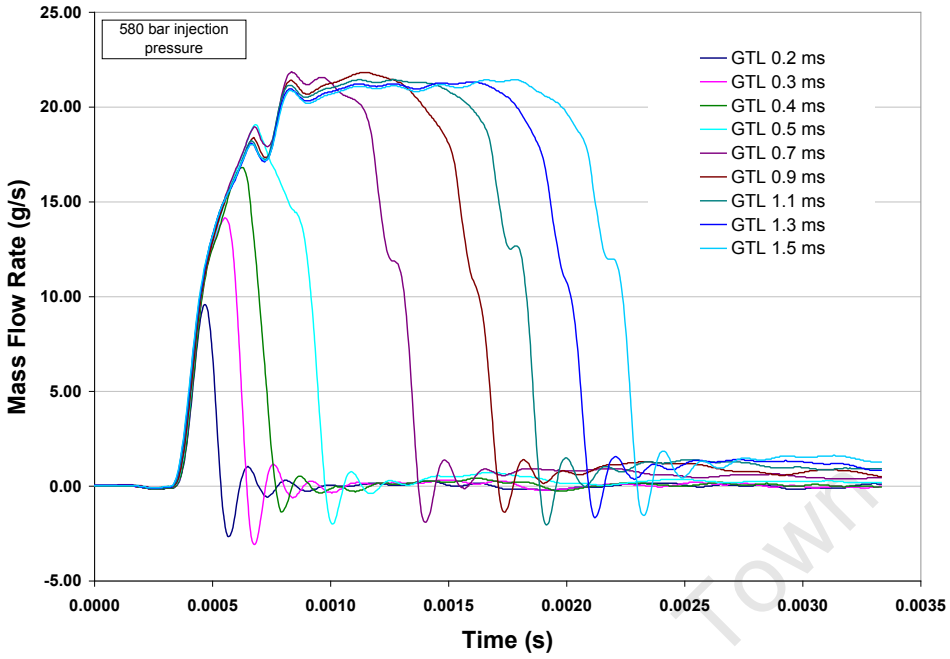

Figure 5- 9. Injection rate shape curves for the GTL in a solenoid injector at 580 bar.

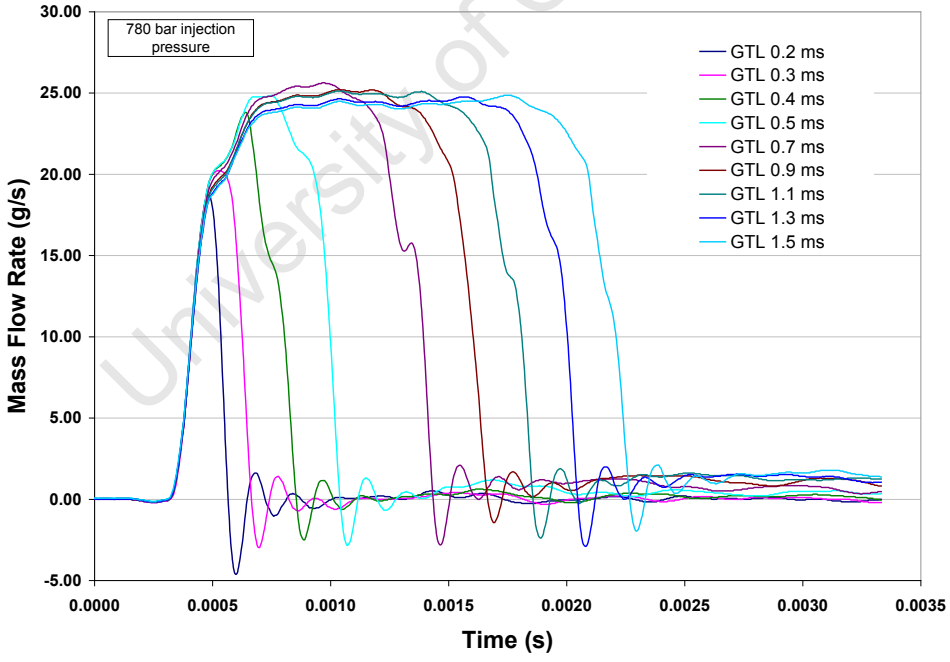

Figure 5- 10. Injection rate shape curves for the GTL in a solenoid injector at 780 bar.

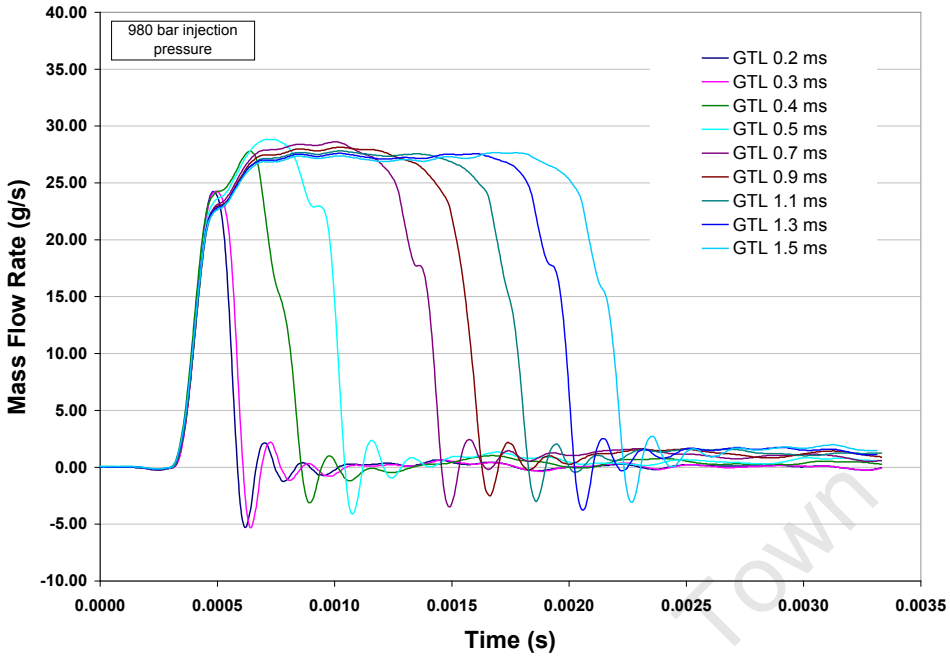

Figure 5- 11. Injection rate shape curves for the GTL in a solenoid injector at 980 bar.

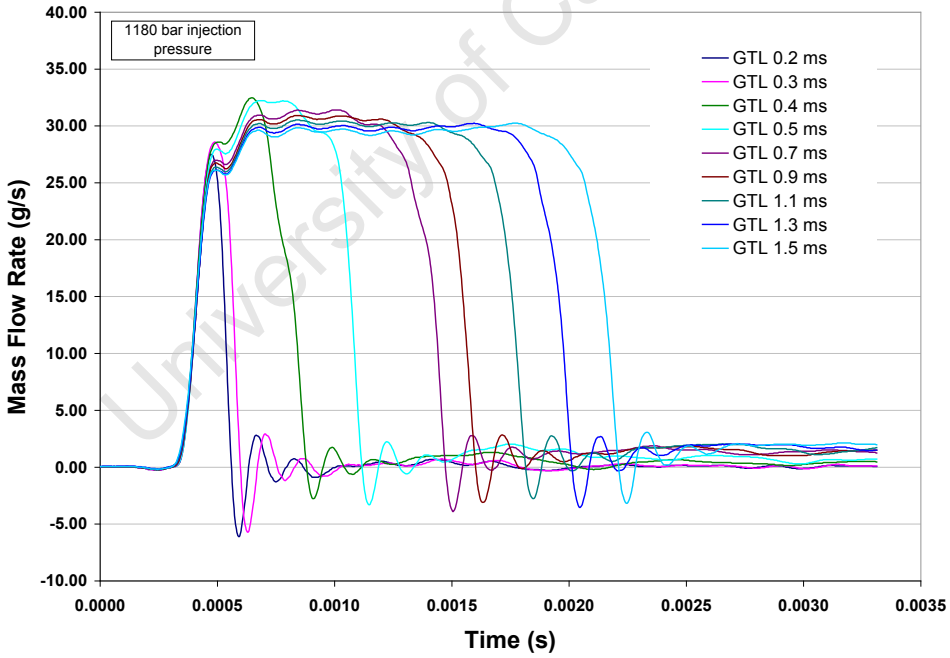

Figure 5- 12. Injection rate shape curves for the GTL in a solenoid injector at 1180 bar.

The pulse width of an injection event is the duration of the energising signal sent by the ECU to the injector. The flow duration however, was deemed to be the time between the first rise in the flow rate, and the end of the main flow event (where the flow curve crossed the zero line). As illustrated in figure 5-13, the flow duration was not equal to the pulse width:

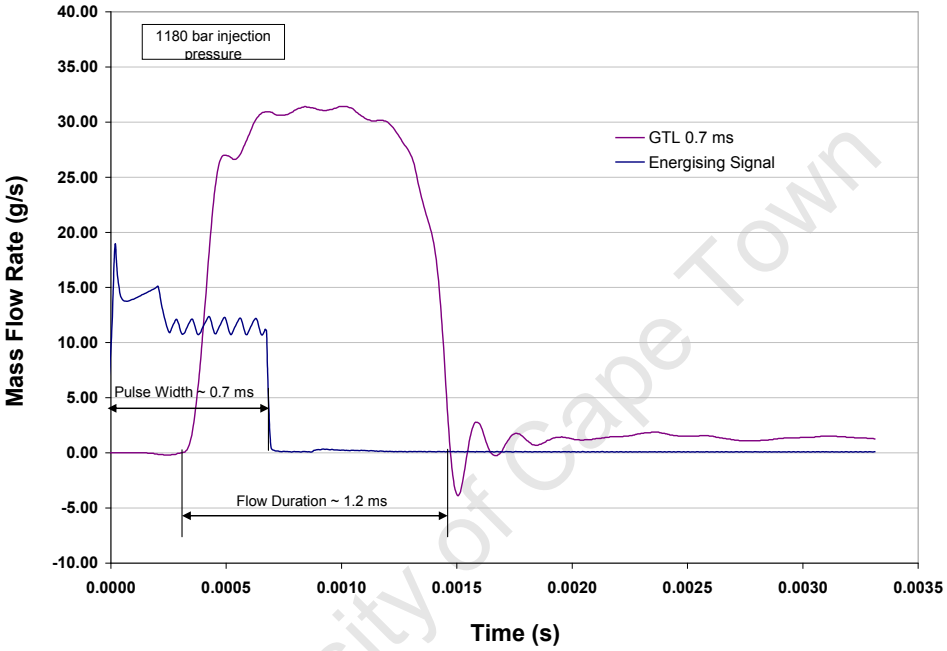

Figure 5- 13. Illustration of the flow duration measurement.

The mass flow of GTL through the solenoid injector at various injection pressures and flow durations is shown in figure 5-14.

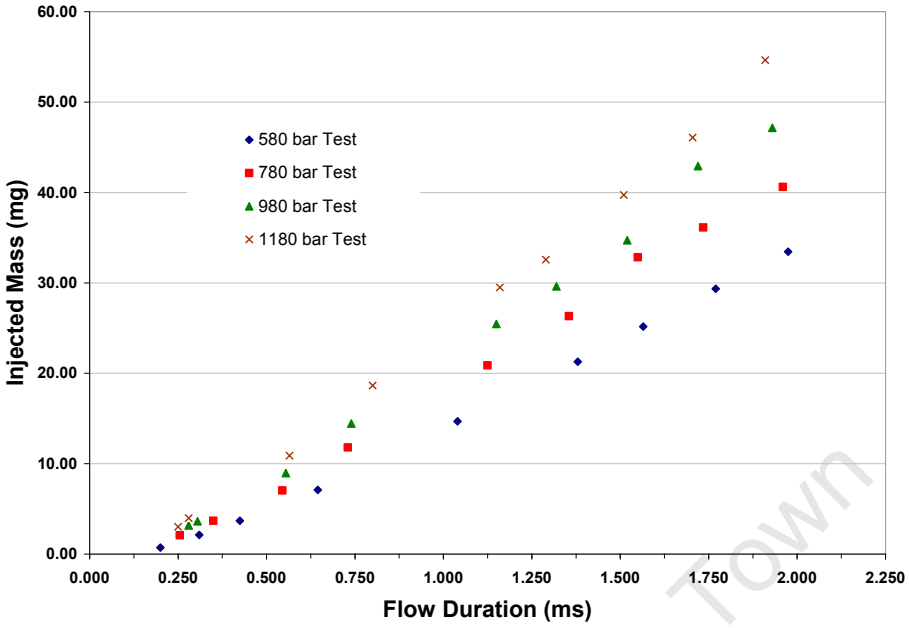

Figure 5- 14. Mass flow of GTL through the solenoid injector.

Figures 5-15 through 5-18 below illustrate the injection rate shape curves for EN590 diesel in the solenoid injector at each test pressure.

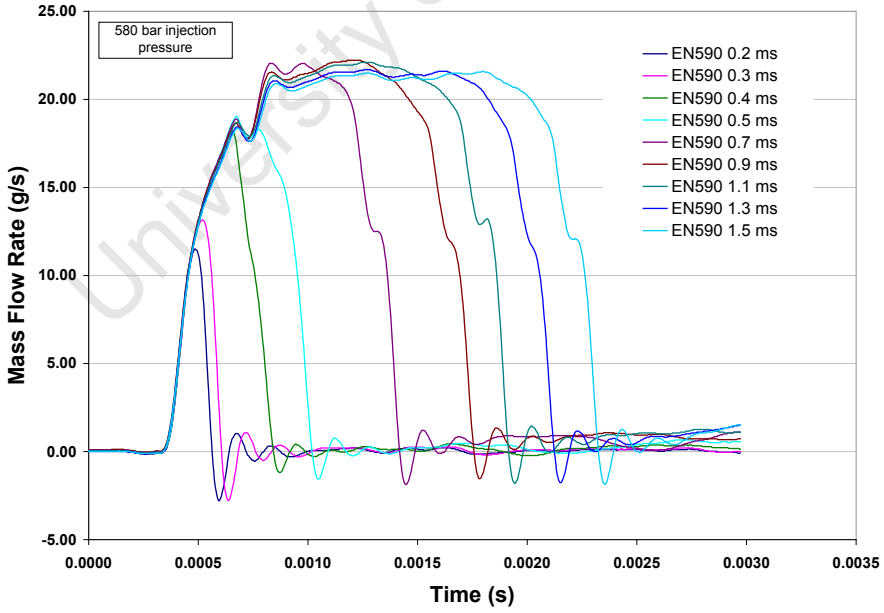

Figure 5- 15. Injection rate shape curves for EN590 in a solenoid injector at 580 bar.

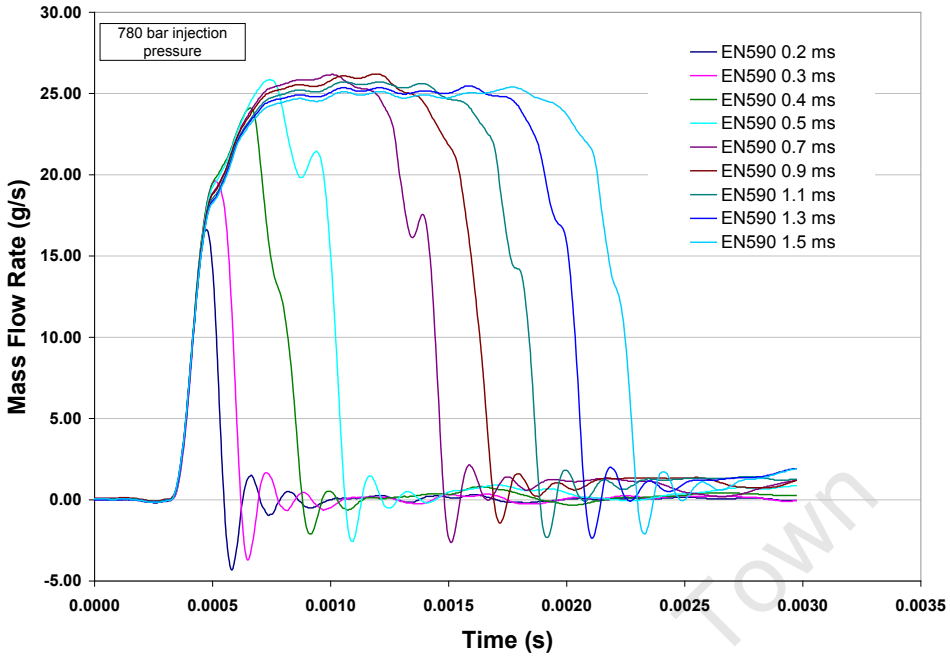

Figure 5- 16. Injection rate shape curves for EN590 in a solenoid injector at 780 bar.

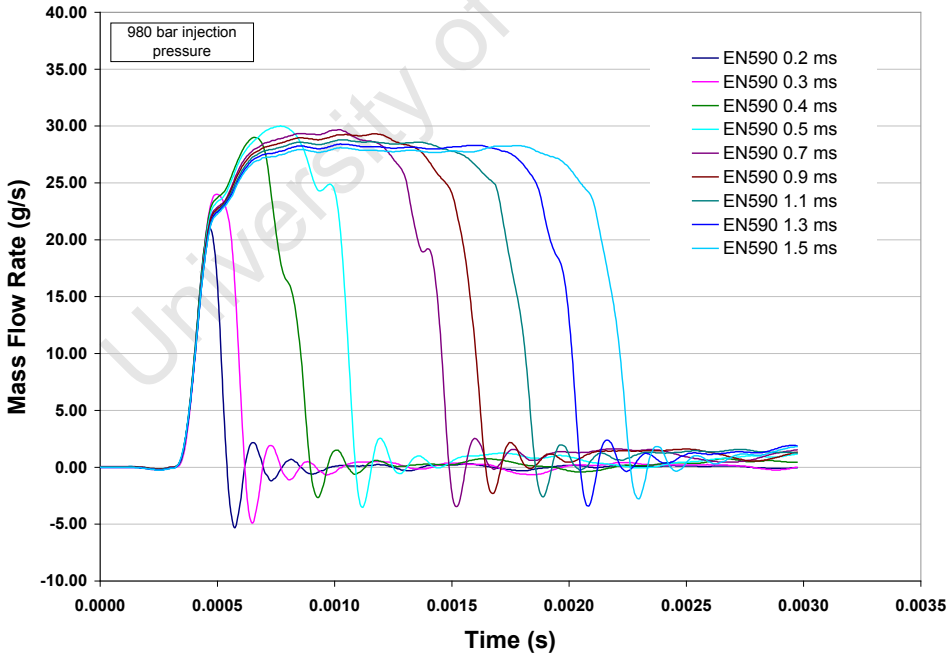

Figure 5- 17. Injection rate shape curves for EN590 in a solenoid injector at 980 bar.

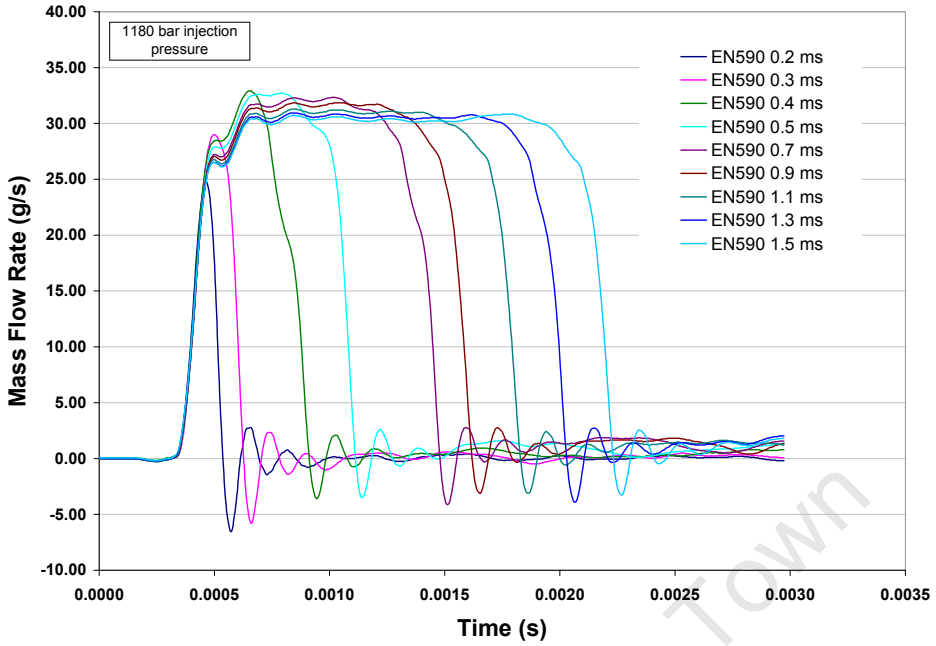

Figure 5- 18. Injection rate shape curves for EN590 in a solenoid injector at 1180 bar.

The mass flow of EN590 through the solenoid injector at various injection pressures and flow durations is shown in figure 5-19.

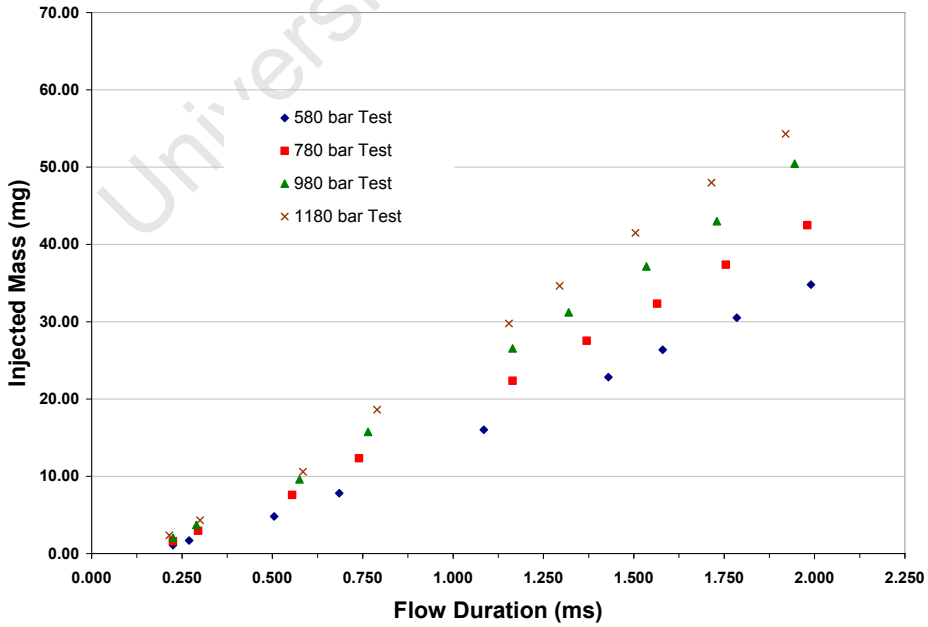

Figure 5- 19. Mass flow of EN590 through the solenoid injector.

Piezo Injector Results

The setup for the piezo injector tests was almost identical to that used for the solenoid injector tests. The same pressure and pulse width set-points were used and the fuels were controlled at the same temperature control set point (80°C). One difference in the testing setup was that the piezo injector required a back pressure to be applied to its fuel return line. This fuel was circulated back to the main fuel drum but did not have any effect on the temperature of the fuel being supplied to the injector intake.

Unfortunately some problems were encountered during the piezo injector flow tests, the first of which involved not being able to control the injector properly at very short pulse widths. Where the pulse width was set to 0.2 ms or 0.3 ms, sometimes the injector would deliver only a fractional amount of fuel and sometimes it would not deliver any fuel at all. It was not clear whether the injection signal was too weak or if the signal profile was not correctly structured, but this problem was not resolved. The injector did however behave correctly at longer pulse-width settings.

The second problem was that the pressure of the fuel delivery from the high pressure pump fluctuated considerably from test to test. The control system had been re-worked in the period between conducting the solenoid tests and the piezo tests, and this had affected the control of the high pressure pump. For each test, the injection pressure set point was selected; however, as shown by the data in table 5-5, the average pressure delivered by the pump during the test would not match the set point. This fluctuating delivery is also evident in figures 5-20 to 5-23, and 5-25 to 5-28, where the maximum flow rates achieved by the piezo injector varied considerably.

Table 5- 5. Variation of injection pressures between tests with a piezo injector.

Injection Pressure Set Point (bar)	Pressure achieved during GTL tests (bar)	Pressure achieved during EN590 tests (bar)
600	612	579
800	797	785
1000	836	958
1200	1040	1034

Figures 5-20 through 5-23 below illustrate the injection rate shape curves for the GTL diesel in the piezo injector at each test pressure.

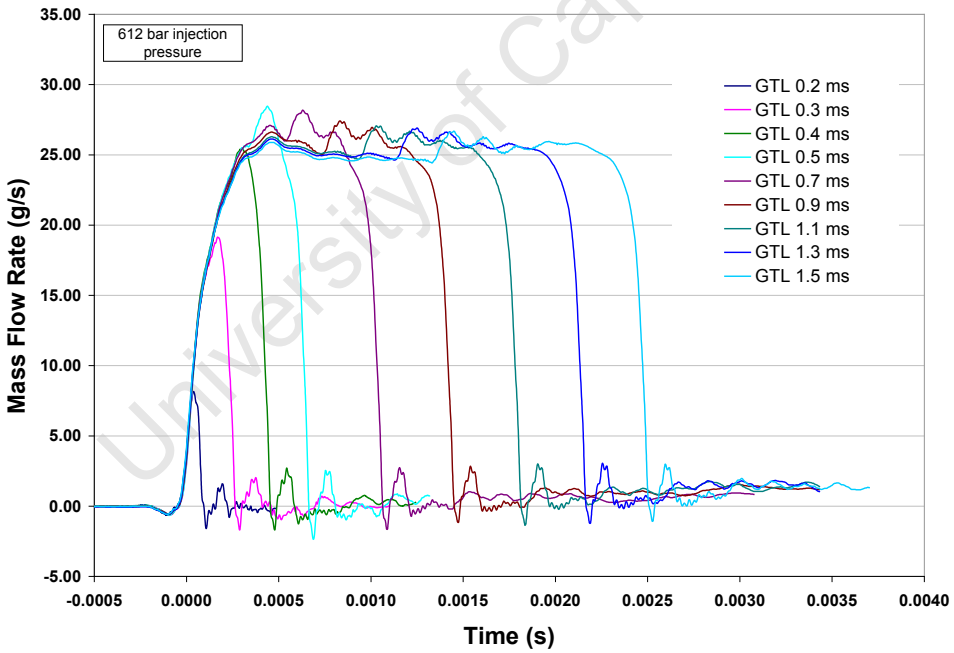

Figure 5- 20. Injection rate shape curves for GTL in a piezo injector at 612 bar.

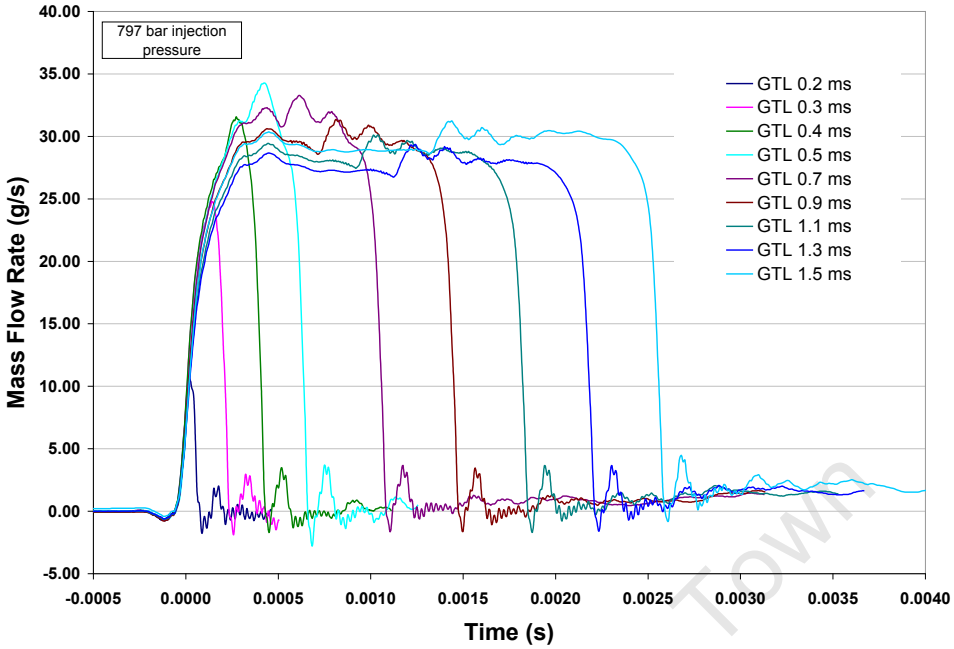

Figure 5- 21. Injection rate shape curves for GTL in a piezo injector at 797 bar.

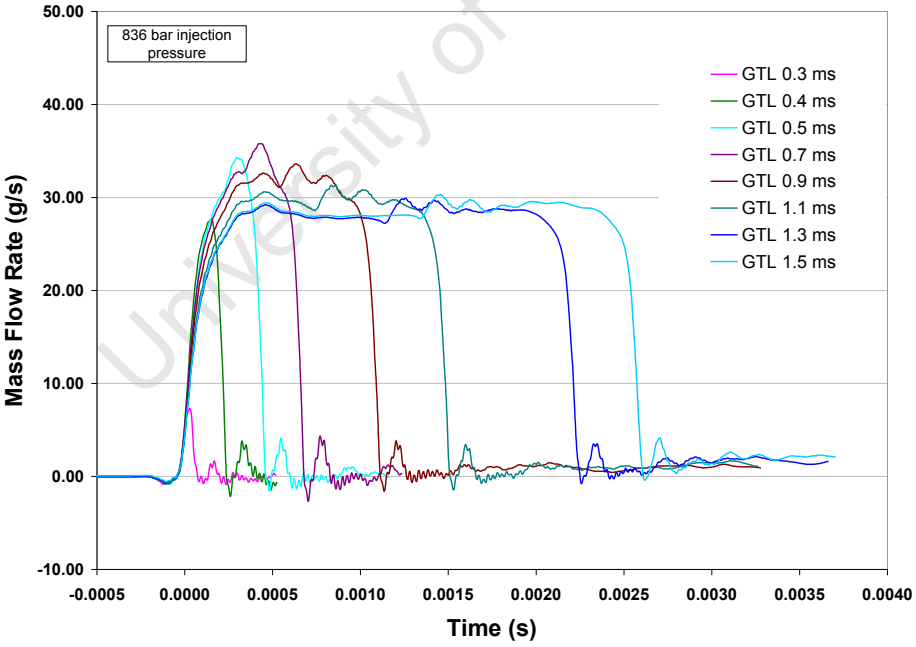

Figure 5- 22. Injection rate shape curves for GTL in a piezo injector at 836 bar.

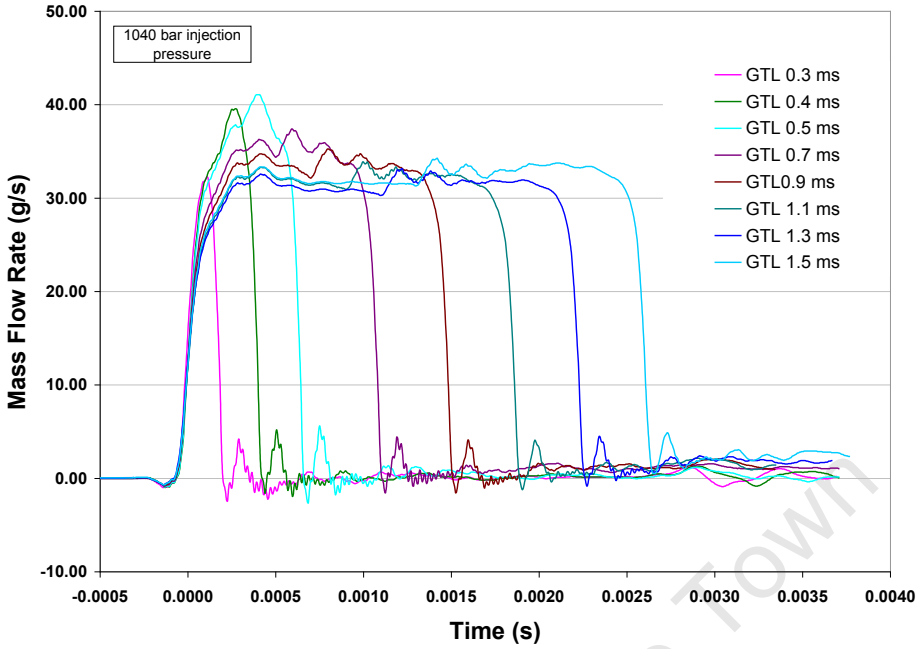

Figure 5- 23. Injection rate shape curves for GTL in a piezo injector at 1040 bar.

The mass flow of GTL through the piezo injector at various injection pressures and pulse width durations is shown in figure 5-24.

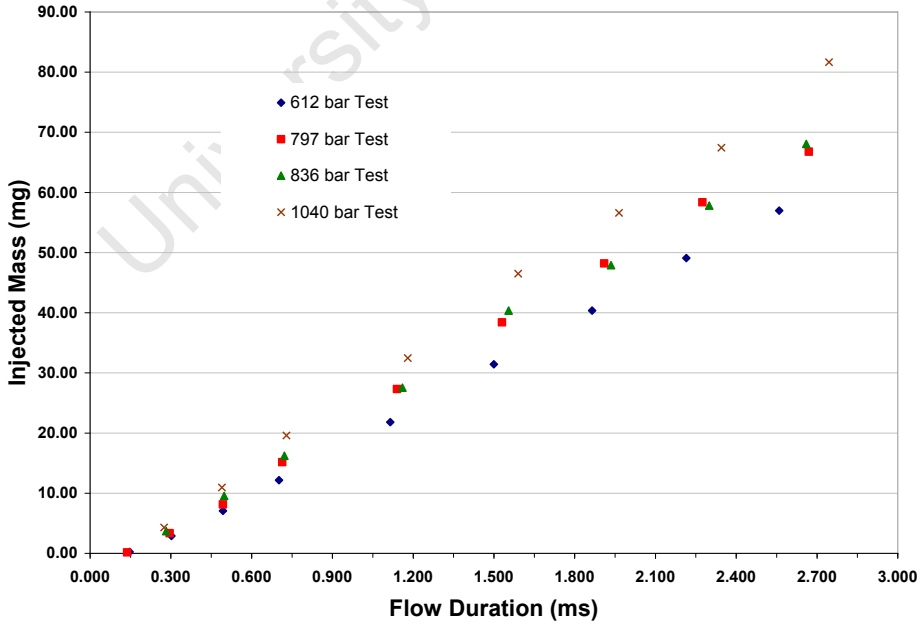

Figure 5- 24. Mass flow of GTL through the piezo injector.

Figures 5-25 through 5-28 below illustrate the injection rate shape curves for EN590 diesel in the piezo injector at each test pressure.

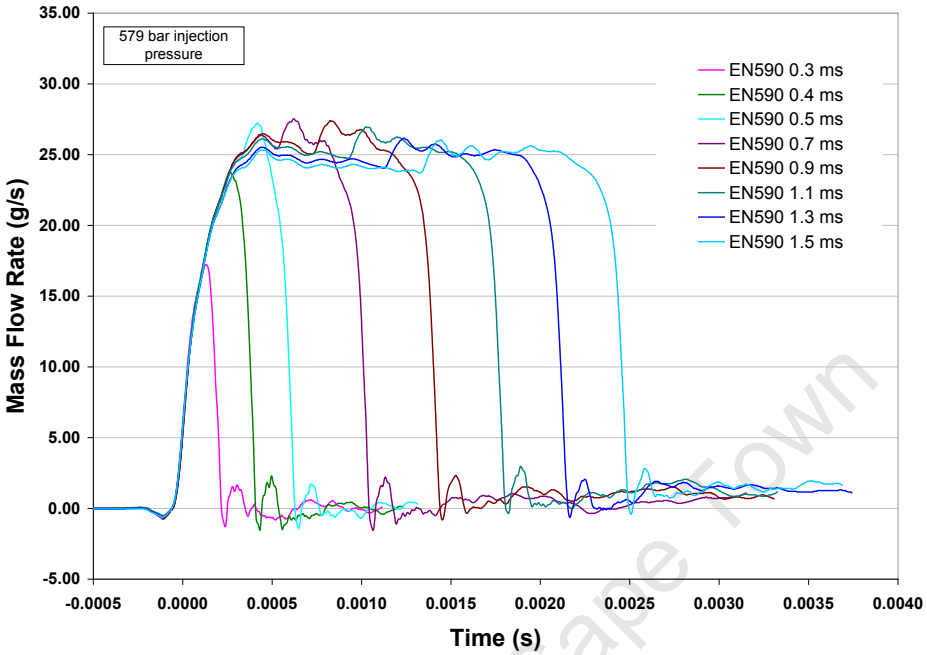

Figure 5- 25. Injection rate shape curves for EN590 in a piezo injector at 579 bar.

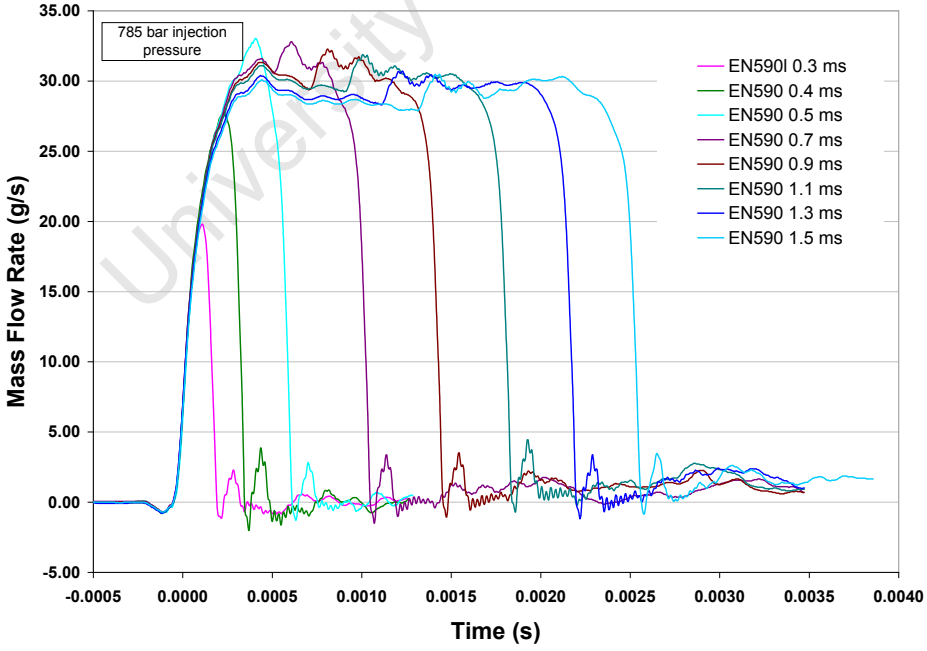

Figure 5- 26. Injection rate shape curves for EN590 in a piezo injector at 785 bar.

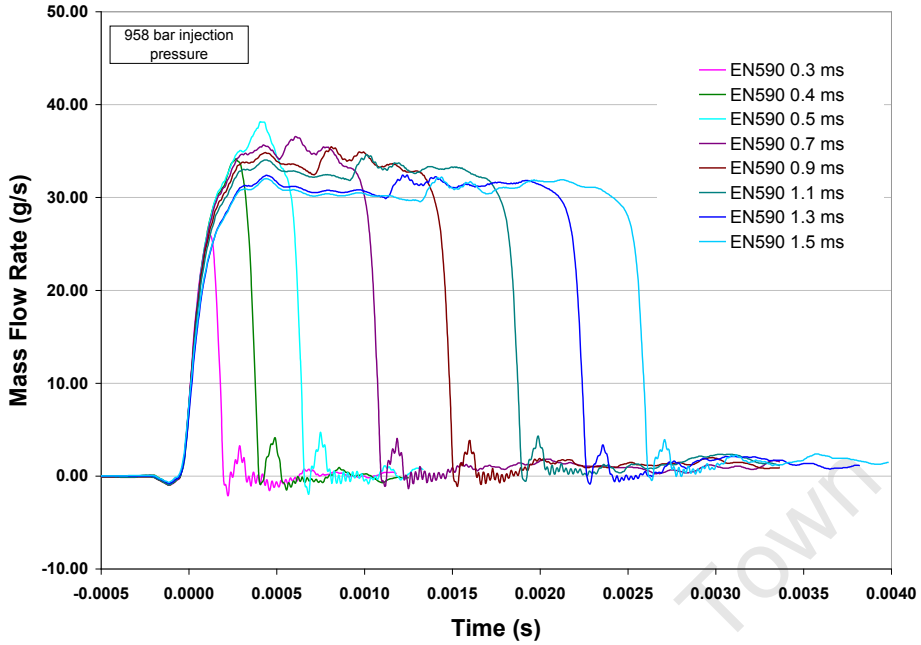

Figure 5- 27. Injection rate shape curves for EN590 in a piezo injector at 958 bar.

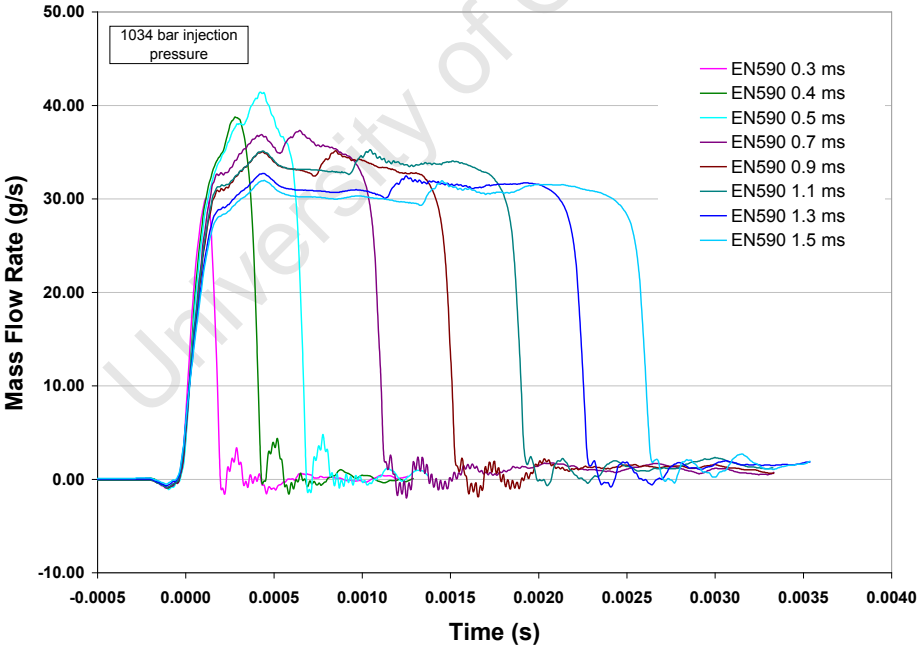

Figure 5- 28. Injection rate shape curves for EN590 in a piezo injector at 1034 bar.

The mass flow of EN590 through the piezo injector at various injection pressures and pulse width durations is shown in figure 5-29.

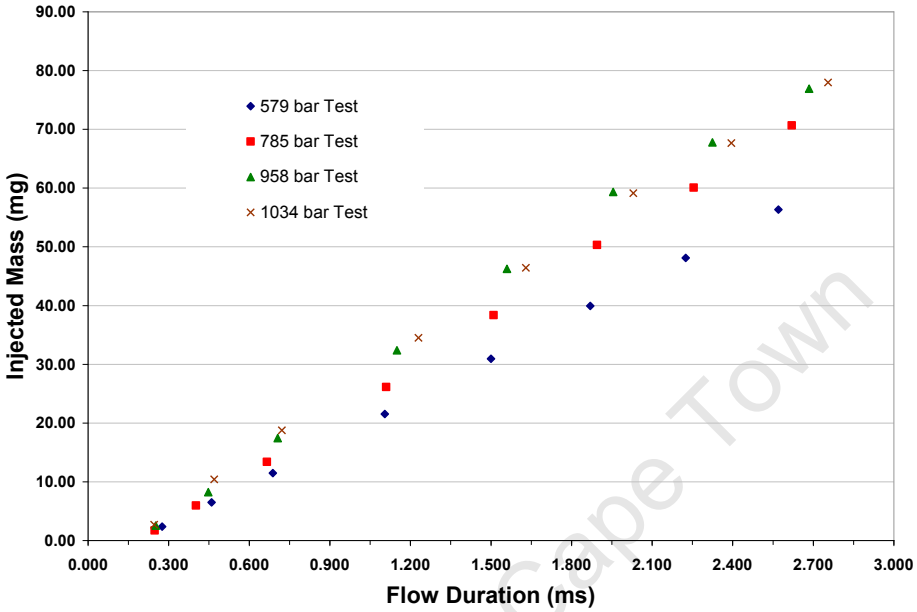

Figure 5- 29. Mass flow of EN590 through the piezo injector.

Having presented data for the validation of the experiments carried out in this study, as well as the experimental data for the fuel properties and the flow measurements, the following chapter will continue with a discussion and analysis of these results.

6. Analysis and Discussion

6.1 Fuel Properties

n-Hexadecane

Although measured at a different test temperature, the n-hexadecane acoustic velocity data from this study correlated very well with the data presented by Ball and Trusler, in terms of both temperature and pressure effects (See figure 5-2). The acoustic velocity values were found to increase with the square of the test pressure, and to decrease with increasing test temperatures.

The inferred density data for n-hexadecane was then indirectly compared to two other data sources via a regression model. The regression model fit the data sources with an R^2 value of 0.999, and as shown in figure 5-3, the results from this study showed very good correlation over the pressure range between 170 and 860 bar.

The bulk modulus data for n-hexadecane was slightly high compared to the DGMK's data (approximately 1.7% higher on average), considering that it was measured at a higher temperature. A possible reason for this inaccuracy may have been that the cross-correlation method took into account the geometry of the fuel pipe, as well as the physical properties of the steel. Small changes in these numbers resulted in varying pipe stiffness values and thus affected the bulk modulus of the fuel. Tat and Van Gerpen (2003) related the acoustic velocity of biodiesel directly to the density and bulk modulus, without taking the stiffness of the pipe into account.

The relationship was presented as follows (Gouw and Vlugter, 1967 and Rolling and Vogt, 1960, Tat and Van Gerpen, 2003):

$$c = \sqrt{\frac{B}{\rho}} \qquad \text{(Eq 6-1)}$$

If the bulk modulus values in this study are re-calculated directly from the acoustic velocity and the density as in equation 6-1, the bulk modulus values come out between 1.8 % and 2.7 % lower over the pressure range, making the comparison with the DGMK's data more favourable.

Overall, the results for n-hexadecane proved very satisfactory and served in verifying the technique for the measurement of acoustic velocity, and the subsequent calculation of densities and bulk modulus values.

GTL and EN590

The GTL and EN590 were tested using the same method as for the n-hexadecane above. The range of pressures over which the acoustic velocities for these two diesels were measured was from 170 bar to 970 bar. The results from these tests were then extrapolated to give fuel data over the pressure range for which the injector flow rate testing was performed (at 600 bar, 800 bar, 1000 bar and 1200 bar). Over this range, EN590 had higher acoustic velocity properties than the GTL. At the lowest pressure (600 bar), EN590 displayed a velocity roughly 1.67 % higher than that of the GTL, and at the highest pressure (1200 bar), this difference dropped to only 0.75%. This comparison is shown in the figure 6-1.

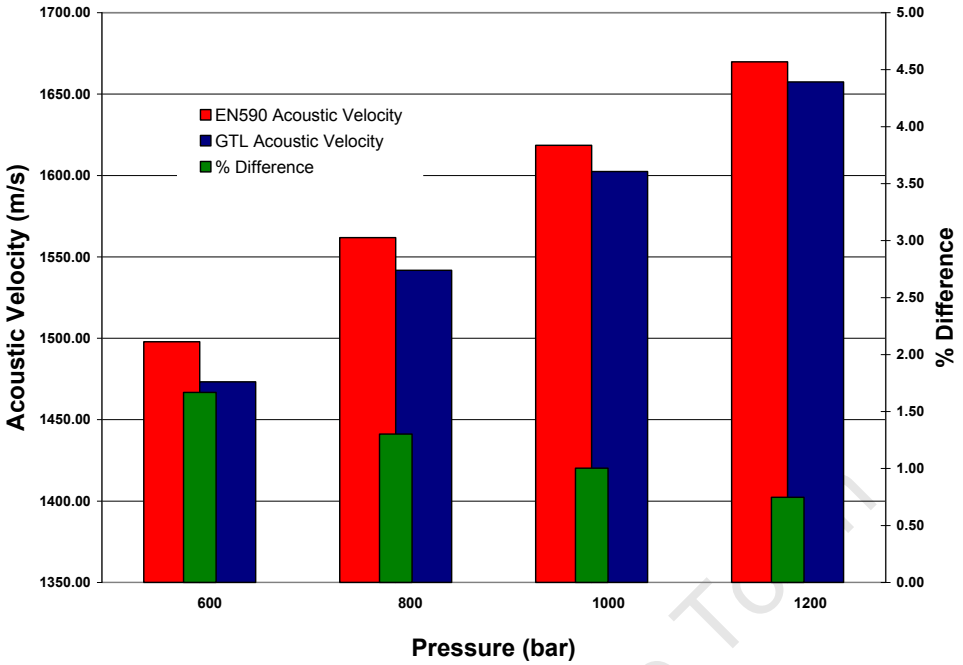

Figure 6- 1. Differences in the acoustic velocity data for diesel fuels at test pressures.

The densities of the EN590 were also higher than the densities of the GTL; with the EN590 being roughly 8.3 % higher than the GTL across the pressure range, as seen in figure 6-2.

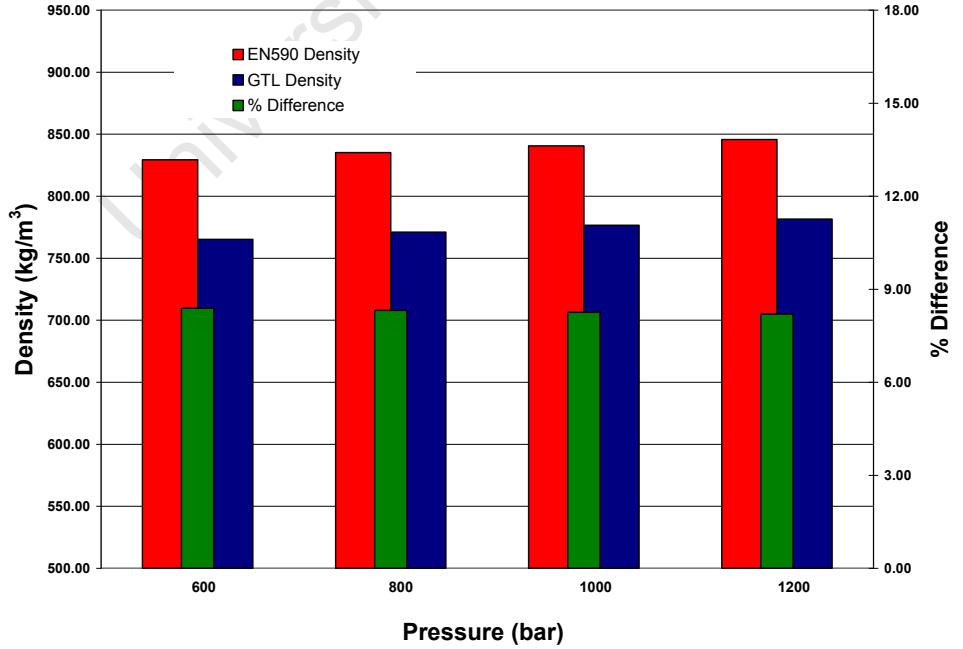

Figure 6- 2. Extrapolate density data for diesel fuels at test pressures.

Considering that density formed an integral part of the cross correlation method calculations, as well as the injected mass calculations for the Bosch indicator, it was interesting to note that across the pressure range, the percentage difference in density between the GTL and the EN590 did not vary significantly. The consequence of this was that any differences in flow characteristics measured between the two fuels (as a result of differing densities) were independent of injection pressure.

Bulk modulus values for EN590 were also consistently higher than the GTL values by roughly 11.7 % across the pressure range, as seen in figure 6-3.

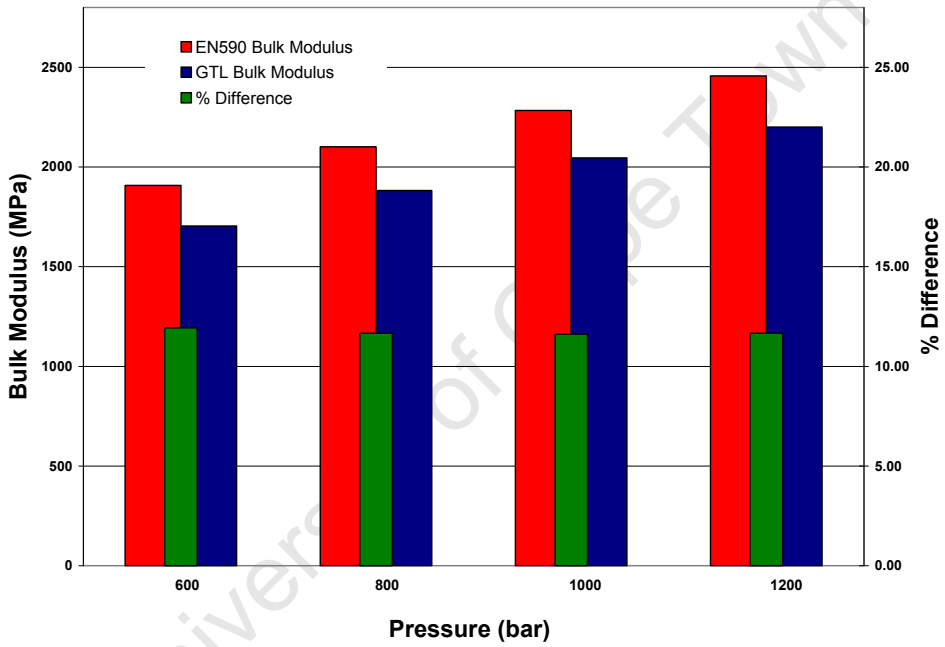

Figure 6- 3. Extrapolated bulk modulus data for diesel fuels at test pressures.

The overall effects of pressure on the physical properties of the diesel fuels were significant in terms of acoustic velocity and bulk modulus, but only very slight in terms of density. Where pressure was increased from 600 bar to 1200 bar, acoustic velocity values for both diesel fuels increased by roughly 12 % and bulk modulus values increased by roughly 29 %, but density values only increased by about 2 %.

6.2 Injector Mass Flow

Injection Rate Shape Characteristics

In chapter 3, the basic principles of operation of a common rail injector unit and, in particular, the movement of the injector needle were explained (Item 'E' in figure 3-1). The injection flow rate curves presented in chapter 5 are very useful for illustrating this needle movement. Looking again at the curves for the GTL in the solenoid injector, it was evident that at the various pulse widths, the injector attained varying peak flow rates. In figure 6-4, at very short pulse widths such as 0.2 milliseconds, the needle only lifted briefly from its seat, and then returned to seal again. In this time, the peak flow rate achieved was approximately 9.5 g/s. When the pulse width was increased to 0.3 milliseconds, the needle lifted a little higher than before, resulting in a slight increase in the available flow area, and thus the peak flow rate increased to approximately 14 g/s.

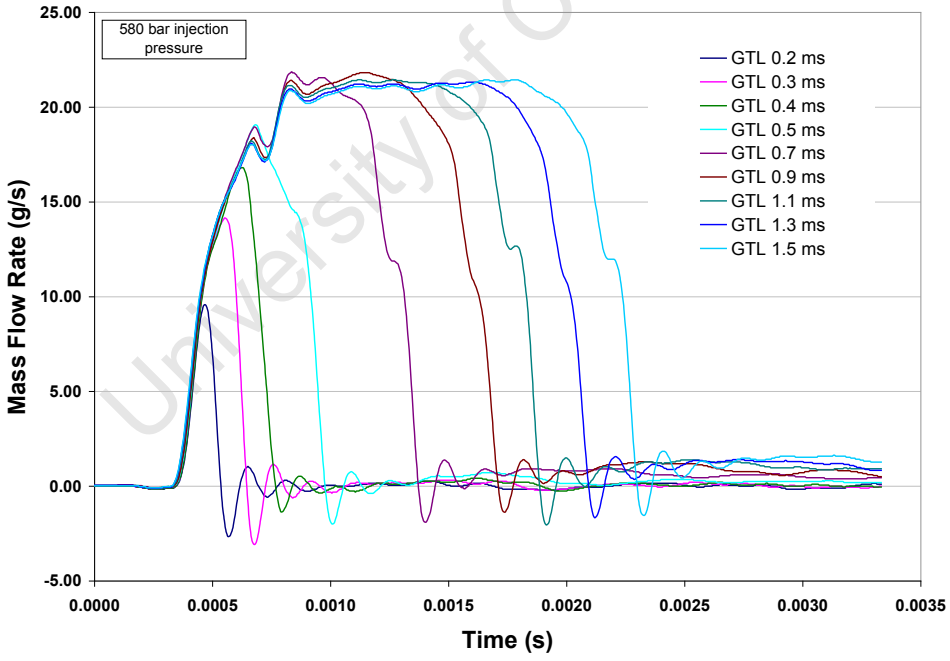

Figure 6- 4. Injection rate shape curves for the GTL in a solenoid injector at 580 bar.

For this particular set of tests, this trend continued up to a pulse width of 0.5 milliseconds, with the needle lifting slightly higher from its seat each time. When a

pulse width of 0.7 milliseconds was used, the needle had enough time to reach its maximum height above the seat, thus giving the maximum flow area. It was at this point that the injector achieved its maximum possible flow rate at the given injection pressure (580 bar in this case). Any subsequent increase in the pulse width resulted in the injector achieving the same maximum flow rate, and simply increased the time for which the injector remained in this fully open state.

For injection tests at the highest injection pressure, as seen in figure 6-5, the results were quite different:

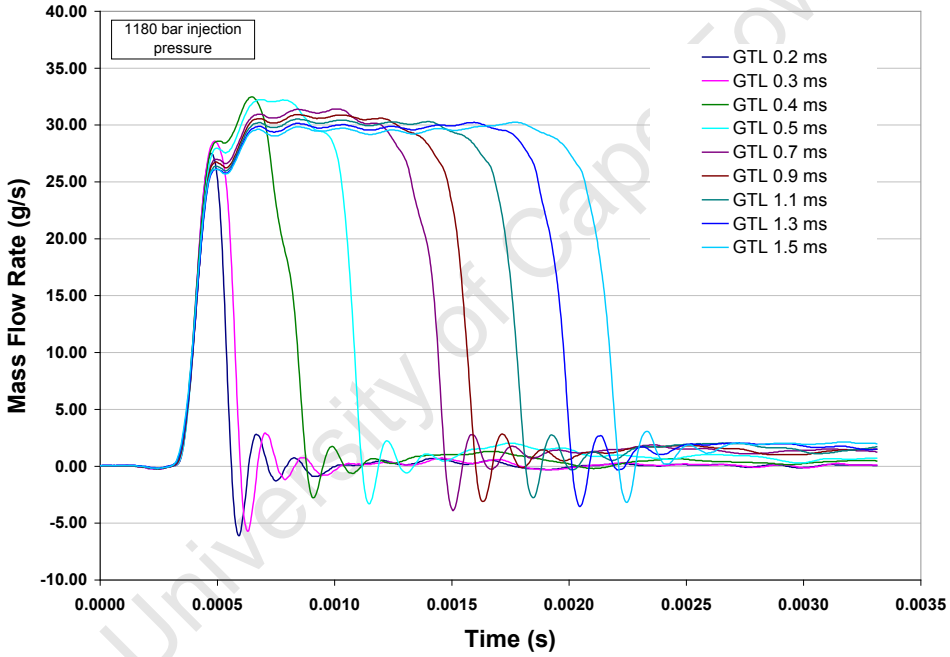

Figure 6- 5. Injection rate shape curves for the GTL in a solenoid injector at 1180 bar.

It was immediately evident that the injector achieved its maximum possible flow rate far earlier in the pulse width regime. At higher injection pressures, the resultant force acting on the injector needle was higher, and the fuel's acoustic velocity was higher, resulting in the pressure waves travelling much faster through the fuel. These two factors combined meant that the injector needle displayed a much quicker response time. The needle required less time to reach the maximum height above its seat, and thus at higher injection pressures, the peak flow rate achieved by the fuel injector was less varied across the pulse-width regime.

To give a more clear indication of the effects of pressure on the injection rate shape curves, figures 6-6 to 6-8 are presented, where the 0.2, 0.7 and 1.5 millisecond pulse-widths were chosen for comparison at four different test pressures:

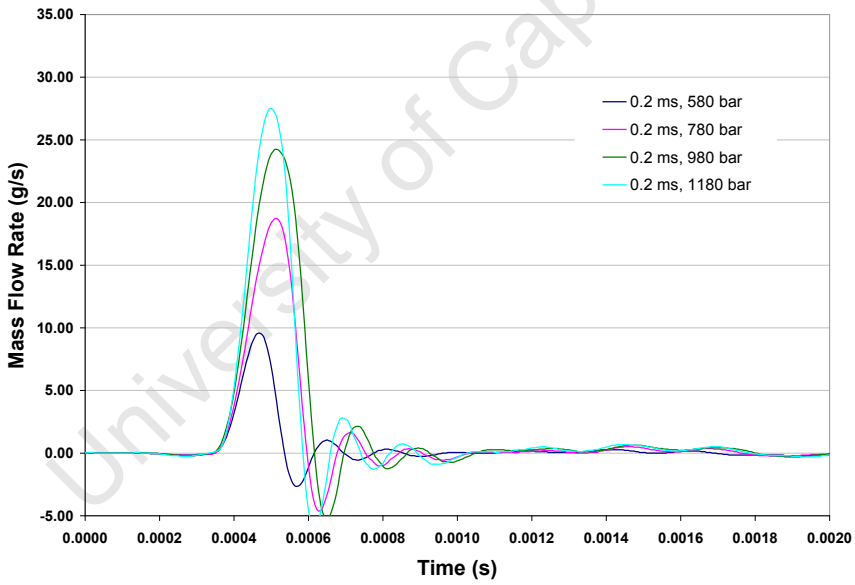

Figure 6- 6. Pressure effects on injection rate shape for the GTL in a solenoid injector at 0.2 ms pulse-width.

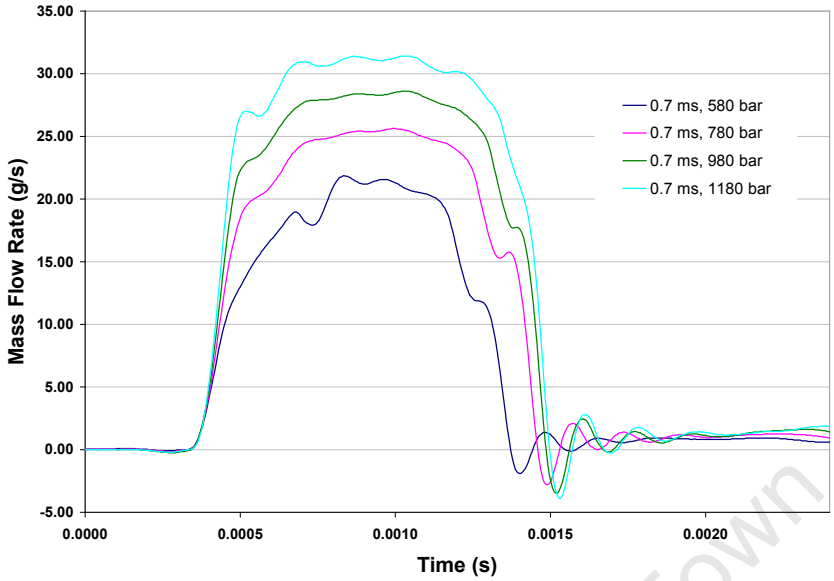

Figure 6- 7. Pressure effects on injection rate shape for the GTL in a solenoid injector at 0.7 ms pulse-width.

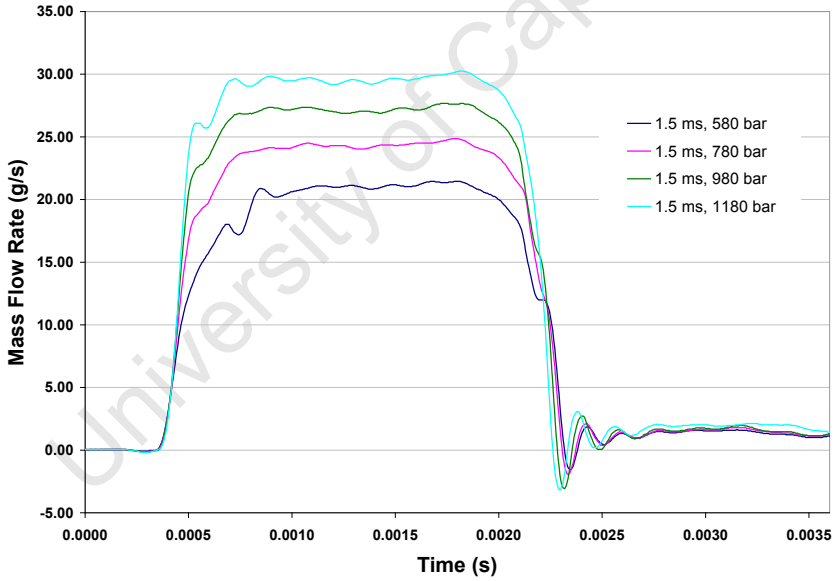

Figure 6- 8. Pressure effects on injection rate shape for the GTL in a solenoid injector at 1.5 ms pulse-width.

From figures 6-6 and 6-7, it was evident that for a given pulse width, the flow duration did not necessarily remain constant. This behaviour was expected at very short pulse widths, as seen in figure 6-6, where the needle had insufficient time to fully lift, but was

not expected at longer pulse widths, where the needle experienced its maximum lift. As these plots were all from the same fuel (GTL), the contrast between figures 6-7 and 6-8 also suggests that the effect was not caused by changing fuel properties resulting from differences in injection pressure. As the injection signals delivered to the injector were identical, this posed a difficult phenomenon to explain.

A possibility may be that the control needle in the injector deformed under movement. The deformation of the needle would occur during a change of acceleration of the needle. This would explain why the higher injection pressures in figure 6-7 resulted in longer flow durations, because the needle displayed a higher degree of deformation, and thus took a fraction longer to re-seat. The effect was diminished in figure 6-8, because the pulse width was long enough to allow the needle to regain its shape before re-seating.

Increases in the injection pressure resulted in corresponding increases in the maximum flow rate achieved by the injector. As expected, the increase in flow rate was far more pronounced at shorter pulse widths. As the injection pressure increased, not only did the peak flow rate increase, but the initial rate of rise in the flow rate also increased. That is to say that the time taken to reach the peak flow rate decreased with an increase in injection pressure.

The effects of pressure on the maximum flow rate are illustrated by figure 6-9:

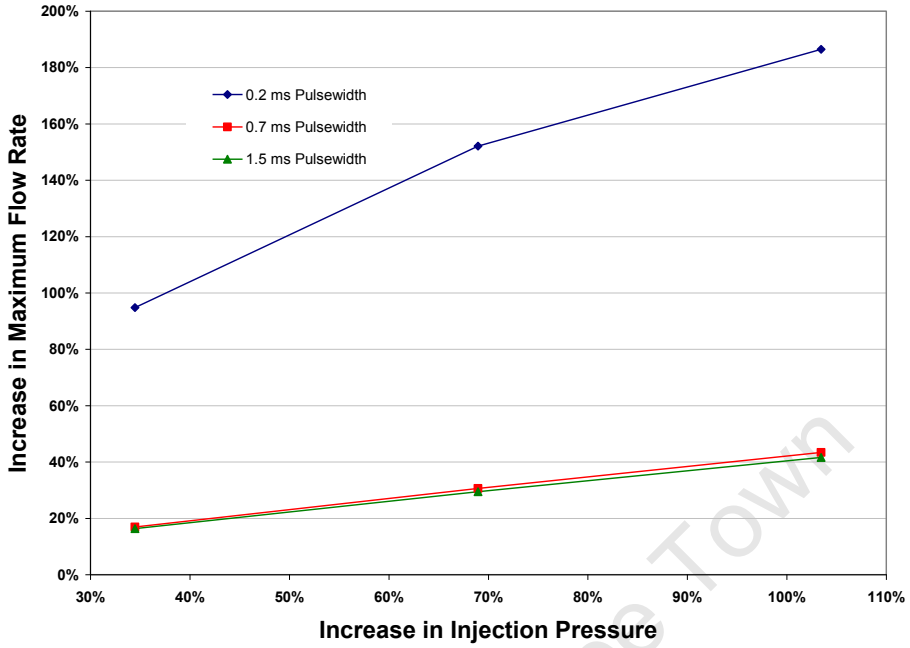

Figure 6- 9. The effects of injection pressure on the maximum flow rate in a solenoid injector.

The effects of pressure on the initial rate of rise in flow rate are illustrated by figure 6-10:

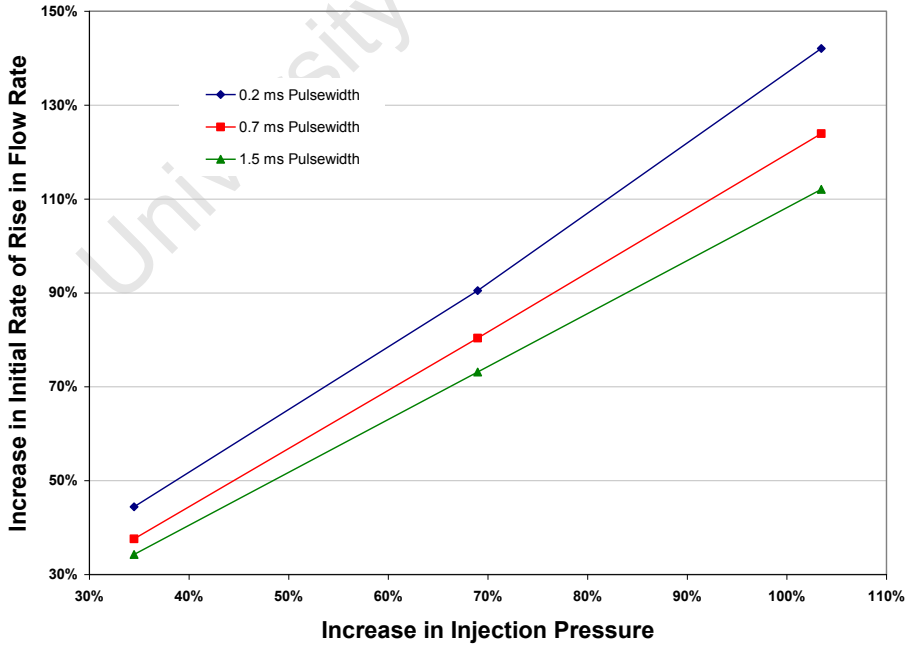

Figure 6- 10. The effects of injection pressure on the initial rate of rise in flow rate in a solenoid injector.

Injector Flow Test Regression Analyses

As mentioned in chapter 5, particularly during the piezo injector flow tests, problems were encountered with regard to the control of the pressure delivered by the fuel pump.

In order to be able to compare the different injectors and the different fuels properly, it was necessary to use data taken at the same operating points (i.e. injection pressure, and pulse width). Having not obtained satisfactory data during testing, it was necessary to perform a regression analysis on the existing data.

The regression models were a set of equations aimed at describing the behaviour of the two fuels at various test conditions in the two injectors. These models were based on basic mass flow formulae, and on a simplified version of Bernoulli's equation as detailed below:

$$\dot{m} = \dot{Q}\rho \qquad \text{(Eq 6-2)}$$

Where $\dot{m}$ = mass flow rate (kg/s)

$\dot{Q}$ = Volume flow rate (m^3/s)

ρ = density (kg/m^3)

And,

$$\dot{Q} = C_d A v \qquad \text{(Eq 6-3)}$$

Where C_d = Flow drag coefficient

A = Flow area (m^2)

v = Flow velocity (m/s)

Now, using the simplified Bernoulli's equation, and with the assumption that upstream velocity is zero:

$$v_2 = \sqrt{2\left|\frac{P_R}{\rho_R} - \frac{P_M}{\rho_M}\right|} \qquad \text{(Eq 6-4)}$$

Where v_2 is the downstream flow velocity (m/s)

P_R is the upstream rail pressure (Pa)

P_M is the downstream measuring tube pressure (Pa)

ρ_R is the upstream fuel density (kg/m^3)

ρ_M is the downstream fuel density (kg/m^3)

This gives the following expression for the mass flowing through the injector,

$$m = C_d A \rho_R \sqrt{2\left|\frac{P_R}{\rho_R} - \frac{P_M}{\rho_M}\right|}\Delta t \qquad \text{(Eq 6-5)}$$

Where m is the injected mass (kg), and

Δt is the flow duration (s) as explained in chapter 5.2.

For each combination of fuel and injector, a statistical regression of the form of equation 6-5 was performed. The density data used for the regressions was based on equations 5-2 and 5-3. For the regression model, the mass term 'm' in equation 6-5 was the dependent term, and the independent term was: $\left(A\rho_R \sqrt{2\left|\frac{P_R}{\rho_R} - \frac{P_M}{\rho_M}\right|}\Delta t \right)$.

The flow discharge coefficient, C_d was then solved for using Microsoft Excel's Solver Tool. The root mean square difference between the measured injected mass and the regression injected mass was used as the 'Solver Target'.

$$Diff_{RMS} = \sqrt{\sum (m_{Exp} - m_{\mathrm{Re}g})^2} \qquad \text{(Eq 6-6)}$$

Initially, the regression equations were developed against the full data sets collected during the fuel mass flow experiments; however, as displayed by figure 6-11, the fit of these regression models to the experimental data was poor at the shorter flow durations, particularly for the solenoid injector.

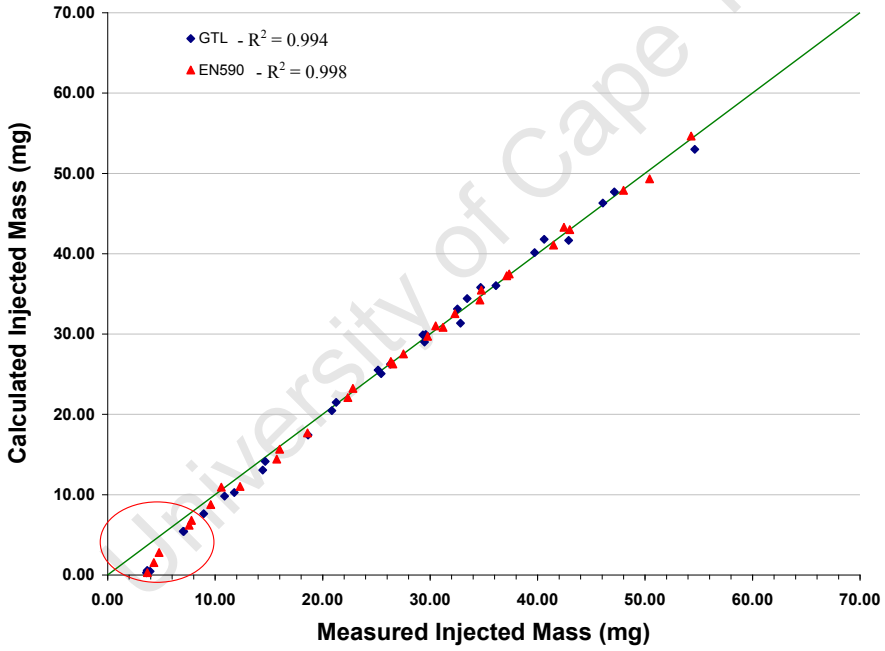

Figure 6- 11. Inaccuracies of the solenoid injector regression models at short flow durations.

The 'Δt' term in equation 6-5 indicates that the regression form approximates the injection rate shape curve as having a "top-hat" shape. This form was not very accurate for modelling the injected mass at pulse widths where the injector needle did not lift fully from its seat. This problem was particularly noticeable in the solenoid injector.

As shown in figure 6-12, the fit of the initial regression models for the piezo injector was better at shorter pulse widths, which would indicate that the control of the injector needle

movement at short pulse widths was far better in the piezo injector than in the solenoid injector.

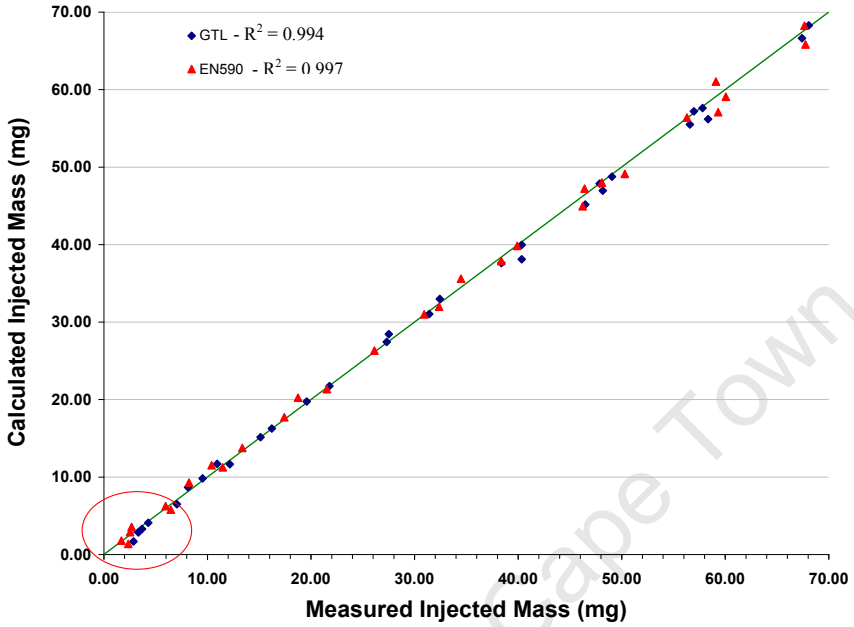

Figure 6- 12. Improved accuracy for the piezo injector regression model relative to solenoid injector model.

Despite this slight improvement in fit for the piezo injector, the following regression models were only fit to the experimental data where the **pulse width** signal was greater than 0.5 milliseconds. The models then yielded data which matched up very well with the experimental flow data.

For GTL in the solenoid injector, the regression equation was:

$$m = 0.725 A \rho_R \sqrt{2\left|\frac{P_R}{\rho_R} - \frac{P_M}{\rho_M}\right|}\Delta t - 8.756 \quad \text{(Eq 6-7)}$$

The flow discharge coefficient was 0.725, and the offset of -8.756 indicates that the injector ceased to deliver fuel before the pulse width signal reached zero. The regression

data fit the experimental data with a coefficient of determination (R^2) of 0.994. Figure 6-13 illustrates the comparison between the experimental data and the regression data.

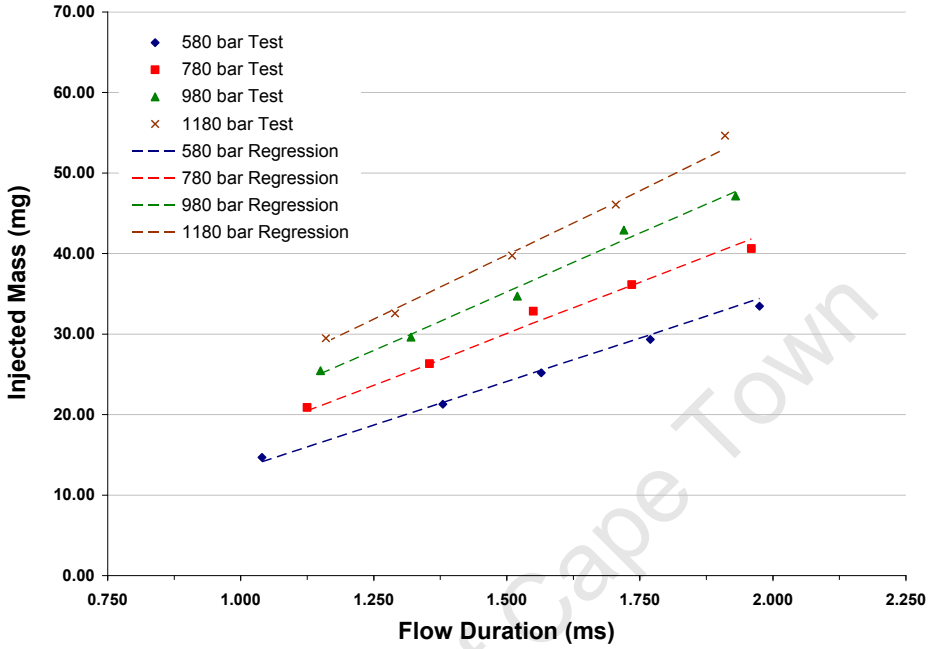

Figure 6- 13. Comparison of test and regression data for the GTL in a solenoid injector.

For EN590 in the solenoid injector, the regression equation was:

$$m = 0.704 A \rho_R \sqrt{2\left|\frac{P_R}{\rho_R} - \frac{P_M}{\rho_M}\right|}\Delta t - 8.392 \qquad \text{(Eq 6-8)}$$

The flow discharge coefficient was 0.704, and again the offset of -8.392 indicates that the injector ceased to deliver fuel before the pulse width signal reached zero. The regression data fit the experimental data with a coefficient of determination (R^2) of 0.998. Figure 6-14 illustrates the comparison between the experimental data and the regression data.

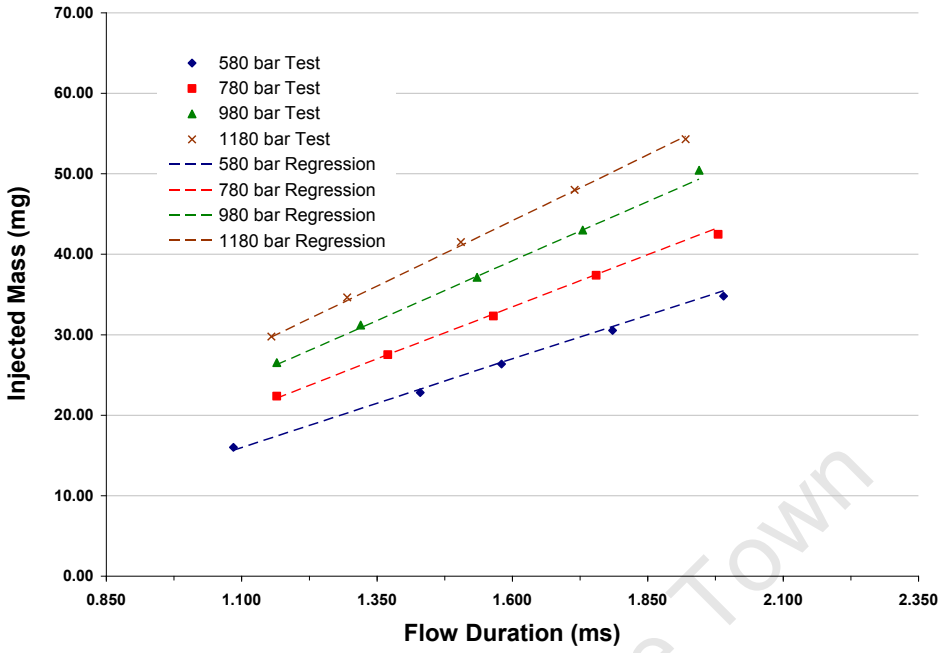

Figure 6- 14. Comparison of test and regression data for EN590 in a solenoid injector.

For GTL in the piezo injector, the regression equation was:

$$m = 0.798 A \rho_R \sqrt{2\left|\frac{P_R}{\rho_R} - \frac{P_M}{\rho_M}\right|}\Delta t - 5.958 \qquad \text{(Eq 6-9)}$$

The flow discharge coefficient was 0.798, and the offset was -5.958. The regression data fit the experimental data with a coefficient of determination (R^2) of 0.994. Figure 6-15 shows the comparison between the experimental data and the regression data.

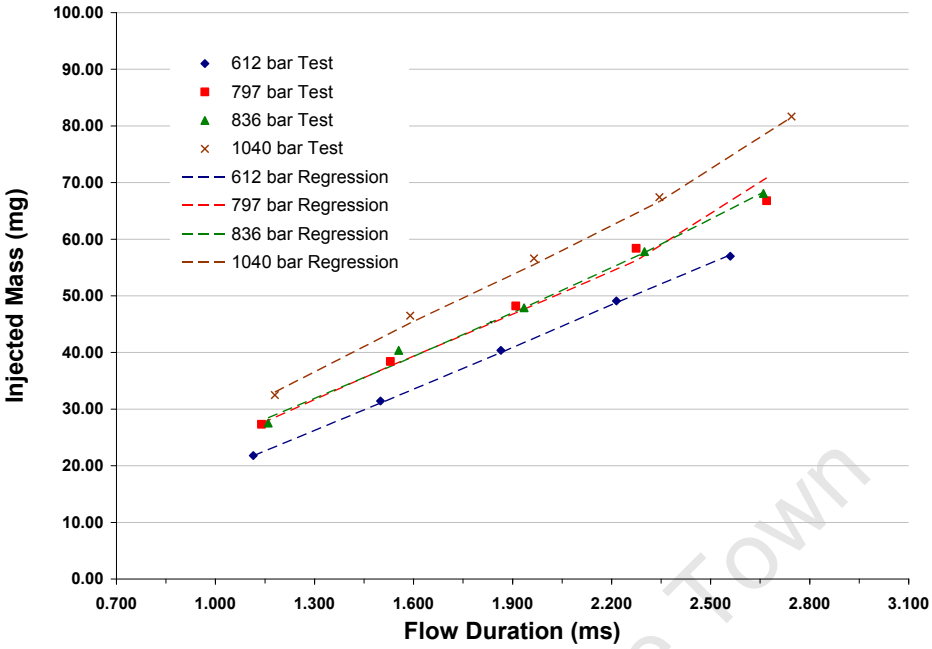

Figure 6- 15. Comparison of test and regression data for GTL in a piezo injector.

For EN590 in the piezo injector, the regression equation was:

$$m = 0.773 A \rho_R \sqrt{2\left|\frac{P_R}{\rho_R} - \frac{P_M}{\rho_M}\right|}\Delta t - 5.272 \qquad \text{(Eq 6-10)}$$

The flow discharge coefficient was 0.773, and the offset was -5.272. The regression data fit the experimental data with a coefficient of determination (R^2) of 0.997. Figure 6-16 shows the comparison between the experimental data and the regression data. When considering that the set points for the injection pressures were separated by intervals of 200 bar, figures 6-15 and 6-16 clearly illustrate how the fuel pump did not deliver fuel at the required intervals. Instead, the injection pressure intervals achieved between data sets dropped as low as 39 bar as seen in figure 6-15, leading to the grouping of the data.

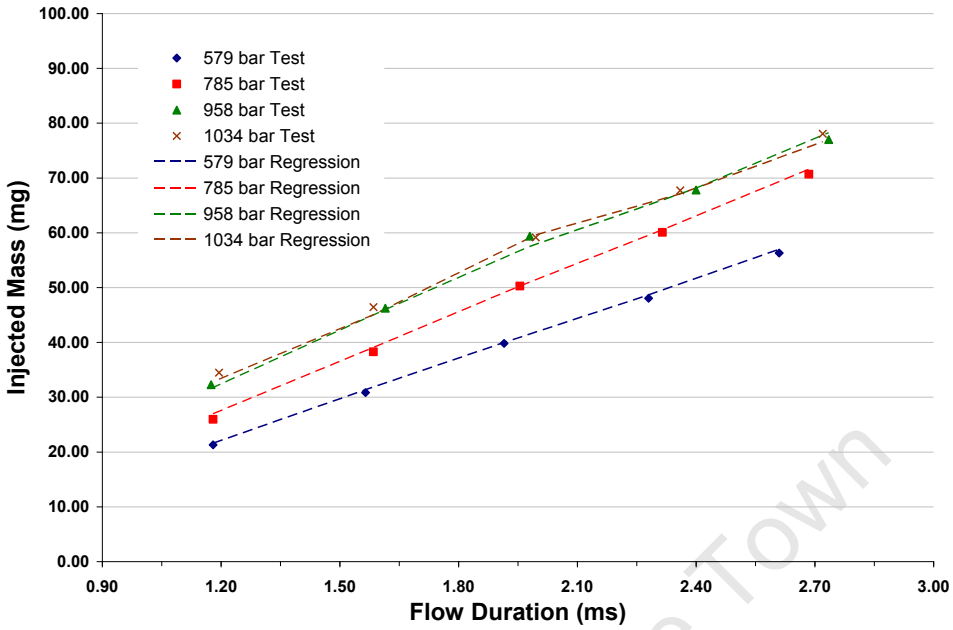

Figure 6- 16. Comparison of test and regression data for EN590 in a piezo injector.

Despite matching the test data very well, there were still a few data points where the errors between the regression data and the test data were significant. These deviations were likely due to an error in the experimental procedure, as they did not conform to the trends shown by the accompanying data. Another explanation could be that during testing, certain combinations of injection pressure and pulse width resulted in a harmonic behaviour of the upstream pressure in the fuel supply line as described by Boudy and Seers (2009). The effect of this was that at certain conditions, the pressure available to the injector was higher or lower than expected. In this study, the injection pressure was measured roughly 100 mm upstream of the injector, and was measured as an average figure over each test consisting of 1000 injection events. Thus it is plausible that the instantaneous injection pressure at the injector's nozzle was not exactly the same as the measured value. This might explain any discrepancies between the regression data and the test data.

6.3 Comparing Diesel Fuel Injection Characteristics

In order to make meaningful comparisons between different fuels and different injectors, a pre-requisite was to have measured data at matching experimental set points. As with any experiment, the proximity of the control values to their respective set points is only as close as the control system permits. Having experienced significant difficulties in this regard, data sets were generated from the regression models, allowing for meaningful comparisons between the two diesel fuels.

Figures 6-17 and 6-18 show the comparison between the GTL and EN590 regression data for the two different injectors.

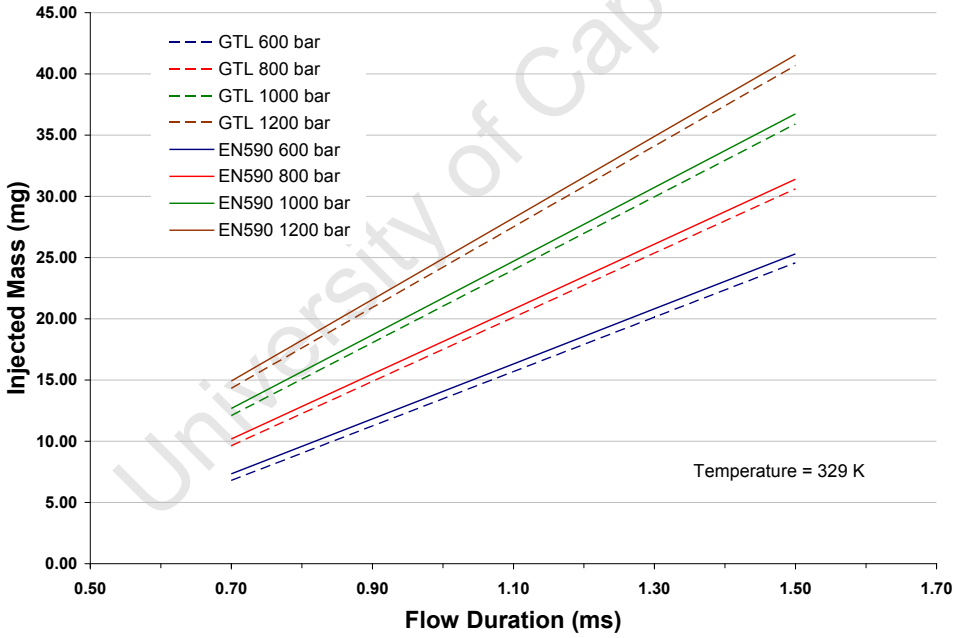

Figure 6- 17. Comparison of the injected mass for GTL and EN590 in a solenoid injector.

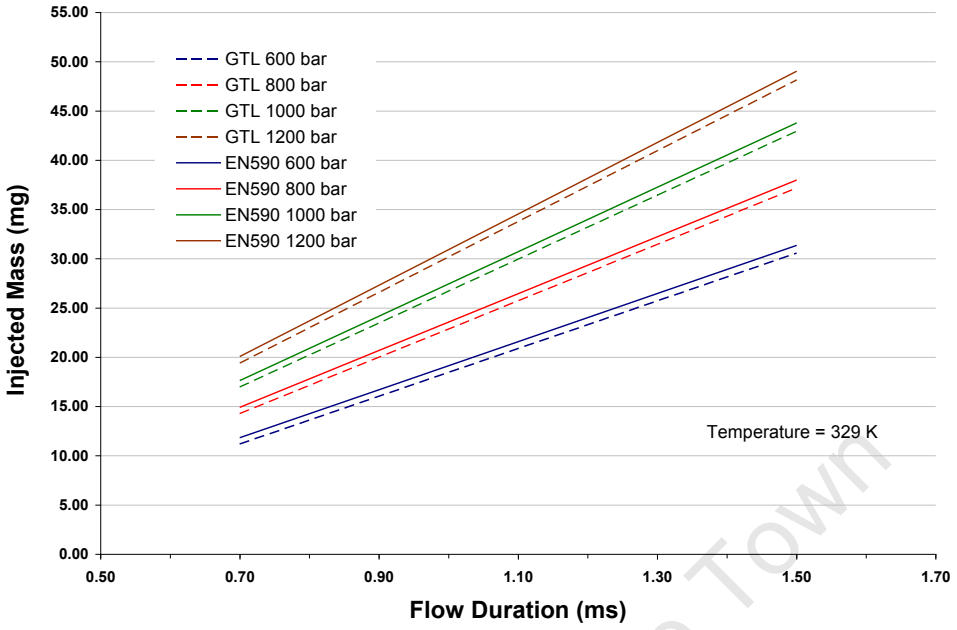

Figure 6- 18. Comparison of the injected mass for GTL and EN590 in a piezo injector.

From the data presented in figures 6-17 and 6-18 above, three pulse widths were chosen to represent the injected mass data across the range, and the respective results are reported below:

Table 6- 1. Comparison of the injected mass for GTL and EN590 in a solenoid injector.

	0.7 ms			1.1 ms			1.5 ms		
Injection Pressure	GTL (g)	EN590 (g)	Diff %	GTL (g)	EN590 (g)	Diff %	GTL (g)	EN590 (g)	Diff %
600	6.79	7.33	7.9%	15.68	16.31	4.0%	24.56	25.29	3.0%
800	9.61	10.17	5.8%	20.11	20.78	3.3%	30.61	31.39	2.6%
1000	12.08	12.66	4.8%	23.99	24.70	2.9%	35.90	36.73	2.3%
1200	14.31	14.91	4.2%	27.50	28.23	2.7%	40.68	41.55	2.1%

Table 6- 2. Comparison of the injected mass for GTL and EN590 in a piezo injector.

	0.7 ms			1.1 ms			1.5 ms		
Injection Pressure	GTL (g)	EN590 (g)	Diff %	GTL (g)	EN590 (g)	Diff %	GTL (g)	EN590 (g)	Diff %
600	11.00	11.82	7.5%	20.68	21.59	4.4%	30.37	31.36	3.3%
800	14.07	14.92	6.0%	25.52	26.45	3.7%	36.96	37.99	2.8%
1000	16.77	17.63	5.1%	29.75	30.71	3.2%	42.74	43.80	2.5%
1200	19.20	20.07	4.5%	33.58	34.55	2.9%	47.95	49.04	2.3%

In both injectors, the EN590 displayed injected mass values of between 2.1 % and 7.9 % higher than the GTL at the same conditions. As injection pressure was raised, so the percentage difference between the injected mass of the two fuels decreased.

The piezo injector also displayed a higher rate of rise in the flow rate than the solenoid injector. This was more noticeable at lower injection pressures. Figures 6-19 and 6-20 are zoomed in shots of the injection rate curves, and illustrate that the delay in reaching maximum flow rate was more pronounced for the solenoid injector.

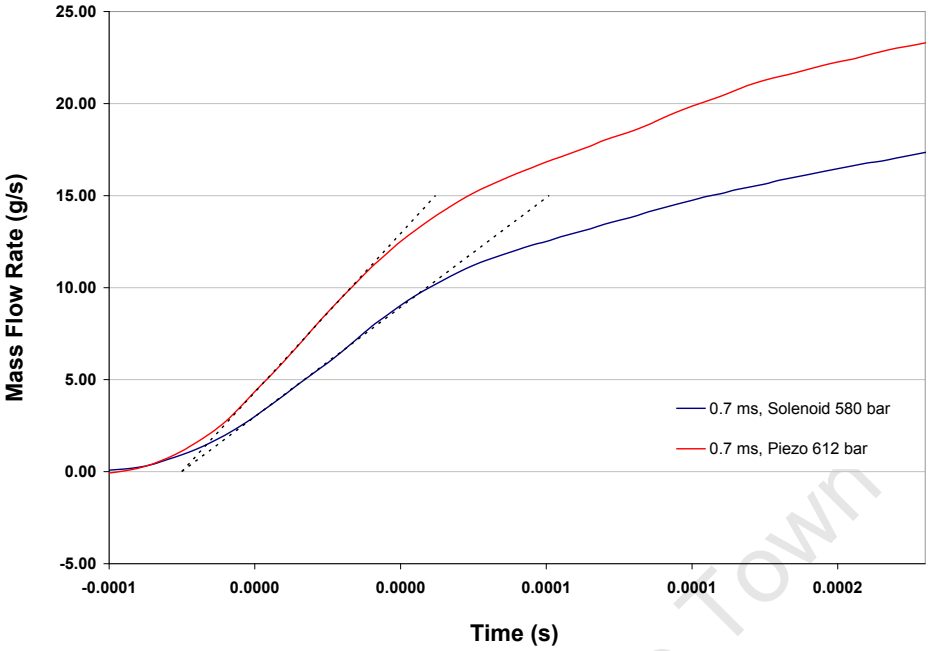

Figure 6- 19 – Rate of rise in flow rate in Solenoid and Piezo injectors.

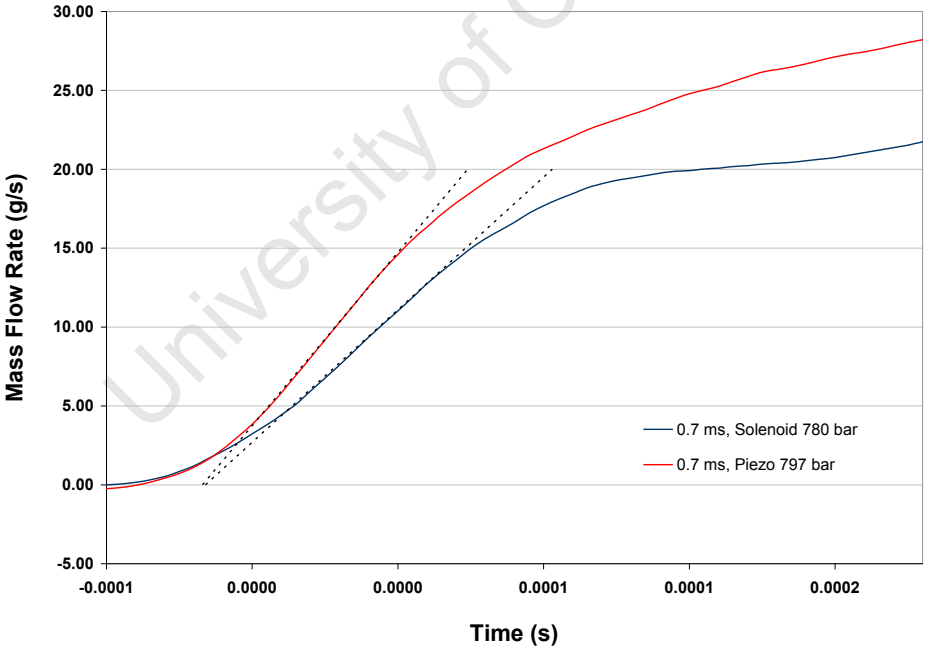

Figure 6- 20 – Rate of rise in flow rate in Solenoid and Piezo injectors.

The rate of increase in flow rate for the piezo injector was roughly 45%, and 31% higher than that for the solenoid injector in figures 6-19 and 6-20 respectively. However due to the varying injection pressures achieved during testing; it was difficult to compare the two injectors directly. The two injectors were fitted with different flow nozzles, which would have contributed to this effect, however, it was also expected that the response time of the piezo injector would be faster than that of the solenoid injector.

6.4 The Effects of Fuel Properties on Injection Characteristics

Density

The regression models discussed earlier in this chapter showed that there was a direct relationship between the injected mass and the density of the diesel fuel being injected. In order to quantify this relationship for each fuel injector, combined regression models were developed using both sets of fuel data. The upstream fuel density values in the models were then independently varied, producing corresponding changes in the injected mass values.

The results that follow again exclude the test results from pulse widths of 0.5 milliseconds and shorter.

For the solenoid injector, the regression equation was as follows ($R^2 = 0.994$):

$$m = 0.710 A \rho_R \sqrt{2\left|\frac{P_R}{\rho_R} - \frac{P_M}{\rho_M}\right|}\Delta t - 8.352 \qquad \text{(Eq 6-11)}$$

And for the piezo injector, as follows ($R^2 = 0.994$):

$$m = 0.782 A \rho_R \sqrt{2\left|\frac{P_R}{\rho_R} - \frac{P_M}{\rho_M}\right|}\Delta t - 4.989 \qquad \text{(Eq 6-12)}$$

For each incremental change in the upstream density, the percentage change in the injected mass data for each injector was then averaged across the pulse width range, resulting in the data shown in figure 6-21 below:

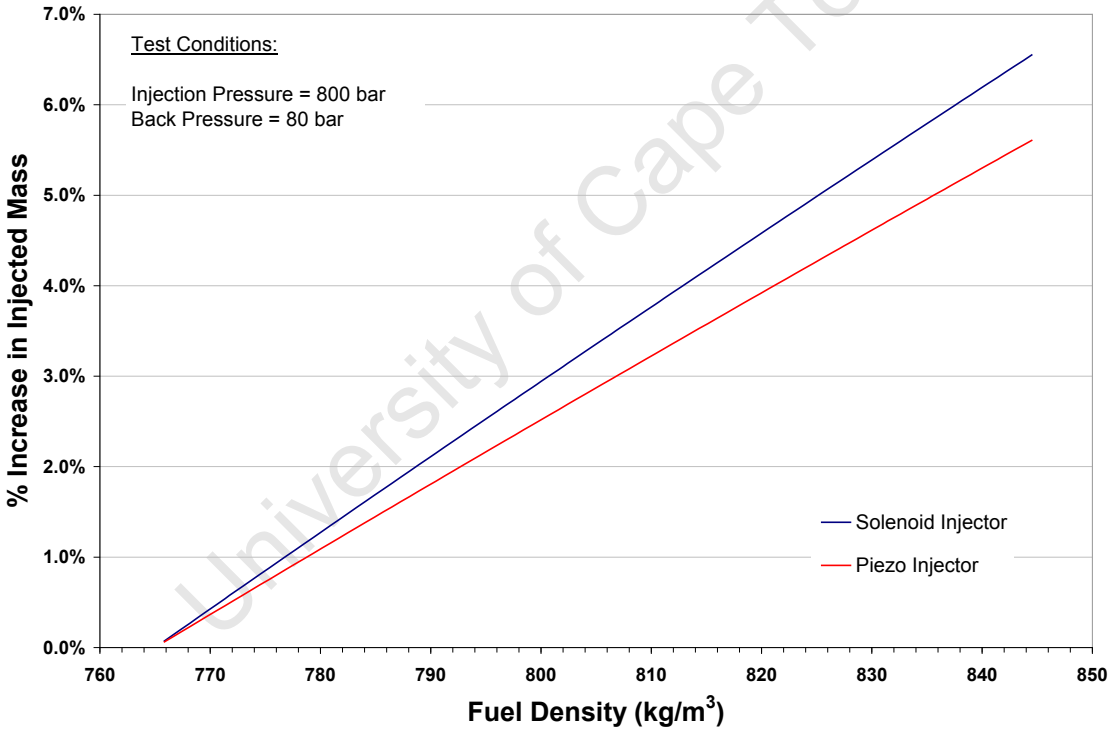

Figure 6- 21. The effects of fuel density on the injected mass.

It was evident that density had a marked effect on the injected mass values. As the density values were increased by up to 10.4 %, the averaged injected mass values rose by up to 6.6 % in the solenoid injector, and by up to 5.6 % in the piezo injector. This is contrary to the findings presented by Boudy and Seers (2009), where it was reported that

density inversely affects the injected mass for single injection events. That is to say that an increase in density results in a lower injected mass.

Viscosity

If it were possible to independently measure the head loss across the injector due to pipe friction losses in the nozzle, the viscosity of the fuel could be taken into account as part of the regression models using the Darcy and Blasius equations. The head loss term would be calculated as follows (Douglas, Gasiorek and Swaffield, 2001, pg 348):

$$h_f = \frac{4fl}{d} \cdot \frac{v^2}{2g} \qquad \text{(Eq 6-13)}$$

Where h_f is the head loss due to friction (m)

l is the length of the nozzle holes (m)

d is the diameter of the nozzles (m)

v is the velocity of the fluid (m/s)

And (Douglas, Gasiorek and Swaffield, 2001, pg 349),

$$f = \frac{0.079}{\mathrm{Re}^{0.25}} \qquad \text{(Eq 6-14)}$$

For GTL in the solenoid injector, at the highest injection pressure (1200 bar) the head loss due to pipe friction losses in the nozzle can be calculated as follows in table 6.3:

Table 6- 3. Calculations illustrating the effect of viscosity increases for GTL in a solenoid injector.

Quantity	Equation	Scenario 1 (Original GTL viscosity)	Scenario 2 (100% increase in GTL viscosity)
GTL Fuel density (ρ)	-	760 kg/m^3	760 kg/m^3
Fuel flow rate ($\dot{m}$)	-	32e^{-03} kg/s	32e^{-03} kg/s
Fuel volumetric flow rate ($\dot{Q}$)	$\dot{Q} = \dot{m} \div \rho$	4.2 e^{-05} m^3/s	4.2 e^{-05} m^3/s
Solenoid Injector Hole diameter (d)	-	152e^{-06} m	152e^{-06} m
C_d	-	0.704	0.704
Effective flow area per hole (A)	$A = C_d \cdot \pi \frac{(d)^2}{4}$	1.28 e^{-08} m^2	1.28 e^{-08} m^2
No. of holes (N)	-	6	6
Velocity of fuel through each hole (v)	$v = \frac{Q}{N \cdot A}$	549 m/s	549 m/s
Length of nozzle hole (l)	-	1.14 e^{-03} m	1.14 e^{-03} m
Kinematic Viscosity (ν)	-	1.7e^{-06} m2/s	3.4e^{-06} m2/s
Reynolds Number	$\mathrm{Re} = \frac{vd}{\nu}$	49117	24558
Friction factor (f)	$f = \frac{0.079}{\mathrm{Re}^{0.25}}$	0.0053	0.0063
Head loss due to friction (h_f)	$h_f = \frac{4flv^2}{d \cdot 2g}$	2449 m	2912 m
Head loss in bar (h_f)	$P = \rho g h_f$	183 bar	217 bar
Difference in head loss	$h_{f1} - h_{f2}$	-	34 bar

The total pressure drop across the solenoid injector was 1120 bar (1200 bar upstream – 80 bar downstream). The 100% increase in viscosity represented in table 6.3 above resulted in a 34 bar increase in the friction losses in the nozzle. This equates to 3% of the total pressure drop over the injector.

Pressure Drop

Looking again at equation 6-5, the pressure drop across the injector is a major factor in affecting the injected mass. Figure 6-22 displays the effects of changes in the injection pressure on the injected mass values, having been calculated in a similar manner to the density effects discussed previously.

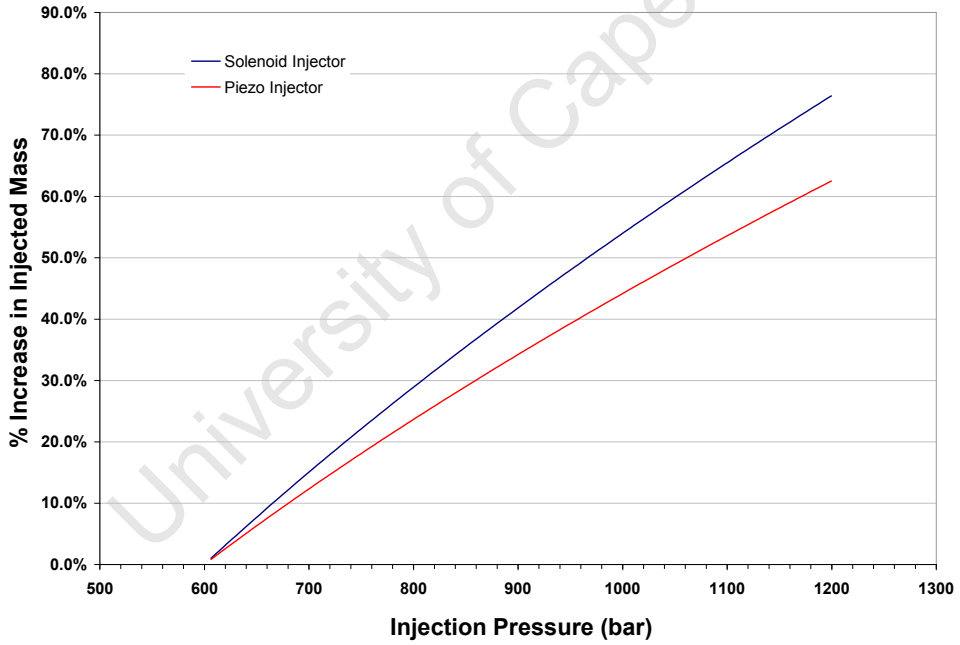

Figure 6- 22. The effects of injection pressure on the injected mass.

With increases of up to 100 % in the injection pressure, the injected mass values for the solenoid injector increased by up to 76.4 %, and by up to 62.5 % in the piezo injector.

The following figures show comparisons between GTL and EN590 in the solenoid and piezo injectors at different injection pressures, and serve to illustrate the subtle differences in the injection rate shape caused by the different fuel properties.

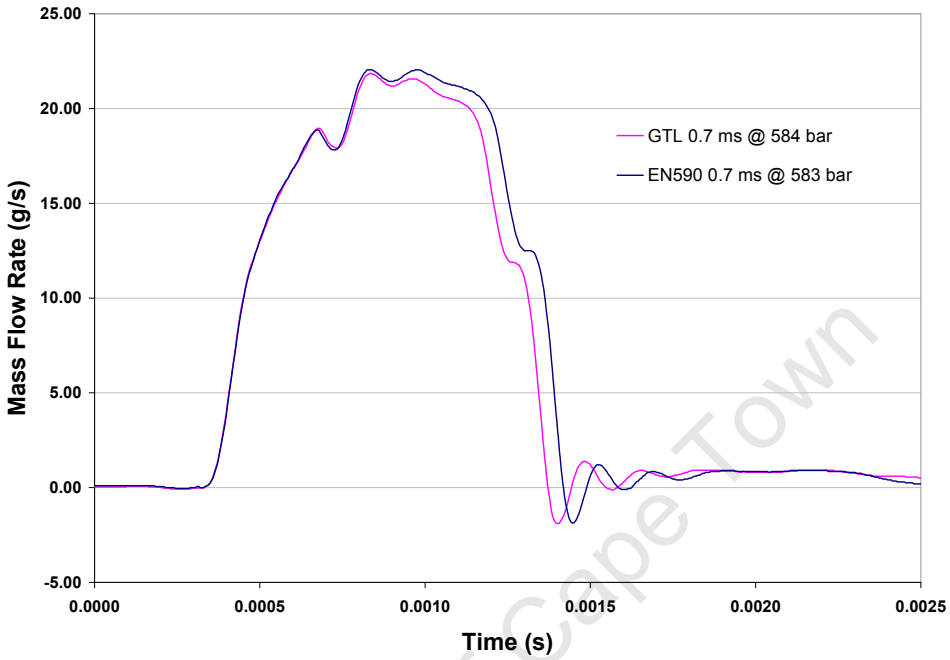

Figure 6- 23. GTL vs EN590 in a solenoid injector at 580 bar injection pressure.

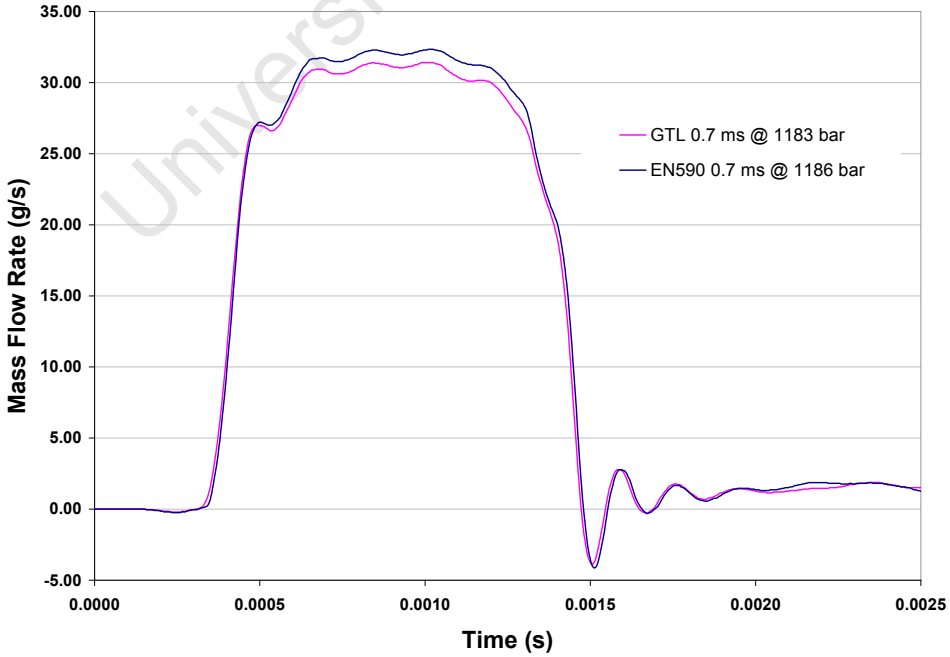

Figure 6- 24. GTL vs EN590 in a solenoid injector at 1180 bar injection pressure.

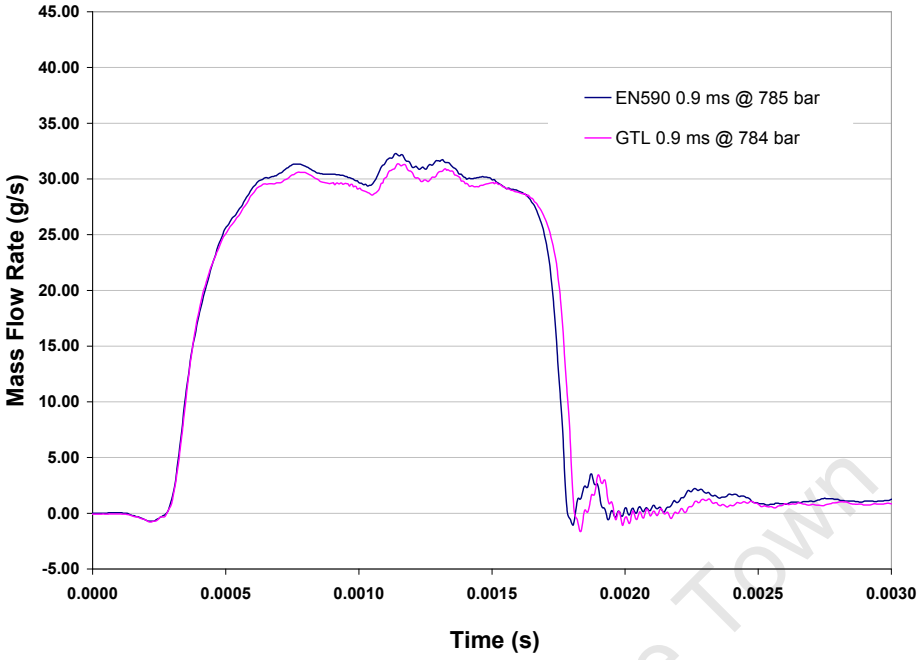

Figure 6- 25. GTL vs EN590 in a piezo injector at 785 bar injection pressure.

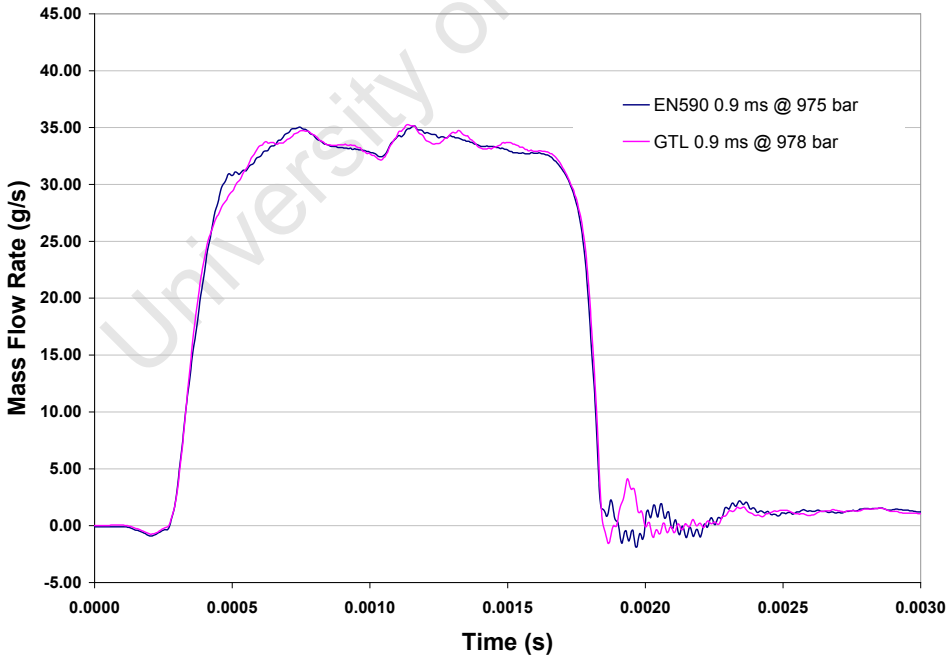

Figure 6- 26. GTL vs EN590 in a piezo injector at 977 bar injection pressure.

The GTL had a lower density and slightly higher viscosity than the EN590, and so as previously discussed, displayed a slightly lower flow rate through the injector at given conditions, resulting in a slightly lower injected mass. The fuel properties did not appear to have any effect on the initial rate of rise in the flow rate, but did affect the maximum flow rate achieved.

From these plots, it was again evident that there were variations in the flow duration at given conditions. The previous discussion around this behaviour (in figures 6-7 and 6-8) suggested that it was not caused by any fuel property variations with pressure, however, looking at figures 6-23 to 6-26, it seems that there was some influence as a result of fuel properties.

The ballistic behaviour of the needle may have been affected by the density and acoustic velocity properties of the fuel. Higher fuel densities would result in a higher inertia of the fuel and, therefore, longer delays for the needle to react to an opening or closing signal. Also, increases in the acoustic velocity of the fuel would result in increases in the speed with which pressure waves travelled through the fuel, and would speed up the reaction of the needle.

Having analysed and discussed all of the results and testing from the study, the following chapter will summarize the key points and trends.

7. Summary and Conclusions

- An experiment for the measurement of acoustic velocity has been verified, with n-hexadecane used as the reference fuel. Values for acoustic velocity, as well as inferred values for density and bulk modulus compared well with data from literature.

- This experiment was then used to determine acoustic velocity, density and bulk modulus values for two diesel fuels, namely EN590 and GTL, at various operating conditions, representative of typical engine operating conditions.

- EN590 was found to have higher acoustic velocity values than the GTL. The difference was 1.67 % at 600 bar and was 0.75 % at 1200 bar.

- Across the pressure range, EN590 was consistently higher in density and in bulk modulus than the GTL by about 8.27 % and 11.71 % respectively. This was an important finding, that across the range of test pressures, pressure had a negligible effect on the relative densities of EN590 and GTL. This in turn meant that any effects on injection characteristics (as a result of fuel density differences) were independent of the injection pressure.

- The relative effects of pressure on the fuel properties for EN590 and for GTL were quantified for the pressure range from 600 bar to 1200 bar. The increase in each property over this pressure range was as follows:

Table 7- 1. The effects of pressure on the fuel properties for EN590 and GTL between 600 and 1200 bar at constant temperature of 329 K.

	Pressure range	Increase in Density	Increase in Acoustic Velocity	Increase in Bulk Modulus
GTL	600 – 1200 bar	2.1 %	12.5 %	29.1 %
EN590	600 – 1200 bar	2.0 %	11.5 %	28.8 %

- Injector mass flow tests were performed on two different types of fuel injector, namely solenoid type and piezo type. Four full sets of tests were performed, one for each combination of fuel and injector type. These tests were run at four different injection pressures, namely 600, 800, 1000, and 1200 bar. The injection pulse widths used were 0.2, 0.3, 0.4, 0.5, 0.7, 0.9, 1.1, 1.3 and 1.5 ms. The injection flow tests were conducted using an apparatus based on the Bosch Indicator design.

- Actual test data were presented in the form of injection rate shape curves. It was observed that, particularly at lower injection pressures, the injectors attained varying maximum flow rates at the different pulse widths.

- An increase in the injection pressure also resulted in a corresponding increase in the maximum flow rate achieved. This effect was more pronounced at shorter pulse widths.

- At higher injection pressures, the diesel fuels displayed a higher acoustic velocity, meaning they reacted quicker in the injector, and this reduced the effect of pulse width on the maximum flow rate achieved. The maximum flow rates for each injector were attained much earlier in the pulse width regime.

- The flow tests conducted with the piezo injector at pulse widths less than 0.4 ms were not very successful. The behaviour of the injector was erratic and it would, on occasion, fail to inject any fuel. The root cause of this problem was not identified.

- Regression models have been presented, which link the mass flow through the injector to the fuel density, and the pressure differential across the injector. These regression models were found to be very accurate at pulse widths longer than 0.5 ms, but were not found to correspond well with the measured data for tests at shorter pulse widths.

- The mismatching of actual data to regression data at shorter pulse widths was likely due to the fact that the regression model approximated the injection rate shape curves as having a 'top hat' shape. At shorter injection pulse widths, such as those in the pilot injection regime, it is known that this is not true, as the needle does not have sufficient time to reach its maximum height above the seat. Instead, the shape of the flow curves at these conditions would be better approximated as a 'pyramid' shape.

- The regression models and the known geometry of the fuel injector nozzles were used to determine flow coefficients for the two injectors. For the solenoid injector, the flow coefficient was 0.725 with GTL, and 0.704 with EN590. For the piezo injector, the flow coefficient was 0.798 with GTL, and 0.773 with EN590.

- On a mass basis, the EN950 yielded higher injection rates than the GTL. In the solenoid injector, for pulse widths between 0.7 ms and 1.5 ms, the EN590 yielded between 2.1 % and 7.9 % more fuel per injection than the GTL. In the piezo injector this difference was between 2.3 % and 7.5 %.

- The piezo injector also displayed a higher rate of rise in the initial part of the injection rate shape curves (by roughly 30 %). This can be attributed to the faster action of the piezo mechanism as opposed to the solenoid.

- Density had a direct effect on the injected mass, with a 10.4 % increase in density yielding an increase in the injected mass of up to 6.6 % in the solenoid injector, and 5.6 % in the piezo injector.

- Although not included as part of the regression model, it was estimated that a 100 % increase in viscosity would yield increases in the nozzle friction losses of roughly 3 % of the total pressure drop across the injector. This figure was based on head loss calculations using the Darcy and Blasius equations, and by evaluating the effect of pressure difference over the injector nozzle on injected mass values.

- Increases in fuel density were found to result in significant increases in the injected mass for single event injections. This did not agree with the study presented by Boudy and Seers (2009), who found that increases in density resulted in slight decreases in the injected mass for single injection events. Boudy and Seers also reported that changes in density played a significant role in the injected mass values, but only where multiple injection events were employed.

- GTL, having a lower density and higher viscosity than EN590, displayed a lower flow rate through the injectors, and thus yielded a lower injected mass at given conditions.

8. Recommendations

8.1 Acoustic Velocity Measurement

- Even though the measurements for n-hexadecane acoustic velocity compared very well with values from literature, there were still some improvements that could be made to the experimental setup. The dead weight tester, for the most part, provided a steady pressure for the testing purposes. At pressures beyond 800 bar however, the tester started to display leakage and there was significant difficulty in capturing the necessary data at these pressures. A more reliable pressure supply would remove a large amount of difficulty from this testing procedure. The solution should also take consideration of the fact that n-hexadecane is a very costly substance, and so volumes required for testing should be minimized wherever possible.

- The fuel properties in this study were measured only up to 970 bar, whereas the fuel mass flow rate tests were performed at over 1150 bar. Ideally the fuel properties should be measured over this full pressure range in order to minimise errors incurred by extrapolating fuel property data.

- The resolution of the signals captured by the oscilloscope for timing the pressure waves was good, but even so, the accuracy of the acoustic velocity measurements could have been made more precise with the use of a device with an even higher sampling rate. The oscilloscope used in this study captured the signals at 200 kHz. Recalling the acoustic velocity measurement procedure from chapter 4, the two pressure signals were superimposed on each other and then shifted until they lined up. At this sampling rate of 200 kHz, for every **two data points** that the graphs were shifted, the acoustic velocity values changed by roughly 1.5 %. This was significant when the difference between the two fuels was only around 12 %.

8.2 Mass Flow Rate Measurement

- One of the elements not considered in this model was the effect of the upstream supply pressure to the injectors. Boudy and Seers (2009) reported that the upstream pressure fluctuated as a result of both fuel properties, and the design of the fuel injection system. In this study, the fuel feed pipe between the common rail and the injector body was roughly 1.6 metres in length. In order to better simulate the behaviour of the injector in an engine, one should rather ensure that this pipe length is as close as possible to the real pipe length on the engine itself. Any harmonic or interference with the supply pressure should then be accurately mimicked by the experimental setup. The effects of the fuel properties on upstream head loss due to pipe friction could also be included in the model, although the benefit in terms of accuracy is not clear.

- The shorter injection events in this study were aimed at simulating pilot injection events in real engine operation. These events are much quicker than the normal main injection events and, as such, the volume through the injector is much smaller. In this study, 1000 injection events were run per test at each combination of injection pressure and pulse width. Perhaps a much higher number of the shorter injection events should be captured, resulting in a higher volume of fuel being collected per test. A factor could also be included in the regression models to correct for the shape of the flow curve and possibly improve the overall accuracy of the results. For instance, the solenoid tests with GTL at 0.2 ms pulse width and 600 bar injection pressure yielded 0.64 grams of fuel into the beaker. The regression model yielded a value which differed by 260 % for the same conditions.

- Even though the much shorter injection events were sufficiently captured on the downstream pressure transducer, perhaps a transducer more suited to small fluctuations in pressure would capture a more accurate signal. The downstream

transducer used in this study was rated for 0-200 bar measurements. A pilot injection event at 600 bar only induced a 7 bar pressure increase in the measuring tube. This only represented 3.5 % of the pressure transducer's range.

- An investigation should be conducted into the proper methods for controlling a piezo type injector at shorter pulse-widths, in order to ensure that the experimental tests performed at these conditions yield results representative of actual injector behaviour in an engine.

- The calculation of mass flow through the injector required, as an input, the time for which the injector was open. In this study this time value was measured directly off the injection rate shape curves, but a more accurate method of measurement would be to install a needle lift sensor on the fuel injectors, allowing one to see exactly when the injector needle opens and closes.

- As has been mentioned, the fuel pump control system did not perform satisfactorily, and resulted in the need for much post processing of the data in order to draw meaningful conclusions. If the control system were more effective, and the pressure delivered by the pump more in line with the set point, then the experimental data would be of a much higher quality, and far less time would be required for extrapolating and correcting the data.

9. References

Ball S., Trusler J., "Speed of Sound of n-Hexane and n-Hexadecane at Temperatures Between 298 and 373K and Pressures up to 100MPa", International Journal of Thermophysics, Vol. 22, No.2, 2001

Benajes J., Pastor J., Payri R., Plazas A., "Analysis of the Influence of Diesel Nozzle Geometry in the Injection Rate Characteristic", ASME Journal of Fluids Engineering, Vol. 126, pg 63, 2004

Bianchi G., Falfari S., Parotto M., "Advanced Modelling of Common Rail Injector Dynamics and Comparison with Experiments", SAE 2003-01-0006, 2003

Bosch W., "The Fuel Rate Indicator: A New Measuring Instrument for Display of the Characteristics of Individual Injection", SAE 660749, 1966

Boudy F., Seers P., "Impact of physical properties of biodiesel on the injection process in a common-rail direct injection system", Energy Convers Manage, 2009

Cerdeirina C., Tovar C., Gonzalez-Salgado D., Carballo E., Romani A., "Isobaric thermal expansivity and thermophysical characterization of liquids and liquid mixtures", PCCP, Vol. 3, pg 5230-5236, 2001

Desantes J., Arregle J., Lopez J., Hermens S., "Experimental characterization of outlet flow for different diesel nozzle geometries", SAE 2005-01-2120, 2005

DGMK Project-4510, "pvt-Data at high pressures", German Association for Petroleum Sciences and Coal Chemistry, 1976

Douglas J., Gasiorek J., Swaffield J., "Fluid Mechanics – 4th Edition", Prentice Hall, 2001

Ganser M., "Common Rail Injectors for 2000 bar and Beyond", SAE 2000-01-0706, 2000

Gouw, T.H., Vlugter, J.G. "Physical Properties of Triglycerides III: Ultrasonic Sound Velocity. Fette-Seifen-Anstrichmittel", 69 Jahrgang, Nr. 3, 1967, 159-164.

Huhtala K., Vilenius M., "Study of a common rail fuel injection system", SAE 2001-01-3184, 2001

Ishikawa S., Ohmori Y., Fukushima S., Suzuki T., Takamura A., "Measurement of Rate of Multiple-Injection in CDI Diesel Engines", SAE 2000-01-1257, 2000

Jinghong Y., Zhaoneng C., Yuanzhang L., "The Variation of Oil Effective Bulk Modulus with Pressure in Hydraulic Systems", ASME Journal of Dynamic Systems, Measurement and Control, Vol 116, 1994

Morgan P., Viljoen C., Roets P., Schaberg P., Myburgh I., Botha J., "Some Comparative Chemical, Physical and Compatibility Properties of Sasol Slurry Phase Distillate Diesel Fuel", SAE 982488, 1998

Mulemane A., Han J., Lu P., Yoon S., Lai M., "Modelling Dynamic Behaviour of Diesel Fuel Injection Systems", SAE 2004-01-0536, 2004

Rolling, R. E., Vogt, C. J. "The Adiabatic Bulk Modulus of Normal Paraffin Hydrocarbons from Hexane to Hexadecane", Transactions of the ASME – Journal of Basic Engineering, 1960, 635-644

Ryan T., “Measurement of the Instantaneous Distribution of Momentum in Diesel Injection Nozzle Fuel Jets”, SAE 962004, 1996

Schmid U., Krötz G., Öing H., Renner G., Schmitt-Landsiedel D., “A Nozzle-Integrated Flow Sensor for Common-Rail Injection Systems”, SAE 2001-01-0614, 2001

Schommers J., Duvinage F., Stotz M., Peters A., Ellwanger S., Koyanagi K., Gildein H., “Potential of Common Rail Injection System for Passenger Car DI Diesel Engines”, SAE 2000-01-0944, 2000

Seykens X., Somers L., Baert R., “Modelling of Common Rail Fuel Injection System and Influence of Fluid Properties on Injection Process”, Proceedings of VAFSEP2004

Smith W., Timoney D., “Fuel Injection Rate Analysis – A New Diagnostic Tool for Combustion Research”, SAE 922224, 1992

Stan C., “Direct Injection Systems for Spark-Ignition and Compression-Ignition Engines”, SAE International, ISBN 0-7680-0610-4

Stumpp G., Ricco M., “Common Rail – An Attractive Fuel Injection System for Passenger Car DI Diesel Engines”, SAE 960870, 1996

Szybist J., Boehman A., Taylor J., McCormick R., “Evaluation of formulation strategies to eliminate the biodiesel NOx effect”, Fuel Processing Technology 86, 2005, 1109-1126

Takamura A., Ohta T., Fukushima S., “A Study on Precise Measurement of Diesel Fuel Injection Rate”, SAE 920630, 1992

Tat M., Van Gerpen J., “Measurement of Biodiesel Speed of Sound and Its Impact on Injection Timing”, NREL/SR-510-31462, 2003

Watton J., “Fluid Power Systems, Modelling, Simulation, Analog and Microcomputer Control”, Prentice Hall, 1989

Zhu Y., Reitz R., “Modelling Fuel System Performance and Its Effects on Spray Characteristics”, SAE 2000-01-1253, 2000

Appendix A

Fuel Properties

n-Hexadecane at 329 K

Pressure (bar)	Temperature (K)	Measured Acoustic Velocity (m/s)	Inferred Bulk Modulus (MPa)	Inferred Density (kg/m^3)
172.0	329.4	1318.4	1335.7	765.7
172.0	329.6	1301.3	1320.5	766.0
172.2	329.7	1318.4	1355.7	765.7
172.1	329.8	1301.3	1320.6	766.0
171.6	329.8	1318.4	1355.7	765.7
391.7	329.0	1401.4	1555.6	775.6
394.6	329.0	1411.3	1577.8	775.4
389.6	329.0	1401.4	1555.4	775.5
393.4	329.1	1401.4	1555.8	775.6
389.0	329.1	1411.3	1577.3	775.2
594.6	329.4	1484.4	1765.8	782.4
541.6	329.5	1473.5	1734.9	780.4
557.8	329.5	1484.4	1762.1	780.8
582.6	329.6	1495.5	1790.8	781.5
567.4	329.6	1484.4	1763.1	781.2
770.1	329.8	1553.5	1950.5	787.2
737.1	329.7	1541.5	1917.7	786.3
773.2	329.1	1553.5	1950.8	787.3
720.9	329.1	1541.5	1916.0	785.6
694.0	329.1	1529.8	1884.5	785.0
866.7	329.3	1578.0	2021.4	789.9
910.7	329.6	1603.2	2090.1	790.5
806.0	329.5	1565.6	1984.3	788.1

EN590 at 329 K

Pressure (bar)	Temperature (K)	Measured Acoustic Velocity (m/s)	Inferred Bulk Modulus (MPa)	Inferred Density (kg/m^3)
173.5	328.9	1301.3	1403.6	813.2
174.3	329.1	1301.3	1403.7	813.3
174.2	328.9	1309.8	1422.2	813.1
174.2	328.8	1318.4	1441.1	813.0
174.3	328.8	1309.8	1422.2	813.1
375.9	328.6	1401.4	1650.8	822.0
376.2	328.6	1411.3	1674.2	821.7
376.6	328.6	1401.4	1650.9	821.9
376.4	328.6	1401.4	1650.8	822.0
376.1	328.5	1401.4	1650.8	822.0
572.4	329.1	1484.4	1872.8	828.6
577.2	329.1	1495.5	1901.2	828.5
578.1	329.1	1484.4	1873.4	828.9
577.7	329.1	1495.5	1901.3	828.5
578.3	329.1	1484.4	1873.4	828.9
773.7	329.2	1565.6	2103.3	834.0
777.9	329.1	1553.5	2071.5	834.7
774.5	329.2	1578.0	2136.4	833.6
772.0	329.1	1565.6	2103.1	834.0
778.4	329.0	1553.5	2071.6	834.7
962.0	329.3	1616.1	2259.5	839.1
971.8	329.4	1603.2	2224.9	840.0
973.4	329.4	1603.2	2225.1	840.1
975.1	329.4	1616.1	2260.8	839.6
974.7	329.3	1616.1	2260.8	839.6

EN590 at Standard Conditions

Fuel Density @ 20°C, 1 bar	828.8	kg/m^3
Fuel Density @ 15°C, 1 bar	832.3	kg/m^3
Fuel Kinematic Viscosity @ 40°C, 1 bar	2.355	mm^2/s

GTL at 329 K

Pressure (bar)	Temperature (K)	Measured Acoustic Velocity (m/s)	Inferred Bulk Modulus (MPa)	Inferred Density (kg/m^3)
178.7	328.5	1281.3	1250.9	749.0
180.9	328.6	1274.8	1238.4	749.3
179.0	328.8	1271.6	1231.9	749.2
182.1	328.8	1281.3	1251.2	749.2
378.1	328.9	1384.0	1480.8	757.7
385.1	329.2	1384.0	1481.5	758.1
384.9	329.1	1384.0	1481.5	758.1
385.5	329.0	1387.8	1489.7	758.0
387.5	328.7	1384.0	1481.8	758.2
574.0	328.7	1464.9	1678.4	764.5
579.7	328.7	1469.2	1688.7	764.6
581.2	328.8	1473.5	1698.7	764.5
577.3	328.7	1464.9	1678.7	764.7
770.2	328.2	1536.8	1865.5	770.2
787.4	328.5	1541.5	1878.6	770.7
788.7	328.6	1541.5	1878.7	770.7
788.0	328.7	1541.5	1878.6	770.7
781.1	328.8	1536.8	1866.6	770.6
971.0	329.5	1590.5	2016.5	775.7
965.6	329.5	1585.4	2003.5	775.7
970.8	329.4	1590.5	2016.5	775.7
973.6	329.2	1595.5	2029.3	775.6

GTL at Standard Conditions

Fuel Density @ 20°C, 1 bar	763.4	kg/m^3
Fuel Density @ 15°C, 1 bar	767	kg/m^3
Fuel Kinematic Viscosity @ 40°C, 1 bar	2.46	mm^2/s

Appendix B – Injected Mass Results

GTL in the Solenoid Injector

Back Pressure (bar)	Injection Pressure (bar)	Pressure Differential (bar)	Pulse Width (s)	Flow duration (s)	Injected Mass (kg)
83	579	495	0.0002	0.000245	0.00064
83	580	497	0.0003	0.000335	0.00204
84	581	497	0.0004	0.000445	0.00367
82	582	500	0.0005	0.000660	0.00706
81	584	503	0.0007	0.001050	0.01464
81	583	501	0.0009	0.001400	0.02125
82	584	502	0.0011	0.001580	0.02513
82	582	500	0.0013	0.001775	0.02930
81	583	502	0.0015	0.001995	0.03340
83	781	698	0.0002	0.000285	0.00196
83	781	698	0.0003	0.000380	0.00362
82	780	699	0.0004	0.000565	0.00697
82	783	702	0.0005	0.000750	0.01173
82	782	700	0.0007	0.001155	0.02080
82	778	696	0.0009	0.001370	0.02629
81	781	700	0.0011	0.001570	0.03278
82	781	699	0.0013	0.001765	0.03604
82	782	700	0.0015	0.001975	0.04054
83	983	900	0.0002	0.000305	0.00302
85	983	898	0.0003	0.000320	0.00348
82	980	898	0.0004	0.000580	0.00886
82	981	899	0.0005	0.000765	0.01433
81	982	901	0.0007	0.001165	0.02533
82	981	899	0.0009	0.001345	0.02949
83	984	901	0.0011	0.001545	0.03456
81	983	902	0.0013	0.001750	0.04278
82	983	901	0.0015	0.001960	0.04701
81	1180	1098	0.0002	0.000280	0.00286
81	1178	1097	0.0003	0.000310	0.00384
77	1179	1102	0.0004	0.000600	0.01082
76	1180	1104	0.0005	0.000830	0.01855
80	1183	1103	0.0007	0.001195	0.02933
81	1181	1101	0.0009	0.001315	0.03240
81	1181	1100	0.0011	0.001525	0.03958
81	1179	1098	0.0013	0.001740	0.04587
81	1184	1103	0.0015	0.001935	0.05448

EN590 in the Solenoid Injector

Back Pressure (bar)	Injection Pressure (bar)	Pressure Differential (bar)	Pulse Width (s)	Flow duration (s)	Injected Mass (kg)
81	581	500	0.0002	0.000265	0.00092
81	584	502	0.0003	0.000300	0.00151
81	582	501	0.0004	0.000530	0.00466
80	582	502	0.0005	0.000705	0.00763
81	583	503	0.0007	0.001105	0.01581
81	584	502	0.0009	0.001445	0.02269
81	584	504	0.0011	0.001610	0.02623
82	583	502	0.0013	0.001820	0.03043
82	583	500	0.0015	0.002030	0.03470
82	780	698	0.0002	0.000250	0.00140
84	781	697	0.0003	0.000320	0.00271
82	781	700	0.0004	0.000585	0.00734
82	781	700	0.0005	0.000765	0.01211
81	780	699	0.0007	0.001180	0.02219
81	784	703	0.0009	0.001400	0.02745
81	782	700	0.0011	0.001590	0.03225
80	780	700	0.0013	0.001785	0.03734
81	780	700	0.0015	0.001995	0.04245
82	976	895	0.0002	0.000245	0.00173
82	982	900	0.0003	0.000320	0.00336
81	979	898	0.0004	0.000605	0.00939
80	980	900	0.0005	0.000800	0.01557
80	980	901	0.0007	0.001200	0.02646
80	980	901	0.0009	0.001350	0.03117
80	983	903	0.0011	0.001565	0.03715
81	983	902	0.0013	0.001755	0.04303
81	982	901	0.0015	0.001965	0.05052
83	1179	1096	0.0002	0.000240	0.00202
82	1181	1100	0.0003	0.000330	0.00399
79	1179	1100	0.0004	0.000615	0.01035
80	1181	1102	0.0005	0.000805	0.01849
80	1186	1106	0.0007	0.001180	0.02975
80	1183	1103	0.0009	0.001320	0.03469
80	1183	1102	0.0011	0.001530	0.04162
80	1181	1101	0.0013	0.001740	0.04815
81	1184	1104	0.0015	0.001945	0.05448

GTL in the Piezo Injector

Back Pressure (bar)	Injection Pressure (bar)	Pressure Differential (bar)	Pulse Width (s)	Flow duration (s)	Injected Mass (kg)
85	612	526	0.0002	0.000166	0.00026
87	612	525	0.0003	0.000334	0.00284
85	614	529	0.0004	0.000518	0.00705
84	614	530	0.0005	0.000730	0.01215
83	609	526	0.0007	0.001135	0.02180
83	606	523	0.0009	0.001515	0.03144
83	608	525	0.0011	0.001885	0.04037
83	614	531	0.0013	0.002240	0.04907
82	615	532	0.0015	0.002575	0.05697
88	818	730	0.0002	0.000148	0.00010
87	817	730	0.0003	0.000279	0.00329
85	821	735	0.0004	0.000516	0.00808
85	822	738	0.0005	0.000740	0.01511
85	819	735	0.0007	0.001170	0.02730
85	785	700	0.0009	0.001565	0.03840
83	751	668	0.0011	0.001935	0.04818
84	736	652	0.0013	0.002295	0.05836
84	809	725	0.0015	0.002670	0.06673
88	966	878	0.0003	0.000279	0.00363
86	927	841	0.0004	0.000524	0.00950
85	887	802	0.0005	0.000742	0.01619
85	839	754	0.0007	0.001195	0.02749
88	781	693	0.0009	0.001590	0.04038
88	762	674	0.0011	0.001965	0.04787
88	756	669	0.0013	0.002320	0.05780
88	772	684	0.0015	0.002670	0.06805
82	1188	1105	0.0003	0.000315	0.00418
81	1170	1088	0.0004	0.000520	0.01088
81	1132	1051	0.0005	0.000760	0.01953
82	1018	936	0.0007	0.001200	0.03241
81	978	897	0.0009	0.001610	0.04647
81	936	855	0.0011	0.001985	0.05656
81	923	842	0.0013	0.002350	0.06739
81	976	896	0.0015	0.002725	0.08165

EN590 in the Piezo Injector

Back Pressure (bar)	Injection Pressure (bar)	Pressure Differential (bar)	Pulse Width (s)	Flow duration (s)	Injected Mass (kg)
85	580	496	0.0003	0.000300	0.00222
83	580	497	0.0004	0.000486	0.00626
81	577	496	0.0005	0.000698	0.01124
80	580	500	0.0007	0.001130	0.02130
78	584	506	0.0009	0.001510	0.03083
78	582	504	0.0011	0.001875	0.03982
77	575	498	0.0013	0.002250	0.04803
76	577	501	0.0015	0.002580	0.05629
85	782	697	0.0003	0.000264	0.00160
84	785	702	0.0004	0.000414	0.00572
83	783	700	0.0005	0.000686	0.01318
82	779	697	0.0007	0.001130	0.02594
82	785	704	0.0009	0.001535	0.03826
82	794	712	0.0011	0.001935	0.05027
82	786	705	0.0013	0.002280	0.06005
81	790	709	0.0015	0.002635	0.07068
84	984	900	0.0003	0.000268	0.00236
83	987	904	0.0004	0.000458	0.00816
83	991	908	0.0005	0.000718	0.01737
83	984	901	0.0007	0.001160	0.03228
83	975	892	0.0009	0.001570	0.04624
83	961	877	0.0011	0.001955	0.05936
84	894	810	0.0013	0.002325	0.06780
84	887	804	0.0015	0.002690	0.07699
85	1189	1103	0.0003	0.000262	0.00263
80	1168	1088	0.0004	0.000474	0.01036
80	1147	1068	0.0005	0.000726	0.01869
81	1029	947	0.0007	0.001170	0.03446
81	976	894	0.0009	0.001580	0.04643
82	1003	921	0.0011	0.001975	0.05913
82	899	816	0.0013	0.002355	0.06771
83	865	782	0.0015	0.002700	0.07806

Appendix C - Drawings

Materials list for the drawings.

Item Description	Material
Injector Holder	316 Stainless Steel
Cylinder	316 Stainless Steel
Endcap	316 Stainless Steel
Collar	316 Stainless Steel
Piston Head	316 Stainless Steel
Piston Cap	Brass

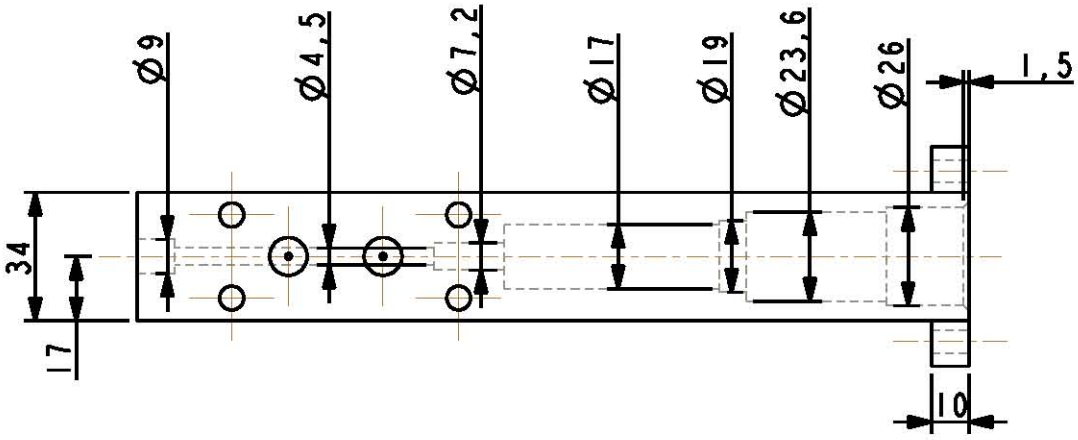

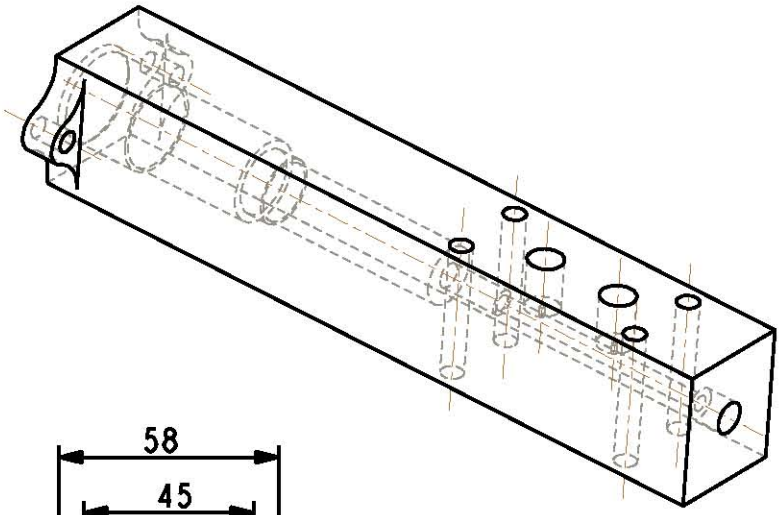

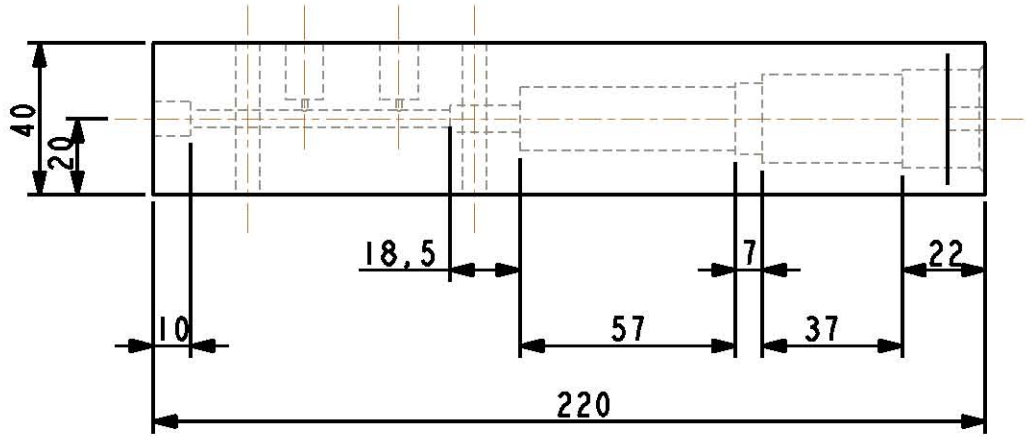

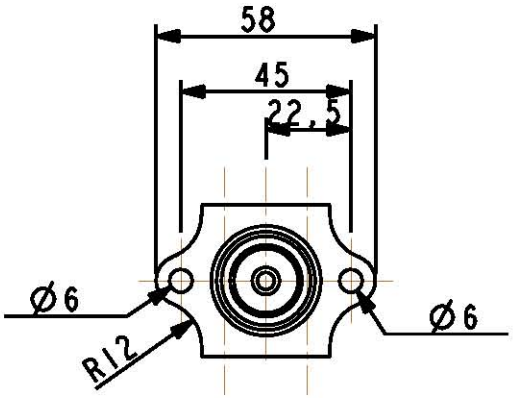

Item	Name	Qty	Material

University of Cape Town
Department of Mechanical Engineering

Title: Injector Holder

Dimensions in mm Tolerance B.O.S.	Scale	Date	Sheet	of
0.1	0,500	30-Dec-06	01	02
	Drawn By: Brenainn Cross		Drawing Number: P01 D01	

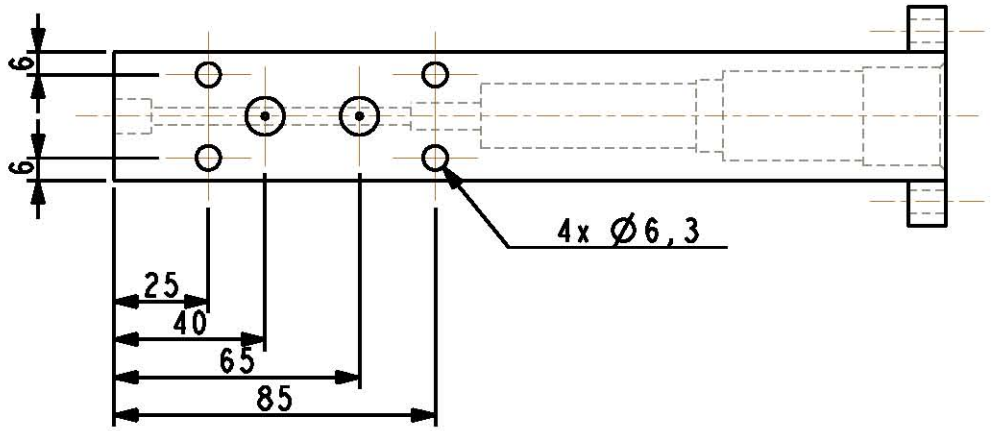

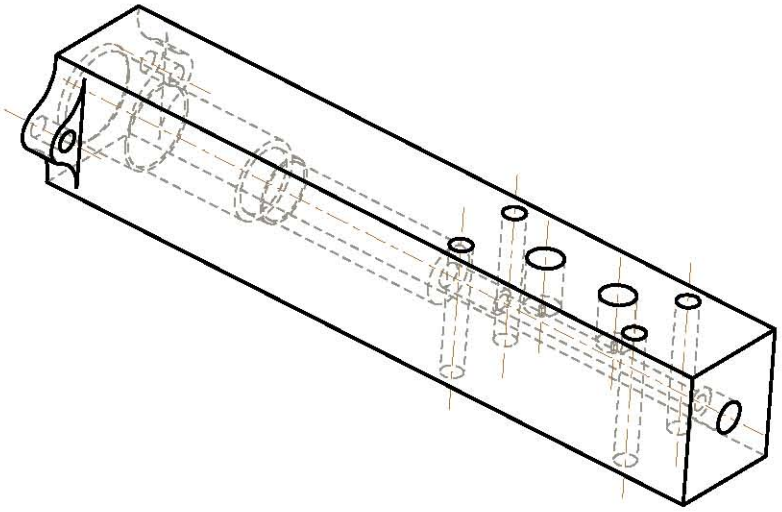

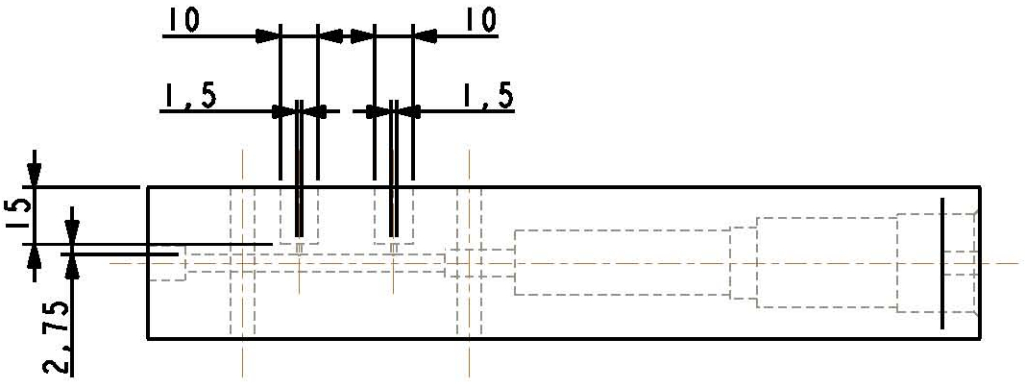

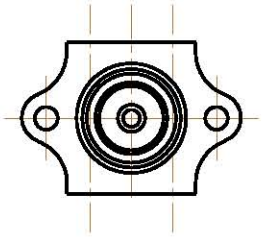

Item	Name	Qty	Material

University of Cape Town
Department of Mechanical Engineering

Title: Injector Holder

Dimensions in mm Tolerance B.O.S.	Scale	Date	Sheet	of
0.1	0,500	30-Dec-06	02	02
	Drawn By: Brenainn Cross		Drawing Number: P01 D02	

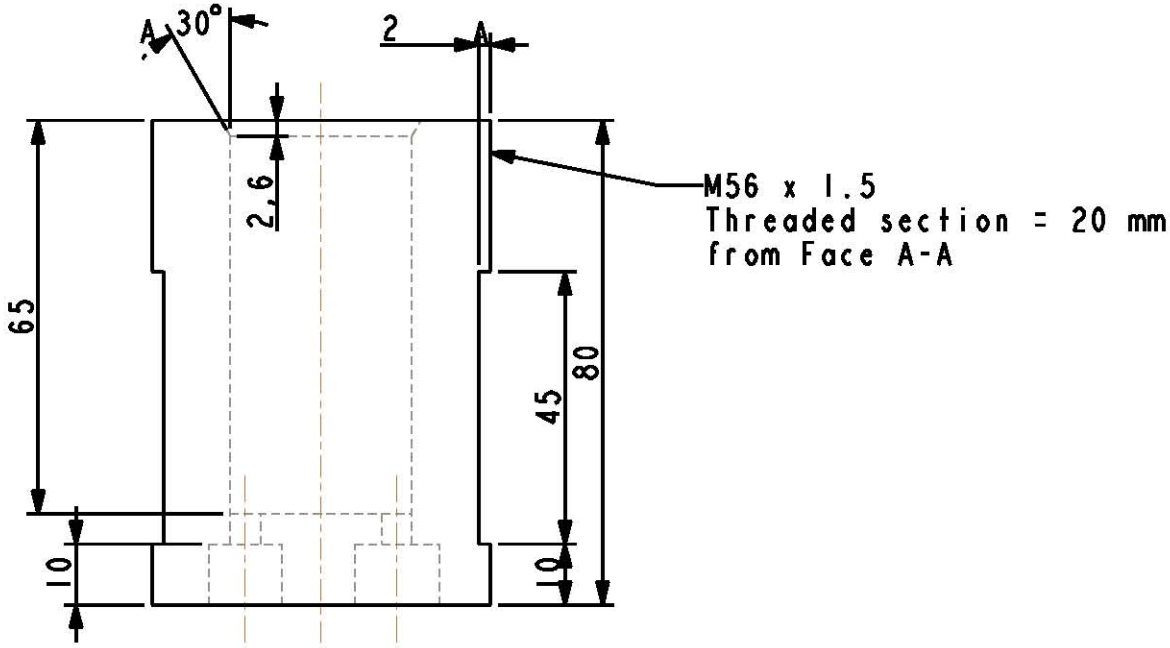

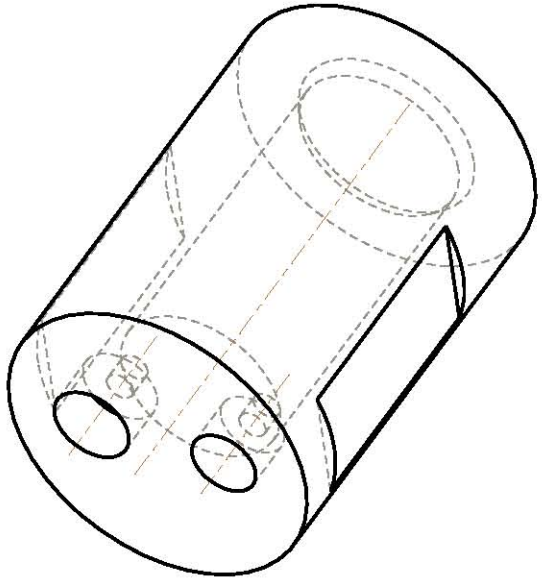

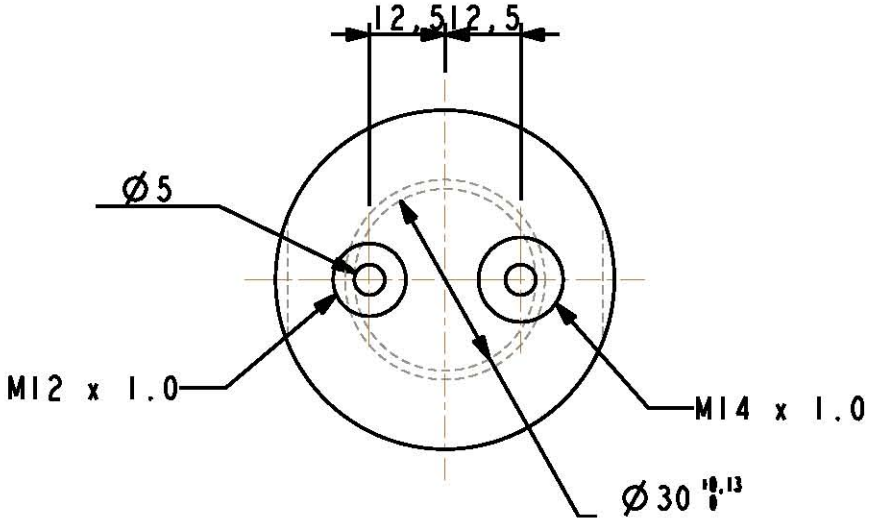

Item	Name	Qty	Material

University of Cape Town
Department of Mechanical Engineering

Title: Cylinder

Dimensions in mm Tolerance B.O.S.	Scale	Date	Sheet	of
0.1	0,800	22-Aug-07	01	06
	Drawn By: Brenainn Cross		Drawing Number: 1	

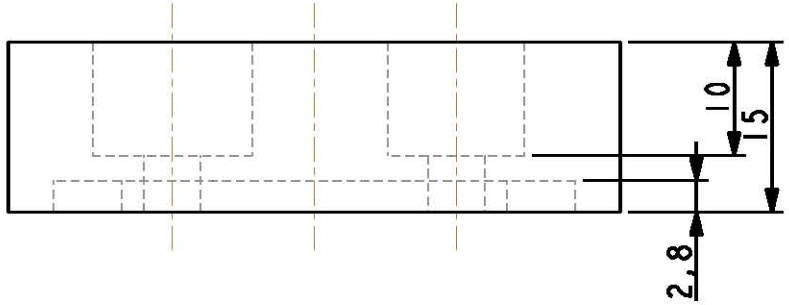

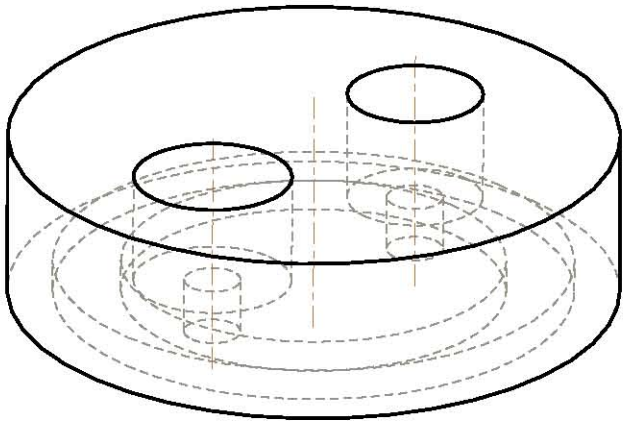

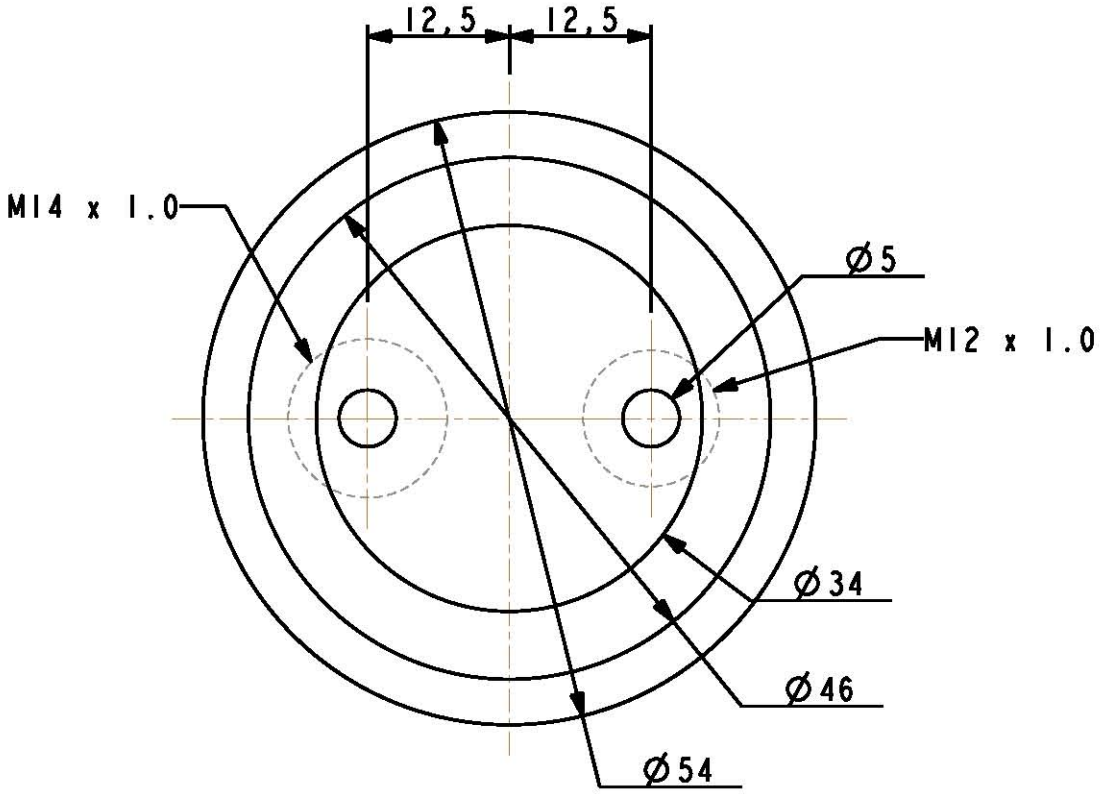

Item	Name	Qty	Material

University of Cape Town
Department of Mechanical Engineering

Title: Endcap

Dimensions in mm Tolerance B.O.S.	Scale	Date	Sheet	of
0.1	1,500	22-Aug-07	02	06
	Drawn By: Brenainn Cross		Drawing Number: 2	

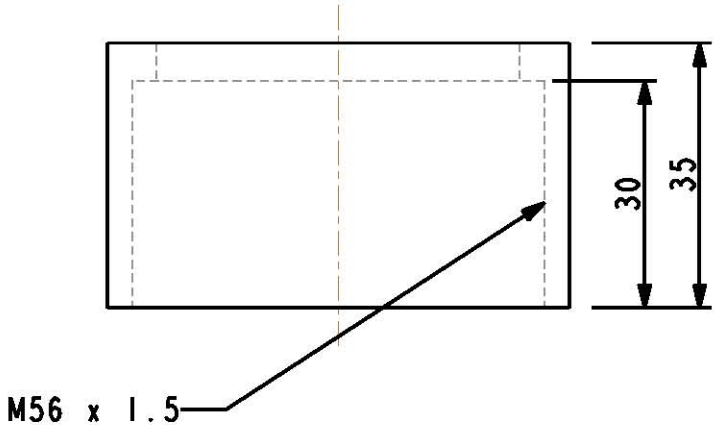

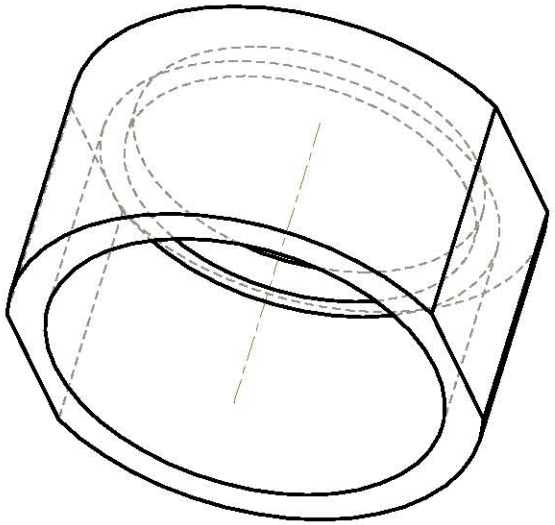

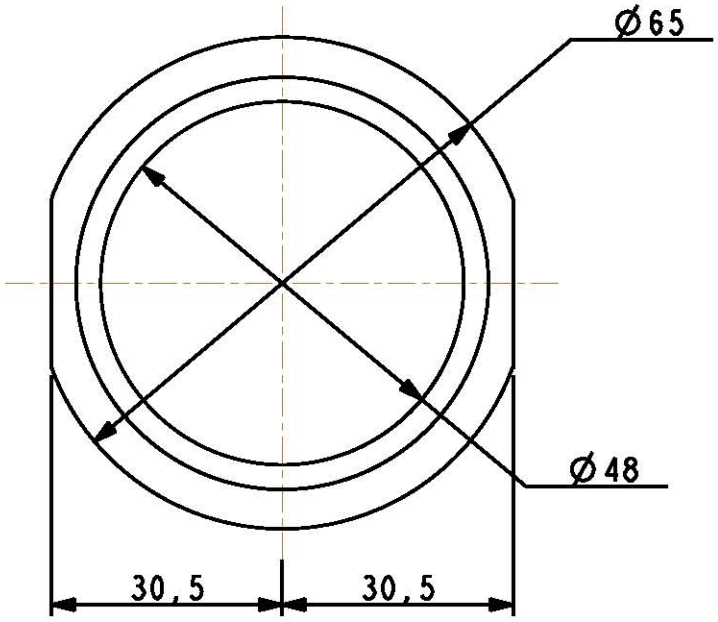

Item	Name	Qty	Material

University of Cape Town
Department of Mechanical Engineering

Title: Collar

Dimensions in mm Tolerance B.O.S.	Scale	Date	Sheet	of
0.1	1,000	23-Aug-07	03	06
	Drawn By: Brenainn Cross		Drawing Number: 3	

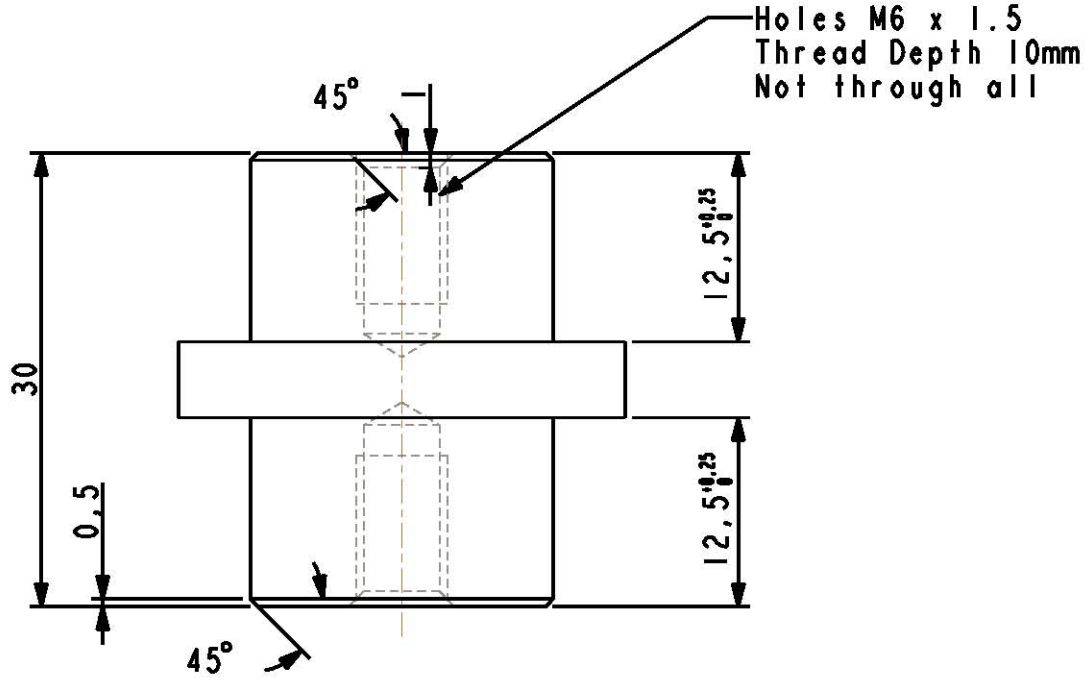

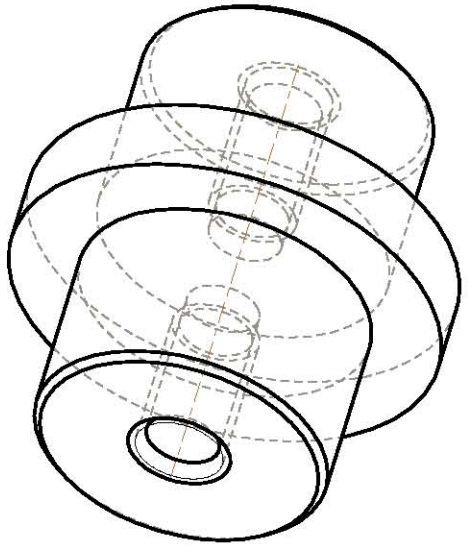

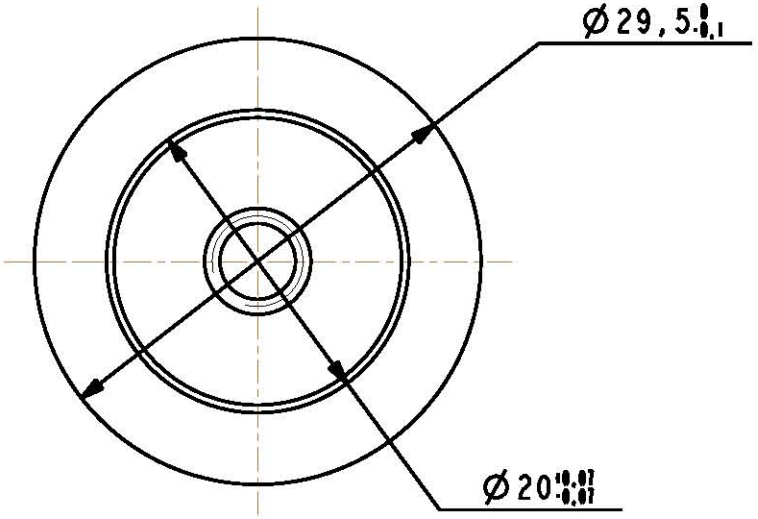

Critical Tolerance

Item	Name	Qty	Material

University of Cape Town
Department of Mechanical Engineering

Title: Piston Head

Dimensions in mm Tolerance B.O.S.	Scale	Date	Sheet	of
0.1	2,000	23-Aug-07	04	06
	Drawn By: Brenainn Cross		Drawing Number: 4	

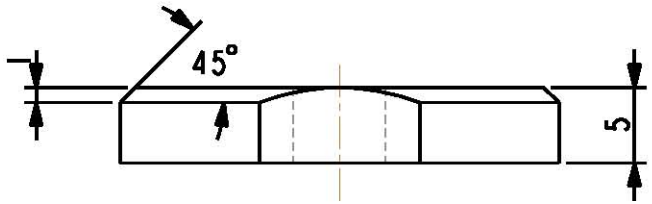

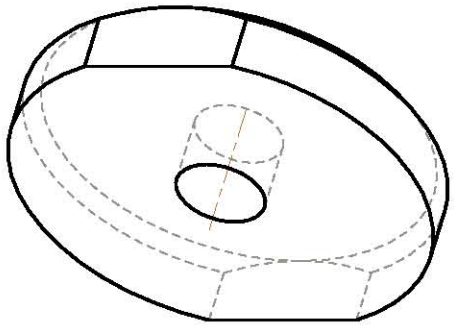

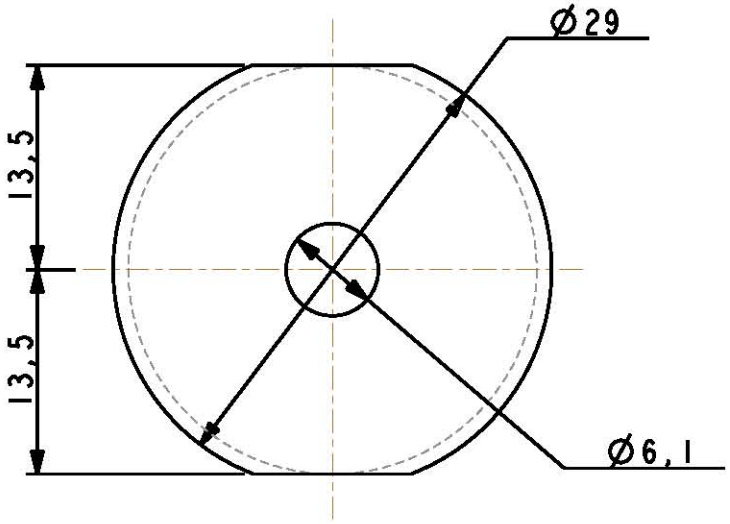

Item	Name	Qty	Material
	University of Cape Town Department of Mechanical Engineering		
	Title Piston Cap		
Dimensions in mm Tolerance B.O.S. 0.1	Scale 2,000	Date 23-Aug-07	Sheet 05 of 06
	Drawn By Brenainn Cross		Drawing Number 5